LIFE-CYCLE COST-BASED DESIGN OF WIND EXCITED TALL BUILDINGS

Dissertation

submitted to and approved by the

Department of Architecture, Civil Engineering and Environmental Sciences
University of Braunschweig – Institute of Technology

and the

Department of Civil and Environmental Engineering
University of Florence

in candidacy for the degree of a
Doktor-Ingenieurin (Dr.-Ing.) /
Dottore di Ricerca in Civil and Environmental Engineering*)

by
Laura Ierimonti
born 16/05/1987
from Perugia, Italy

Submitted on	20 February, 2018
Oral examination on	7 May, 2018
Professorial advisors	Prof. Klaus Thiele Prof. Annibale Luigi Materazzi

2018

*) Either the German or the Italian form of the title may be used.

Acknowledgements

First of all, I would like to thank my supervisors Professor Materazzi and Professor Thiele for their valuable advice, guidance and kind assistance during these three years. A special thank you goes to my co-supervisor Professor Ilaria Venanzi for the enthusiasm and passion for research that she has transmitted to me. I deeply appreciate all her contributions of time and ideas to make my PhD experience productive and stimulating. Thank you to Professor Luca Caracoglia, whose observations and passion for wind engineering inspired me to greatly improve my work. I would also like to express my gratitude to Professor Vincent Denoël, who gave me confidence in my research.

This thesis is dedicated:

To my wonderful travel friends, the group of XXX Cycle PhD students, with whom I have had the opportunity to share this experience. To Silvia, who brought me into her world of laughter and lightheartedness as if we had always known each other; to Giulia who, with her brilliant statements, was able to brighten up the mood on any day; to Antonio, Davide, Giovanna, Laura, Lorenzo, Luca, Sara, Tommaso.

To Mum and Dad, who have always believed in me since I was a little girl; they taught me freedom of thought, love for art, music and poetry, and to face life with courage and determination. I owe every goal I have achieved to them.

To my little brother, Dario, who always inspires me with its unconventional way of seeing life;

To my husband and dance partner, Andrea. I could not have reached this point without his unwavering loving patience, support and encouragement.

PhD is a special journey. Keep calm and enjoy.

Contents

1 Introduction **1**

1.1 General overview of the topic 1
1.2 Motivations 3
1.3 The LCCWD procedure 4
1.4 Main results 6
1.5 Summary of the main contributions 6
1.6 Structure of the thesis 7
1.7 Glossary of common wind engineering terms 8

2 Literature background and main contributions **11**

2.1 Introduction 11
2.2 Life-Cycle Cost Analysis 13
2.2.1 Probability-based and cost-based codes 14
2.2.2 The Performance-Based Design (PBD) approach 15
2.2.3 Formulation of life-cycle cost 19
2.3 LCCA in wind engineering 20
2.4 The structural control in a LCCA perspective 24
2.5 Literature gap 25
2.6 Innovative contributions 26

3 Response of tall buildings to dynamic wind loading **30**

3.1 Introduction 30
3.2 Wind load characterization 32
3.2.1 Wind turbulence 32
3.2.2 Vortex shedding 37
3.3 Dynamic response of wind-excited tall buildings 39

3.3.1 Literature background . . . 39
3.3.2 Frequency-domain response of tall buildings . . . 42
3.3.2.1 Alongwind response . . . 45
3.3.2.2 Acrosswind and torsional response . . . 46
3.4 Wind tunnel tests . . . 46
3.5 Control methodologies for wind-excited tall buildings . . . 49
3.5.1 Tuned Mass Damper . . . 51

4 The proposed Life-Cycle Cost Wind Design (LCCWD) 55
4.1 Introduction . . . 55
4.2 Structural model . . . 58
4.3 Structural control system . . . 59
4.4 Wind hazard model . . . 60
4.4.1 Wind load time histories . . . 60
4.4.2 Joint probability distribution of mean-wind velocity and direction . . . 63
4.5 Structural analysis . . . 63
4.6 Fragility model . . . 66
4.7 Damage analysis . . . 70
4.8 Cost analysis . . . 73
4.9 Alternative design solutions . . . 75
4.9.1 Structural configuration . . . 75
4.9.2 Building orientation . . . 77
4.9.3 Structural control . . . 77
4.9.4 Nonstructural elements: indoor distribution . . . 78
4.10 LCCWD global results . . . 78

5 The case study 79
5.1 Description of the structure and the FE modeling . . . 79
5.2 Characterization of the wind load . . . 85
5.2.1 Wind tunnel records . . . 85
5.2.2 Joint PDF of the mean-wind speed and direction . . . 87
5.2.2.1 PDF of the mean-wind direction . . . 89
5.2.2.2 PDF of the mean-wind annual maximum . . . 89
5.3 Non structural elements . . . 90
5.4 Control systems characteristics . . . 93
5.5 Cost models . . . 95

6 Numerical results **97**
6.1 Introduction . . . 97
6.2 Preliminary design configuration . . . 98
6.2.1 Parametric analysis on building's natural frequencies . . . 100
6.3 Choice of the building orientation . . . 103
6.3.1 Damage probability results . . . 103
6.3.2 Orientation-dependent damage cost accumulation results . . . 104
6.4 Design of the structural control systems . . . 107
6.4.1 Uncontrolled and controlled building response . . . 108
6.4.2 Damage probability results . . . 109
6.4.3 Cost accumulation results . . . 110
6.4.4 Parametric analyses on the variation of the cost model parameters . 111
6.5 Design of nonstructural components . . . 117
6.5.1 Indoor spaces distribution . . . 117
6.6 LCCWD global results . . . 121

7 Conclusions **124**
7.1 Summary of the work . . . 125
7.2 Main outcomes . . . 125
7.3 Future developments . . . 127

List of Figures

1.1 The best design solution is recognized by stakeholders and designers. 3
1.2 LCCWD basic steps. 5

2.1 Schematic representation of the multidisciplinary subject. 12
2.2 Performance-based design diagram (*Design guide for improving School Safety in Earthquakes, Floods and High Winds - Chapter 2*). 16
2.3 PEER performance-based evaluation framework (PEER-TBI 2010). 18
2.4 Performance based wind Engineering scheme (Ciampoli et al. 2011). 21

3.1 World's tallest buildings average heights (*Council on Tall Buildings and Urban Habitat, CTBUH*). 31
3.2 Horizontal wind speed spectrum at Vrookhaven National Laboratory at about 100-m height in synoptic conditions (Hoven 1957). 33
3.3 Principal directions u, v, w of wind velocity and of wind turbulence. 33
3.4 a schematic representation of the mean wind speed of a generic tall building. . . . 34
3.5 Flow around bluff bodies (*Bluff-body aerodynamics*). 38
3.6 Regimes of fluid flow across smooth circular cilinders (Lienhard 1996). 40
3.7 Tridimensional view of a generic tall building with the indication of alongwind, acrosswind and torsional response. 41
3.8 Davenports wind load chain (Davenport 1964). 42
3.9 An example of an experimental set up in a boundery layer wind tunnel (*Azioni ed effetti del vento su edifici alti*). 47
3.10 Wind tunnel test: a) An example of force balance (*Azioni ed effetti del vento su edifici alti*), b) Wind tunnel blades (courtesy of Prof. I. Venanzi), c) pressure taps on scaled models (courtesy of Prof. I. Venanzi). 48
3.11 Means to suppress wind-induced response of buildings (Kareem et al. 1999). . . . 50

3.12 A schematic representation of a system equipped with a TMD (*Tuned Mass Damper Applet*). 51
3.13 Amplification factor as a function of $\beta = 0.05, \alpha = 1$ (Constantinou et al. 1998). . 53
3.14 Optimum absorbers parameters (Warburton 1982). 54

4.1 Outline of the LCCWD procedure. 56
4.2 Design alternatives flowchart. 57
4.3 Schematic view of the tall building denoting: (a) building orientation angle δ, relative mean-wind incidence angle θ; (b) torsional rotation ψ. 59
4.4 World's 100 tallest classified by function (*Council on Tall Buildings and Urban Habitat, CTBUH*). 67

5.1 Schematic view of the 60-stories building. 80
5.2 Schematic view along the height of the central core in the two main directions. . . 81
5.3 3D-view of the 60-story building. 83
5.4 Discrete-mode (FEM) vs continuous power-law function vibrations modes: a) flexural mode in direction x, b) flexural mode in direction y, c) torsional mode. 84
5.5 Pressure taps location (measures in cm). 85
5.6 Wind tunnel set-up, suburban terrain. 86
5.7 i^{th} Pressure coefficient map corresponding to a wind tunnel realization and $\theta = 0°$. 86
5.8 A realization of the generalized force spectrum [Eq. (4.7)], experimentally measured for $(\theta + \delta) = 0°$. 87
5.9 Reduced torque spectrum. 88
5.10 Empirical marginal distribution of the mean-wind direction derived from the database. The angles are measured from the North direction. 89
5.11 3-second gust wind-speed (in miles per hour) at 10 m above ground for Exposure category C and for different return periods ASCE7-16 (2017). 91
5.12 Probability density function of the mean-wind speed annual maxima (10-minute averaging time) at the reference elevation, $f(V_{ref})$ for the city of Boston. 92
5.13 Partition walls fragility curve as a function of *IDR* (a); Glass façade fragility curve as a function of *IDR* (b); Suspended ceiling fragility curve as a function of a (c). . 93
5.14 Schematic plan view of the building considering the torsional rotation ψ with the indication of torque-induced displacements along each side (a), reference and border perimeters (b). 94
5.15 Plan view with selected locations of the partition walls (a), and the suspended ceilings (b). 94

5.16 An example of a PACT graph showing upper and lower bound repair cost data. 96

6.1 $f(EDP, V_{ref,\theta})$ for direction x in the case of $(\theta + \delta = 0°)$: a) $f[EDP|V_{ref} = \{40\}$ m/s] and partition walls fragility curve; b) numerical PDF, $f[EDP|V_{ref} = 40$ m/s], vs. experimental points. 99

6.2 Peak top floor IDR (a) and a (b) for directions x, y (local coordinate system) with $V_{ref} = 40$ m/s, as a function of the relative mean-wind incidence angle $(0° \leq \theta < 360°)$. 99

6.3 Structural response as a function of the floor height (z): (a) glass façades (IDR_{gf}) and (b) partition walls (IDR_{pw}) for directions x, y (local coordinate system) and (c) suspended ceilings (acc_{sc}) with $V_{ref} = 40$ m/s and building orientation $\theta + \delta = 0°$ (wind that blows from the North). 100

6.4 Peak top floor IDR for directions x (a) and y (b) as a function of α_n and V_{ref}. . . 101

6.5 Peak top floor a with respect to α_n and V_{ref} a), Peak top floor a by varying α_n for: $V_{ref} = 30m/s$ b), $V_{ref} = 35m/s$ c), $V_{ref} = 40m/s$ d). 102

6.6 Top floor annual damage probability P_j associated with $V_{ref} = 40$ m/s as a function of α_n: (a) partition walls (x,y direction); (b) glass façades (x,y direction); (c) suspended ceilings. 103

6.7 Top floor annual damage probability P_j associated to each unit element with $V_{ref} = 40$ m/s as a function of the relative mean-wind incidence angle $0° \leq \theta < 360°$: (a) glass façades (curtain walls) for direction x (face B) and direction y (face A);(b) partition walls for direction x (face $\hat{B}$) and direction y (face $\hat{A}$); (c) suspended ceilings. 104

6.8 Top floor annual damage probability for glass façades (a), partition walls (b) for direction x and direction y and suspended ceilings (c) as a function of the building orientation angle δ. 105

6.9 Expected value of the life-cycle cost as a function of the building orientation δ for $t = 50$ years, along the two principal axes: (a) galss façades ;(b) partition walls; (c) suspended ceilings. 106

6.10 Expected total life-cycle cost, normalized according to Equation (4.39), as a function of the building orientation angle δ and for various lifetimes t (years). 107

6.11 3D plot of the expected total life-cycle cost, normalized according to Equation (4.39), as a function of the building orientation angle δ and for various lifetimes t (years) 108

6.12 Top floor peak response (x-displacements, y-displacements, acceleration) obtained for $i = 1$, $V_{ref} = 40\ m/s$ (at full scale) mean-wind incidence angle $\theta = 0°$ and building orientation 90°, normalized with respect to the uncontrolled case. 109
6.13 Annual damage probability as a function of the floor height (z): a) partition walls (x direction); b) partition walls (y direction). 110
6.14 Annual damage probability as a function of the floor height (z): a) glass façades (x direction); b) glass façades (y direction); c) suspended ceilings. 111
6.15 Comparison between the expected values of the total life-cycle cost, accounting for wind-induced damage and intervention/repair cost, with and without TMDs: a) TMDs installed at $t = 0$ years; b) TMDs installed $t = 10$ years after building construction/opening. 112
6.16 Total normalized lifetime cost, accounting for wind-induced damage and intervention/repair cost, for different values of $c_{0,cs} = C_{0,cs}/C_{0,s}$. 113
6.17 Break-even time (BET) as a function of the initial normalized cost of the TMDs, $c_{0,cs} = C_{0,cs}/C_{0,s}$. 114
6.18 Peak top floor IDR for directions x (a) and y (b) and peak top floor a (c) with respect to μ ($V_{ref} = 40$ m/s). 115
6.19 Top floor annual damage probability for partition walls (a), glass façades (b) for directions x and y and suspendend ceilings (c). 115
6.20 Total normalized lifetime investment costs, accounting for wind-induced damage and intervention/repair cost, for different values of μ. 116
6.21 Group 1 internal nonstructural components distribution (G_1). 118
6.22 Group 2 internal nonstructural components distribution (G_2). 118
6.23 Group 3 internal nonstructural components distribution (G_3). 119
6.24 Total normalized lifetime expected costs, accounting for the two different configurations of non structural elements (A,B) with respect to the initial one. 120
6.25 Comparison between the expected values of the total investment cost, accounting for wind-induced damage and intervention/repair cost, with and without TMD: a) $c_{0,cs} = 0.002$, b) $c_{0,cs} = 0.002, 0.01, 0.02$. 121
6.26 LCCWD Global results: total normalized life-cycle costs, accounting for different design alternatives. 123

List of Tables

3.1 Sir. Francis Beaufort (1805) wind scale 31

4.1 Drift ratios used to define median values of damage for nonstructural drift-sensitive components (Hazus 2017). 69
4.2 Peak floor accelerations used to define median values of damage for non-structural acceleration-sensitive components (Hazus 2017). 69

5.1 Geometrical characteristics of the columns. 82
5.2 Geometrical characteristics of the diagonal cross-bracing. 82
5.3 Geometrical characteristics of the I-beams. 82
5.4 Modal characteristics of the simplified dynamic model of the building and coefficients of the power-law function mode shapes 84
5.5 Number of units and normalized unit costs for non-structural elements . . . 96
5.6 Parameters adopted for the cost analysis 96

6.1 TMD parameters by varying the mass ratio μ 114
6.2 Total normalized investment cost as a function of the discount rate λ for different lifetimes (*note*: t_{10}, ten years; t_{50}, fifty years; t_{100}, one hundred years). 116
6.3 Total normalized life-cycle cost disaggregation for $t = 50$ years (*note*: $c_{pw,x}$, partition walls in x direction; $c_{pw,y}$, partition walls in y direction; c_{sc}, suspended ceilings). 117
6.4 Nonstructural components number of units 119

List of Symbols

$\alpha = \omega/\omega_0$ Frequency ratio of a sinusoidal force

α_n Foundamental frequencies percentage of variation

$\beta = \omega_{\text{TMD}}/\omega_0$ Frequency ratio

δ Building orientation angle

δ_{gr} Gradient height

ϵ Torque spectrum correction factor

γ_k Exponential coefficient of the mode shape power law

$\hat{n}_j(z)$ Number of units of nonstructural elements

κ Von Karman constant

λ Discount rate per year

μ TMD mass ratio

ν Mean arrival rate per unit time (i.e., number of events per year)

ω_0 Natural frequency of the structural system

ω_{TMD} Natural frequency of the TMD

$\Phi_k(z)$ k-th mode shape

ψ Torsional rotation

τ Time lag

θ Mean-wind incidence angle

$\tilde{\mu}$ Air dynamic viscosity

$\tilde{\nu}$ Air kinematic viscosity

$\tilde{c}$ Damping of a generic degree of freedom

$\tilde{k}$ Stiffness of a generic degree of freedom

$\tilde{m}$ Mass per unit length of a generic degree of freedom

ξ Structural damping ratio

ξ_{TMD} Damping ratio of TMD

a Acceleration

$a_i(z)$ Peak acceleration at a generic floor

B Reference lateral shorter dimension of the structure

C_p Pressure coefficient

$C_{0,cs}$ Initial cost of the TMD

$c_{0,cs}$ Normalized initial cost of the TMD

$C_{0,s}$ Initial cost of the building (without the TMD)

C_0 Initial construction cost

c_{TMD} Damping coefficient of TMD

$c_{cs}(t,\delta)$ Total expected lifetime repair/maintenance cost

C_j Unit replacement/repair cost of the selected nonstructural element

c_j Normalized unit replacement/repair cost of the selected nonstructural element

cs Control system

D Reference lateral longer dimension of the structure

$D_{i,x}(z)$ Peak displacement in x direction at a generic floor

$D_{i,y}(z)$ Peak displacement in y direction at a generic floor

DS Damage state

$E[.]$ Expected value

EDP Engineering demand parameters

$f(\cdot)$ Probability density function (PDF) of the $\cdot$ variable

$f_{i,k}(z,t)$ Realization of the experimental aerodynamic force per unit height

$F_{Q_{i,k}}(t)$ Generalized lateral force

$G(\cdot)$ Complementary cumulative distribution function of the $\cdot$ variable (Chapter 2)

$g_{i,k}$ Peak factor

$g^a_{i,k}$ Acceleration-related peak factor

H Reference height of the structure

h h^{th} direction: x,y,

$H_{i,k}(n)$ Admittance function

i i^{th} realization of the generalized force

IDR Interstory drift ratio

IM Intensity measure

IP Interaction parameter

j j^{th} damage state

k k^{th} direction: x,y,ψ

L Total number of loading occurrences

l Loading occurrence number

m_{TMD} Mass of TMD

M_k k^{th} modal generalized mass

N Total number of realizations of the generalized force

n Frequency

$n_{0,k}$ k^{th} modal natural frequency

$P(\cdot)$ Complementary cumulative distribution function of the $\cdot$ variable (Chapter 4)

P_j^k Annual damage probability in the k direction associated with limit state j

R_e Reynolds number

RMS Root Mean Square

$S_{Q_{i,k}}(n)$ Response power spectral density

$S_{F_{Q_{i,k}}}(n)$ Power spectral density of the i^{th} experimental realization of the generalized force in the k direction

SP Structural parameter

t Time

t_l Loading occurrence time for the Poisson process

u_* Friction velocity

V_{gr} Gradient velocity

V_{ref} Reference value of the mean-wind speed (ten-minute average) at the roof height

X, Y Horizontal global axes

x, y Horizontal local axes

z Vertical axis

CCDF Complementary cumulative distribution function

DC Design configuration

LCCA Life-cycle cost analysis

LCCWD Life-cycle cost wind design

PBD Performance Based Design

PBWE Performance Based Wind Engineering

PEER Pacific Earthquake Engineering Research Center

SDOF Single degree of freedom

TMD Tuned mass damper

Chapter 1

Introduction

1.1 General overview of the topic

In this thesis a life-cycle cost analysis (LCCA) procedure is proposed as a practical design approach for wind-sensitive structures, aimed at predicting monetary losses over the structure lifetime. The general formulation of the LCCA (see Section 2.2), based on performance-based design (PBD), examines the suitableness of a structure or its design by considering a set of performance criteria on the basis of key Decision Variables (DV) in a probabilistic setting. As an example the annual losses due to the overcoming of one or more established limit states can be considered as a DV in the design procedure. LCCA is based on the evaluation of the sum of the initial construction costs and the lifetime expenses, according to a certain level of the performance requested.
In this context, the following main research question needs to be answered:

- *it is possible to develop a life-cycle cost-based design method specific for tall buildings that responds to the needs of designer and stakeholders in terms of decision-making quantities that can be understood by both?*

Moreover, in order to tailor the design methodology to wind-excited tall buildings a subquestion is also formulated:

- *how to account for all the uncertainties involved in the design process of tall buildings under wind load with an acceptable computational effort?*

In order to get answer to these questions, the challenge of this study is the development of a modern life-cycle cost-based approach for the wind-resistant design of tall buildings by considering all the types of uncertainties involved in the problem: those related to the stochastic nature of the wind speed and direction, to the aerodynamic model, to the structural properties and to the damage model.
With this aim, an automated procedure named Life-Cycle Cost Wind Design (LCCWD) is proposed. The acronym LCCWD emphasizes the peculiar features of the procedure:

- it estimates the life-cycle cost (LCC) of the building;
- it is specific for tall buildings under wind load (W);
- it is a practical design approach (D), effective in comparing different design alternatives.

Since LCCA has evolved recently from earthquake engineering, the basic LCCA methodology is consequently adapted in LCCWD in order to account for the different typology of natural hazard and for the related damages. For example in tall slender buildings, damage is mainly non-structural and it can affect façades, partition walls, installations or ceilings. Only in the case of occurrence of very strong wind events like tornadoes, the structure can experience structural damage and collapse of structural members.
One of the advantages of the use of the LCCWD procedure is that appropriate considerations during the first phase of the design can avoid unexpected problems during the building's lifetime. Another advantage, as schematically represented in Figure 1.1, is that a cost-based ($) approach can broaden the perspective of managers and stakeholders by including all the aspects related to the structure lifetime. Hence LCCWD tries to reconcile two opposing needs: to optimize the invested capital cost (stakeholder) while maintaining a selected performance level over time (designer). Therefore several phases are necessary for the application of the LCCWD:

1. define the type of choice and goals;
2. define the project and the alternatives;
3. establish the design lifetime that is the time in which costs and benefits linked to a certain investment have affected the interests of the investor who has to make the decision;

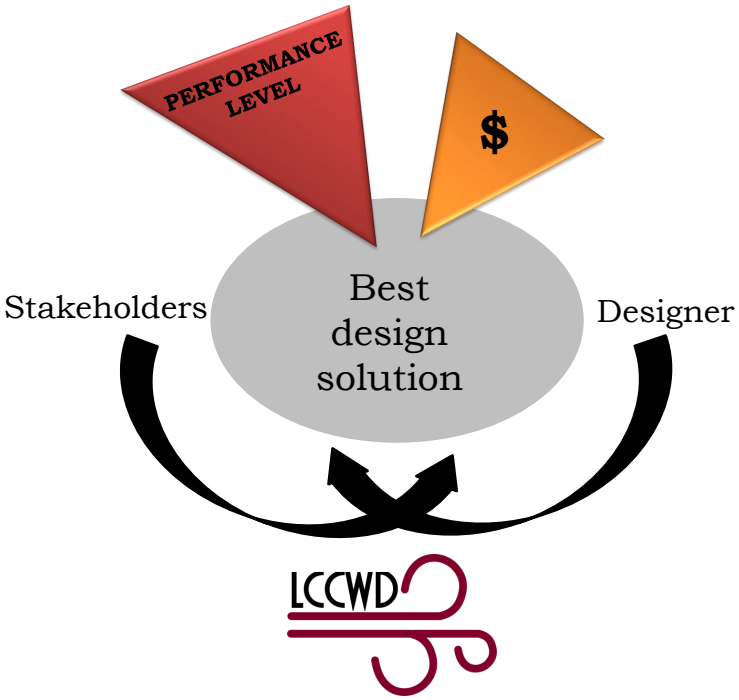

Fig. 1.1: The best design solution is recognized by stakeholders and designers.

4. identify the relevant costs and parameters for the comparison of the different alternatives.

Following each decision step it is possible to accept or to reject design alternatives and select optimal and technically valid systems (for example the type of construction for structural and nonstructural elements) or to decide among different structural control systems that meet specific technical performance.

1.2 Motivations

- Scientific motivation.
  Nowadays, a general trend is being established in design practice towards progressively taller and lightly damped structures, with a consequent increase of the sensitivity to wind loads. In particular, modern tall buildings can experience significant wind-induced vibrations causing serviceability limit states crossing, non structural damages and discomfort to occupants. Since many uncertainties are involved in the design process, a traditional deterministic approach turns out to be inaccurate. Suitable and effective design techniques need to be available to engineers in order to achieve the best solution, according to pre-established performance targets.

On the one hand, in the case of the seismic design, probabilistic methods are widely used and deeply treated in literature with the possibility of establishing different performance objectives. On the other hand, performance-based methods are currently not completely embraced in wind engineering and nowadays probabilistic theories based on the PBD for the design of wind-sensitive structures represent an interesting open issue.

- Economic motivation.
  The overall cost of a durable building construction is represented by the initial cost as well as the expenses for the utilization during its lifetime. In particular, the economic aspect associated with the damage to nonstructural elements under serviceability conditions, is today largely underestimated.
  The estimation of the global cost can help decision-makers in choosing about the opportunity to invest in the structure, considering the phases of design, construction, and management of the building. An effective global design approach which shows the least long-term cost is a difficult achievement to obtain. As a matter of fact there are typical problems and conflicts of interest. As well as the performances requested from reliability engineering, the capital outlay can influence the design choices given a number of alternatives from which to select, since it is usually clearly defined. This last aspect can be considered in opposition to the criteria of the minimum maintenance and repair cost. With different solutions it is possible to optimize operational and maintenance costs over time and preserve future financial resources.

1.3 The LCCWD procedure

LCCWD consists of several steps, from preliminary design to cost evaluation. As schematically reported in Fig. 1.2, the outline of the procedure can be summarized as follows:

1. *Preliminary design configuration.* Depending on the customer requirements, on the constraints imposed by the neighboring buildings and on the main characteristics of the site, it is firstly necessary the development of a preliminary design of the structure (structural elements, shape of the building, materials and so on). This phase is necessary and needs to be carefully developed as the building's characteristics influence the subsequent stages of the analysis and they are an important source of expenses.

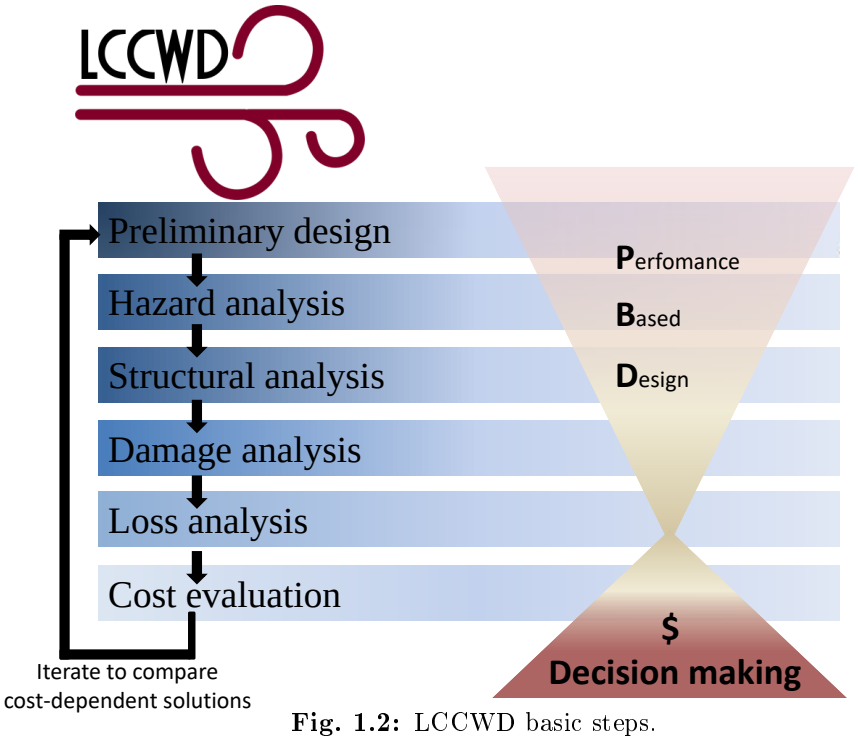

Fig. 1.2: LCCWD basic steps.

2. *Hazard analysis.* In order to consider the realistic uncertainty related to wind load characterization it is necessary to carry out experimental wind tunnel tests in a reduced scale-model reproducing the exact geometry of the building. The possibility of exploring different values of the wind speed and different wind directions allows to include in the analyses the inherent stochastic nature of the wind hazard.

3. *Structural analysis.* The structural response is evaluated in terms of peak displacements and accelerations for each specific wind hazard combination (wind speed intensity and wind direction).

4. *Damage analysis.* As the first stage of the damage analysis, it is necessary to select the most sensitive elements susceptible to the damage. Under the actions of moderate winds, i.e., serviceability conditions, the damage can mostly pertain to non structural elements (partitions, equipment, contents, etc...). The damage analysis is in probabilistic terms and depends on the fragility information on the element type.

5. *Loss analysis.* Once the damage analysis is completed it is possible to evaluate the losses over time of the building in terms of damage probability according to the PEER (Performance Earthquake Engineering Research) approach. The probability of damage can be associated with a certain level of performance.

6. *Cost evaluation.* All the above steps allow the calculation of the expected life-cycle cost including initial costs, operating costs (cost of failures, repair cost, downtime cost) and maintenance costs. With the aim of minimizing or optimizing the cost over time, steps 1 to 6 are repeated and different design cost-based scenarios are analyzed and compared for a specific class of buildings.

The LCCWD procedure is deeply investigated in Chapter 4.

1.4 Main results

The main result of the research is the LCCWD methodology that offers an enhanced approach to the design of tall buildings, combining the needs of designers and investors. The effectiveness of the LCCWD has been demonstrated by the numerical simulations on a benchmark tall building by exploring different design solutions. Wind loads are evaluated from experimental wind tunnel tests. Several configurations are compared and results show the optimal design arrangement corresponding to the best cost-saving scenario.
Results obtained are clearly understandable with a cohesive representation for both technical and nontechnical audience.
Results can be divided into two groups:

1. Intermediate results
   Considering the complexity of the LCCWD procedure, results are presented with intermediate step by step explanations. The basic idea is that the procedure can be easily reproduced and implemented in large scale for different applications.

2. The LLCWD global results
   This part of the results intend to explain the LCCWD in a nontechnical language with the aim to link the best economic design solution to specific engineering aspects and the related achievable performance levels with comparative costs to reach these levels. A global chart is proposed to compare the different solutions proposed.

1.5 Summary of the main contributions

LCCWD approach provides an automated tool that is easily adaptable to specific real applications in order to achieve a design that simultaneously accounts for the needs of customers and designers. The main features and novel contributions with respect to the

existing literature on LCCA are deeply investigated in Chapter 2 and introduced as follows. Various design aspects are included in the project such as:

- the capability of accounting for structural control systems in the damage probability estimation and cost assessment;
- the effect of the wind directionality and the building orientation at a specific site;
- the design of outdoor and indoor distribution of non nonstructural elements.

LCCWD procedure accounts for the main sources of uncertainties:

- the wind load modeling;
- the structural modeling;
- the fragility models (related to the damage assessment of nonstructural elements).

The uncertainty associated with the aerodynamic load estimation and the structural model is efficiently taken into account by parsing the experimentally measured generalized wind forces (Section 4.4.1).
For the characterization of nonstructural wind-induced damages, the proposed LCCWD emphasizes the need for considering probabilistic experimental models.

1.6 Structure of the thesis

This thesis consists in 6 chapters and final conclusions. The main contents of each chapter is summarized as follows:

- **Chapter** 1
  A general overview of the topic is presented and the motivations that make the topic an interesting research area are highlighted. The basic concepts and the main novelty associated with LCCWD are briefly introduced.
- **Chapter** 2
  A literature overview about LCCA for tall buildings is developed, highlighting the differences with the seismic LCCA. In this chapter it is also introduced the concept of structural control in a LCCA perspective. The LCCWD main novel contributions with respect to the existing literature are highlighted.

- **Chapter** 3
  The basic concepts on the characterization of the dynamic response of tall buildings under wind loads are explored. The last part of the chapter is devoted to briefly introduce the currently used control methodologies for wind-sensitive structures.
- **Chapter** 4
  The proposed wind-related LCCWD is deeply investigated with step by step explanations.
- **Chapter** 5
  The case study is described. Accurate indications are given about: the structural FE modeling, the characterization of the wind load, the control system characteristics and the adopted cost models.
- **Chapter** 6
  Numerical results are carried out in terms of structural response, damage probability and life-cycle cost. Different cost-effective design solutions are analyzed and compared.
- **Chapter** 7
  This part collects conclusions of the thesis.

1.7 Glossary of common wind engineering terms

A glossary of common wind engineering terms is defined as follows (Holmes 2007; Simiu and Scanlan 1996):

Aerodynamic damping Aerodynamic forces proportional to the velocity of a structure, and additional to (or subtractional from) the structural damping.

Aerodynamics The study of the motion of air and its interaction with a solid object.

Aeroelasticity The study of the interactions among inertial, elastic and aerodynamic forces.

Atmospheric boundary layer The lowest layer of air in the troposphere which is about one km thick and forms the layer where the ground surface (land or sea) influences the behavior of the atmospheric flows.

Bluff body Body with a large frontal dimension, from which the airflow separates.

Background response That part of dynamic response to wind excluding the effects of resonant amplifications.

Boundary layer Region of reduced air velocities near the ground or the surface of a body.

Correlation Statistical relationship between two fluctuating random variables.

Gradient wind Upper level wind that can be calculated from the gradient wind equation

Gust factor Ratio of expected maximum to mean value of wind speed, pressure or force.

Gust response factor Ratio of expected maximum to mean structural response.

Lock-in The enhancement of fluctuating forces produced by vortex shedding due to the motion of the vibrating body.

Logarithmic law A mathematical representation of the profile of mean velocity with height in the lower part of the atmospheric boundary layer.

Mean-wind speed The average speed of wind flow expressed with a variety of averaging times: fastest mile, three-second gust, one minute mean velocity, and mean hourly velocity, typically measured at 10 m height.

Mechanical admittance Transfer function relating the spectral density of aerodynamic forces to the spectral density of structural response

Peak factor Ratio of maximum minus mean value, to standard deviation, for wind velocity, pressure, force or response.

Pressure coefficient Surface pressure made non-dimensional by the dynamic pressure in the wind flow.

Quasi-steady A model of wind loading that assumes that wind pressures on buildings fluctuate directly with the fluctuations in wind speed immediately upstream.

Resonant Response A result of the turbulent component of the wind velocity, whose frequencies coincide with the natural frequencies of the structure.

Return period Inverse of probability of exceedence of an extreme value.

Reynolds number Ratio of inertial forces to viscous forces in fluid flow.

Roughness length A measure of the aerodynamic roughness of a surface, which affects the boundary-layer flow over

Spectral density A measure of the contribution to a fluctuating quantity (e.g. wind velocity, wind pressure, deflection) within a defined frequency bandwidth.

Stationary Description of a random process whose statistical properties do not change with time.

Strouhal number Non-dimensional vortex-shedding frequency.

Turbulence Fluctuations in fluid flow. In meteorology and wind engineering the term *gustiness* is also used.

Vortex shedding The periodic shedding of eddies formed from the rolling-up of the boundary shed from a bluff body.

Wake The area of low velocity and turbulent flow in the region downstream of a body.

Wind Motion of air with respect to the Earth's surface.

Wind tunnel boundary layer It is a testing section with flow characteristics that mimics a target full-scale boundary layer used in aerodynamic research to study the effects of wind on the built environment.

Chapter 2

Literature background and main contributions

2.1 Introduction

Life cycle cost analysis (LCCA) is a type of approach aimed at evaluating the total lifetime costs of a structure related to construction, maintenance, repair and disposal. It is used in many research fields and it can be considered as a multidisciplinary subject. In the context of the structural design, the LCCA embraces:

- the evaluation of the damage probability, adopting Performance-Based Design (PBD) approach, devoted to the fulfillment of selected performance levels in a probabilistic context;
- the analysis in terms of cost which associates a monetary value to the achievement of the prefixed performance target.

With reference to Figure 2.1 (top left), LCCA can be considered as the conjunction of PBD and the cost analysis, a design approach widely used in seismic engineering.
Recently, the PBD principles have been extended from the seismic field to wind engineer-

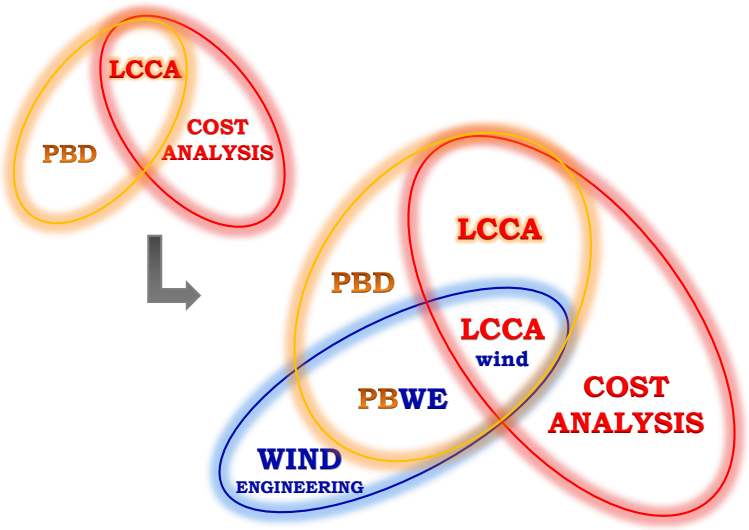

Fig. 2.1: Schematic representation of the multidisciplinary subject.

ing (blue line in Figure 2.1) and the discipline of Performance-Based Wind Engineering (PBWE) is emerging. Moreover when the PBWE joins up the basic concepts of the cost analysis, LCCA is specialized for wind-sensitive structures.
In this context, the project focuses on the application of the LCCA in wind engineering with the aim to use it as a design tool for tall buildings that enables comparison between alternative design options, eventually including structural control systems. The design approach is named LCCWD (Section 1.1).
With the main objective of framing the problem by identifying the major research trends, the chapter is organized as follows:
Section 2.2 introduces the LCCA in the context of earthquake engineering by exploring the literature background with reference to the basic PBD theory.
Section 2.3 treats the PBWE underlining the main differences with respect to the seismic approach and presents a literature background on LCCA for wind-excited structures.
Section 2.4 shows some literature references in which the optimization of the building's control systems is carried out exploiting a life-cycle approach.
Section 2.5 illustrates the literature gap in the field of LCCA for wind-excited structures.
Section 2.6 highlights the main improvements of LCCWD approach with respect to the existing literature.

2.2 Life-Cycle Cost Analysis

The LCCA is a probabilistic approach that has been recently considered in the structural design and it is a well established procedure in earthquake engineering. The LCCA computes, in a probabilistic setting, the total lifetime cost of a specific design solution, accounting for initial costs, repair and maintenance costs, downtime costs, disposal costs and all the possible sources of cost that a structure encounters during its life-cycle.
The main goal of a LCCA approach is not reaching a certain performance level but maintaining it in time by considering materials' deterioration, damage of structural and non-structural elements, by performing consequent maintenance and repair interventions during the lifetime of a building.
In recent years, since probabilistic approaches are replacing deterministic methodologies, the LCCA is becoming a valid design tool as it allows accounting for the effects of uncertainties involved in the design such as uncertainty in the wind load characterization, in the structural and aerodynamic properties and in the damage occurrence (Mitropoulou et al. 2011). The early applications of the LCCA design approach go back to 1980s in USA and are devoted to the optimization of ownership over the life span of an asset, as reported in Arditi and Messiah (1996).
The basic theory of LCCA is presented in Wen and Kang (2001) where an analytic formulation is proposed in order to evaluate expected total life-cycle cost (see Section 2.2.3). In order to account for structural deterioration, structural and nonstructural damage, maintenance and repair losses, many contributions have been given in the last decade for developing different loss estimation models (Liu et al. 2004; Aslani and Miranda 2004; Mitropoulou et al. 2011).
LCCA is often used in conjunction with optimization methods, with the aim of minimizing the expected life-cycle cost (Frangopol and Maute 2003; Liu et al. 2004; Kaveh et al. 2014; Barone and Frangopol 2014). In this framework the LCCA is considered as an integrated aspect in the structural design procedure to reach a preselected structural performance (Lagaros 2007). For example, in Liu et al. (2004), Lagaros (2013), and Lagaros and Karlaftis (2016), the construction cost is used as an objective function for the structural design optimization of steel structures.
Yamin et al. (2017) proposes a methodology for the evaluation of the seismic vulnerability of a specific site in terms of monetary losses. Different levels of structural performance can be related to multiple earthquake hazard levels (Mitropoulou et al. 2015).
In Pandey and Weide (2017) the LCCA basic theory is adjusted to take into account re-

newal processes.
Many applications of LCCA are devoted to comparing different retrofitting solutions and planning maintenance schemes in existing bridges (Padgett et al. 2010; Okasha and Frangopol 2011; Wang et al. 2015).
In Liu and Boaxia (2017) the LCCA method is presented to evaluate the long-term cost-effectiveness of energy-efficient buildings.

2.2.1 Probability-based and cost-based codes

Since the early 1970, a number of probability-based codes and standards were internationally developed. With the aim to give an ideal temporal evolution, some references are reported in the following list:

- *SEAOC Vision 2000* (Vision 1995) formulated by the Structural Engineers Association of California, gives detailed discussions of performance-based approaches considering the design, construction and maintenance of buildings.
- *Standard Practice for Measuring Life-Cycle Costs of Buildings and Building Systems* (ASTM/E917-02 2002) published by the American Society for Testing and Materials represents the standard industry procedure for analyzing life-cycle costs;
- FEMA (Federal Emergency Management Agency) standards: *Performance-Based Seismic Design of Buildings – An Action Plan for Future Studies* (FEMA-283 1996); *Action Plan for Performance-based Seismic Design* (FEMA-349 2000); *Guidelines for Seismic Rehabilitation of Buildings* (FEMA-356 2000);
- *Next-Generation Performance Based Seismic Design Guidelines* (FEMA-445 2006) developed according to the Program Plan for New and Existing Buildings which is a program addressed to engineers and designers to better work with stakeholders in identifying the probable seismic performance of new and existing buildings. The programs, as a collaboration project between the FEMA and the Applied Technology Council (ATC), begun in 2001 and develops the general approach outlined in the FEMA Action plan (FEMA-349 2000);
- *Buildings and constructed assets* (ISO-15686 2017). This international standard, divided in 10 parts, provides an in-depth guide to life-cycle costing.

- *Minimum Design Loads for Buildings and Other Structures* (ASCE6/7-10 2010). In the commentary of current codes was introduced the concept of risk of structural failure or collapse;
- *Seismic Performance Assessment of Building 1,2,3* (FEMA-P-58 2012b; FEMA-P-58 2012c; FEMA-P-58 2012d) and the electronic *Performance Assessment Calculation Tool* (FEMA-P-58 2012a). These three volumes and the electronic calculation tool are the product of the 10-years work developed in the program plan with the collaboration of FEMA and ATC. These codes offer a methodology for the seismic performance assessment with a large number of examples in a logical format.

It is worth noticing that the previous list is focused on the American standards and on the International Organization for Standardization (ISO) but it should be noted that life-cycle approach is spreading in the worldwide codes.

2.2.2 The Performance-Based Design (PBD) approach

In all the methods briefly reviewed above, the monetary loss assessment is related to the estimation of the damage probability carried out in the context of the PBD approach.
This method is capable of taking into account the uncertainties related to the hazard event occurrence, the actual response of building systems and the potential effects of the performance of these systems on the correct functionality. The achievement of certain pre-established performance levels becomes therefore a key issue in the structural design process.
Figure 2.2 illustrates the iterative design process which involves the following key steps (*Design guide for improving School Safety in Earthquakes, Floods and High Winds - Chapter 2*):

- Selection of *performance objectives* (ultimate limit states or service limit states thresholds considering structural or nonstructural damages with the derived economic losses);
- Development of *preliminary design*;
- Evaluation of the *performance capability*;
- Comparison between the *performance level obtained and the preselected one*;
- Review of the initial design up to *convergence*.

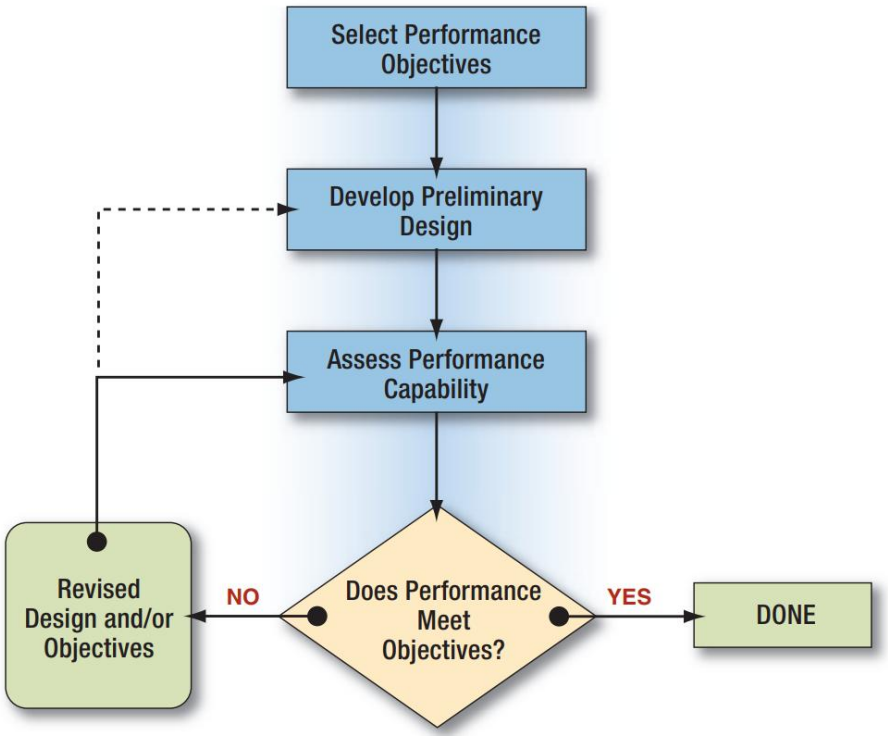

Fig. 2.2: Performance-based design diagram (*Design guide for improving School Safety in Earthquakes, Floods and High Winds - Chapter 2*).

The assessment of the performance is based on the *Pacific Earthquake Engineering Research* (PEER) equation, which allows computing the probability of exceeding a pre-defined damage threshold. Once the failure probability is obtained, the related economic losses can be computed (Kunnath 2006; PEER-TBI 2010; Ramirez et al. 2012; Ramirez and Miranda 2012). This procedure allows to take into account several uncertainty sources in the load, structural and damage models.
The PEER equation, is based on the total probability theorem (Cornell and Krawinkler 2000; Kunnath 2006; PEER-TBI 2010). The total probability theorem, given the events $A, E_1, ..., E_N$ can be summarized by the following equation:

$$P(A) = \sum_{i=1}^{N} P(A|E_i)P(E_i) \tag{2.1}$$

where E_i are mutually exclusive events. Equation (2.1) means that the knowledge of the conditional probabilities $P(A|E_i)$ and of the singular probabilities $P(E_i)$ enables the computation of the unconditional probability $P(A)$. Considering a distributed random variables x, Equation 2.1 can be used to evaluate the (complementary cumulative distribution function) CCDF of the continuous x:

$$\text{CCDF}(x) = \int_{-\infty}^{+\infty} \text{CCDF}(x|y)f(y)dy \tag{2.2}$$

where $\text{CCDF}(x|y)$ is the CCDF of x given a certain outcome of a continuous variable y.
As shown in Figure 2.3, the PEER-based approach can be divided into the following steps:

1. *hazard analysis*, for the load characterization;
2. *structural analysis*, for the evaluation of the structural response;
3. *damage analysis*, to relate the structural response to the probability of damage;
4. *loss analysis*, to relate the damage to the associated life-cycle cost.

The application of the methodology requires the evaluation and the choice of the following parameters (PEER-TBI 2010):

- *Intensity Measure* (IM) which represents a measure of the seismic intensity useful to be used for the subsequent steps. It could be defined in terms of peak ground acceleration, spectral acceleration and magnitude;

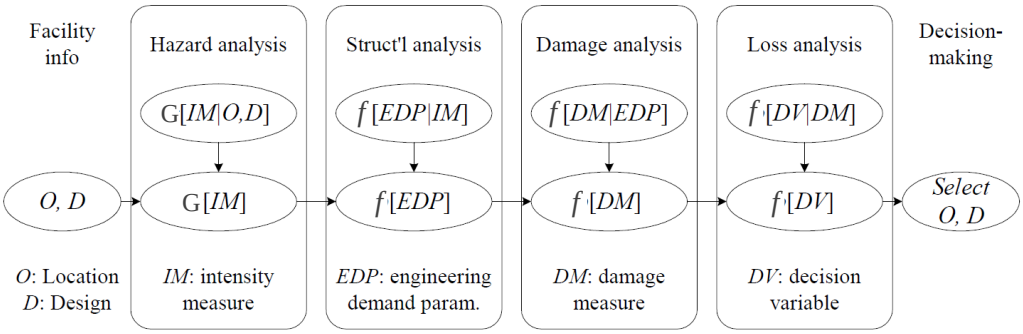

Fig. 2.3: PEER performance-based evaluation framework (PEER-TBI 2010).

- *Engineering Demand Parameters* ($EDPs$) which represent a limited set of variables that characterize the structural response (displacements, accelerations, stresses and so on). These variables need to be correlated to a damage state and to a performance level. The measure of interest is the conditional probability $f(EDP|IM)$;
- *Damage Measures* (DMs) which represent the connection between EDP and the damage. Usually DMs are expressed in terms of fragility functions $f(DM|EDP)$ (Section 4.6);
- *Decision Variables* (DVs). An example of DVs are the expected annual economic loss, mean annual frequency of collapse, fatalities, repair duration or injuries which are correlated with DMs.

Note that IM, EDP, DM and DV can potentially also be vectors.
Considering Equation (2.2), the total probability theorem can be used to evaluate the CCDF of a DV. In principle, as highlighted in Figure 2.3, DV depends on the state of the structure as characterized by a set of damage measures (DMs). Moreover DMs depend on $EDPs$ which in turn depend on IM. Therefore, in general it is possible to write $DV(DM(EDP(IM)))$. In probabilistic terms, the previous relation means that three conditional probabilities $DV|DM$, $DM|EDP$ and $EDP|IM$ need to be evaluated.
Hence, the CCDF of DV, i.e. $G(DV)$, according to Equation (2.2), can be evaluated with a triple integral:

$$G(DV) = \int\int\int G(DV|DM)\,|f(DM|EDP)|\,|f(EDP|IM)|\,f(IM)\mathrm{d}IM\mathrm{d}EDP\mathrm{d}DM \tag{2.3}$$

where $f(\cdot)$ is the probability density function.

2.2.3 Formulation of life-cycle cost

The LCCA allows to determine the global cost of a structure, considering its entire lifetime. The global cost of a structure is the sum of the initial construction costs and all the expenses that are encountered during the lifetime. Typical LCC analyses are therefore based on (*Life Cycle Costing*):

- investment costs and all the associated costs such as installation, design expenses;
- operating costs, including utility costs, disposal costs and maintenance costs;
- end-of-life costs such as removal, recycling or refurbishment.

The estimation of the global cost is aimed at assisting decision makers in the choices regarding the opportunity to invest in the building process considering the phases of design, construction and management of the building. Hence, the initial cost needs to be compared with life-cycle costs to determine the design that performs best.
In Wen and Kang (2001), a general equation for the evaluation of the expected life-cycle cost is proposed:

$$E[C(t)] = C_0 + E[\sum_{l=1}^{L}\sum_{j=1}^{K} C_j e^{-\lambda t_l} P_{lj}(t_l)] + \int_0^t C_m e^{-\lambda t_l} \mathrm{d}\tau \tag{2.4}$$

In the previous equation $E[.]$ denotes expected value; l is the loading occurrence number; L is the total number of loading occurrences between time 0 and time t; j is the limit state number; K is the total number of limit states under consideration; P_{lj} is the probability of exceedence of the j^{th} limit state; C_j is the cost of the j^{th} limit state reached supposed as a deterministic quantity; C_m is the operation and maintenance cost per year; λ is the discount rate per year which allows the conversion of the costs in present dollar values; t_l is the loading occurrence time (random variable).
Implicit in the formulation of Equation (2.4) is the assumption that after each hazard occurrence the structure is restored to its original condition.
Equation (2.4) can be evaluated in closed form under the hypothesis that the hazard occurrence is modeled by a Poisson process with occurrence rate of ν per year.
A continuous-time stochastic process $L(t) : t \geq 0$ is a Poisson process with rate $\lambda > 0$ (Last and Penrose 2017) if:

- $L(0) = 0$;
- it has stationary and independents increments;

- $L(t)$ follows a Poisson distribution, i.e. a discrete probability distribution for the counts of events that occur randomly in a given interval of time (or space), with mean λt:

$$P(L(t) = l) = \frac{(\lambda t)^l}{k!} e^{-\lambda t} \tag{2.5}$$

with $l = 0, 1, 2, ...$

Conditional on $L(t)$ the occurrence times t_l are independent and uniformly distributed in $(0, t)$. Therefore the expectation terms in Equation (2.4) with respect to t_l can be evaluated as follows:

$$E\left[\sum_{l=1}^{L} e^{-\lambda t_l}\right] = \sum_{l=1}^{L} E e^{-\lambda t_l} = l \int_0^t \frac{e^{-\lambda t} d\tau}{t} = \frac{l}{t\lambda}[1 - e^{-\lambda t}] \tag{2.6}$$

considering the number of occurrences:

$$\sum_{l=0}^{\infty} \frac{l}{t\lambda}(1 - e^{-\lambda t}) \frac{(\nu t)^l}{l!} e^{-\nu t} = \frac{1}{t\lambda}[1 - e^{-\lambda t}] \sum_{l=0}^{\infty} l \frac{(\nu t)^l}{l!} e^{-\nu t} = \frac{1}{t\lambda}[1 - e^{-\lambda t}]\nu t = \frac{\nu}{\lambda}[1 - e^{-\lambda t}] \tag{2.7}$$

By substituting Equation (2.7) in (2.4) the expected cost can be written in closed form (Wen and Kang 2001; Kiureghian 2005):

$$E[C(t)] = C_0 + (C_1 P_1 + C_2 P_2 + ... + C_j P_j) \frac{\nu(1 - e^{-\lambda t})}{\lambda} + \frac{C_m}{\lambda}(1 - e^{-\lambda t}) \tag{2.8}$$

Note that λ is called rate of the process and as λ increases, severe loads tend to arrive faster.

Equation (2.8) can be adjusted in order to consider different loading sources. Moreover the approach is general and different limit states can be considered (Lagaros 2013).

2.3 LCCA in wind engineering

LCCA is a well established process in earthquake engineering, as confirmed by the temporal evolution of the probability-based codes and by the literature on the topic (Sections 2.2.1 and 2.2), while in wind engineering considerable efforts are still needed to improve applicability of the methods and models. In the case of wind engineering, theory related to the performance-based design needs to be increased in order to consider the strong correlation between the structure and the wind field which can cause aerodynamic and aeroelastic phenomena (Norton et al. 2008).

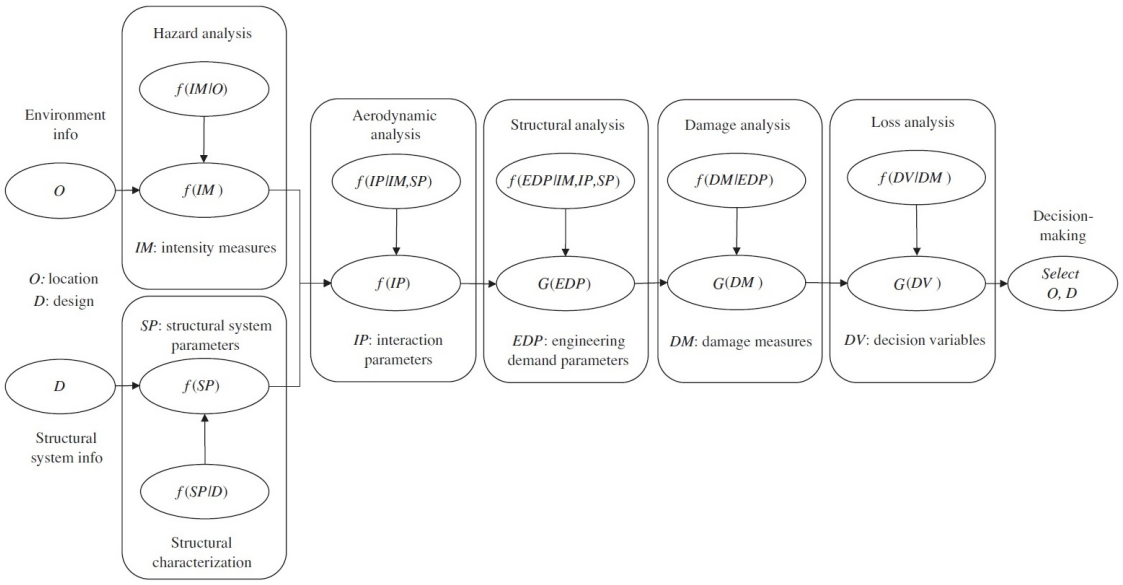

Fig. 2.4: Performance based wind Engineering scheme (Ciampoli et al. 2011).

In Ciampoli et al. (2011) a performance-based design approach for wind engineering called PBWE (Performance Based Wind Engineering) is formalized for the first time. The basic concepts of PBWE are summarized in Figure 2.4. The general framework proposed takes into account the uncertainty related to the wind load characterization due to its inherent stochastic nature and the uncertainty in the aerodynamic models and structural properties of the building which can be relevant to the response estimation.
On the basis of the previous considerations, Equation (2.3) is modified as follows:

$$G(DV) = \int\int\int\int\int G(DV|DM)f(DM|EDP)f(EDP|IM,IP,SP) \\ f(IP|IM,SP)f(IM)f(SP)\mathrm{d}DM\mathrm{d}EDP\mathrm{d}IM\mathrm{d}IP\mathrm{d}SP \quad (2.9)$$

where f stands for probability density function.
With respect to Equation (2.3) symbols assume different meaning as outlined below (Petrini et al. 2013; Tessari et al. 2017):

- *Intensity Measures* (IMs) include the parameters that describe the site-specific hazard (mean-wind velocity, turbulence, mean-wind direction);
- *Interaction parameters* (IPs), added with respect to the original formulation, repre-

sent the interaction between the environment and the structure (aerodynamic coefficients and aeroelastic derivatives);

- *Structural parameters* (SPs), added with respect to the original formulation, represent the randomness of material and geometrical properties which can influence the structural and the dynamic behavior. The probabilistic correlation between IP and IM can be based on wind tunnels tests (Section 3.4) or simulation techniques;
- *Engineering Demand Parameters* ($EDPs$), related to a damage state and consequently to a performance level, represent the variables that characterize the structural response (interstory drift, accelerations, stresses and so on);
- *Damage Measures* (DMs) represent the connection between EDP and the damage due to the wind action. As in the seismic field, DMs are usually expressed in terms of fragility functions $f(DM|EDP)$ (Section 4.6). Typical DMs, caused by excessive vibration or displacements, can be described by the damage associated to structural or nonstructural components or by the downtime losses caused by occupants' discomfort;
- *Decision Variables* (DVs) quantify the performance objectives as a function of DMs by considering two categories (Augusti and Ciampoli 2008): low performance levels (structural integrity, safeguarding human life); high performance levels (occupants' comfort, structural serviceability).

With reference to Figure 2.4 the $PBWE$ assessment can be divided into the following categories:

1. *site-structure hazard analysis.* Outcomes: $f(IP|IM, SP)$, $f(IM)$ and $f(SP)$;
2. *structural analysis.* Outcome: $f(EDP|IM, IP, SP)$;
3. *damage analysis.* Outcome: $f(DM|EDP)$;
4. *loss analysis.* Outcome: $G(DV|DM)$.

Capitalizing from the PEER approach (Section 2.2.2), the major advance (Tessari et al. 2017) provided by the PBWE methodology is the possibility to consider separately the parameters that characterize the structural behavior (SP) from parameters that qualify the wind field (IM) which are assumed as uncorrelated.
Moreover, unlike earthquakes, winds have instability phenomena related to fluid–structure

interaction and for this reason the IPs (interaction parameters) have been introduced. The parameters IPs depend on both IM and SP.
Some recent works present relevant contributions in the design of wind-sensitive structures according to probabilistic approaches derived from seismic engineering field. Among the others in Ciampoli and Petrini (2012) the method is employed to assess the risk of exceeding serviceability limit states in tall buildings subjected to wind load while in Pozzuoli et al. (2013) the occupants' comfort in a high-rise structure is evaluated with a performance-based methodology by including aeroelastic effects. Petrini et al. (2013) performed an extensive literature review on damage and loss analysis in order to expand the PBWE procedure. Griffis et al. (2013) propose a framework procedure for the design of new buildings focusing on nonlinear dynamic analysis of structures. In Bobby et al. (2014) the performance-based approach is used for the structural optimization. In Spence and Kareem (2014) the research focus is devoted to the definition of site-specific wind hazard models and to the derivation of suitable fragility functions as well as of consequence functions that can rationally assess damage and monetary losses. In Bernardini et al. (2015) and Zhao and Yu (2013) the PBD is used as a design indication for the high-rise buildings occupant's comfort. The PBWE was also applied for the evaluation of the performance of steel towers (Tessari et al. 2017).
A few recent works concerning life-cycle cost analysis of structures under wind loads present relevant contributions in this field by adopting several concepts and methods from the seismic engineering field. Seo and Caracoglia (2013), Cui and Caracoglia (2015), and Cui and Caracoglia (2016a) propose a numerical framework to estimate the life-cycle monetary losses due to the wind-induced damage on long-span bridges and tall buildings. A risk design optimization method for optimizing life-cycle costs and functionality of tall buildings is proposed in Li and Hu (2014). Minimization of life-cycle cost is also explored for the optimal design of tall buildings under wind load (Huang et al. 2016; Chen 2011) and for steel wind towers (Lagaros and Karlaftis 2016). More recently a general probabilistic framework for the cost assessment is proposed in Chuang and Spence (2017) by considering probable repair costs and downtime of both collapse and noncollapse performance.
In the case of extreme events the software Hazus-MH, implemented by the Federal Emergency Management Agency (FEMA), could be used for the estimation of potential losses due to hurricanes in the U.S. territory (Vickery et al. 2006). Recently hurricanes and strong winds were treated by some authors (Chung Yau et al. 2011; Bjarnadottir et al. 2014) and a probabilistic framework named PBHE Performance-based Hurricane Engineering is proposed in Barbato et al. (2013).

In recent years, life-cycle loss estimation methodologies have also been proposed for structures subjected to multiple-hazards. A general framework for the LCCA of tall buildings subjected to both seismic and wind excitation is discussed in (Venanzi et al. 2017; Aswegan et al. 2017). In Asprone et al. (2010), a probabilistic model for multi-hazard risk estimation for a reinforced concrete structure subjected to blast threats in the presence of seismic risk is developed. In Jalayer et al. (2011) a methodology is presented for LCCA of critical infrastructures accounting for uncertainty in the occurrence of future events due to different types of hazard and for deterioration of the structure after a series of events. Multi-hazard risk due to earthquakes and hurricanes is considered in Kameshwar and Padgett (2014) for the LCCA of a portfolio of highway bridges. In Mahmoud and Cheng (2017), the life-cycle cost of two different steel buildings under wind and earthquake is examined.
The need for using a life-cycle approach in the field of energy-saving for the energy performance of tall buildings is emphasized in Tschanz and Davenport (2016).

2.4 The structural control in a LCCA perspective

Minimization of the life-cycle cost is also explored for the optimal design of tall buildings under wind load and equipped with control devices.
Most of the existing design methods identify those control systems that satisfy, at the same time, initial economic targets and specific performance levels. The adoption of control systems is an important initial investment that can lead to significant intervention cost savings during the structural lifetime (reduced maintenance and repair). Therefore, the control system optimization procedure should take into account not only the initial cost but also the projected future savings due to the presence of the device in a life-cycle perspective.
In Beck et al. (2014) an approach combining statistical linearization with time-variant reliability analysis concepts is used to formulate a total expected life-cycle cost optimization problem and it is applied to the optimal design of non-linear hysteretic stochastic dynamical systems. In Wang et al. 2016, the life-cycle downtime cost, related to discomfort perception, is explored for the optimal design of tall buildings under wind load and equipped with control devices. In Zhao and Yu (2013) life-cycle cost criteria of high-rise buildings equipped with TMDs is used as a target design indication for occupants' comfort. The human comfort is used as a performance threshold.
The LCCA is also a valid tool to evaluate the performance of structural control systems for seismic vibration mitigation. In Matta (2015) a life-cycle cost-based method for evaluating

the seismic effectiveness of tuned mass dampers on inelastic building structures is presented. In Taflanidis and Beck (2009), a systematic probabilistic framework is presented for the optimization of the life-cycle cost of engineering systems equipped with viscous dampers under seismic load. In Wong and Harris (2013) a cost analysis for actively controlled structures is developed. In Shin and Singh (2017) a life-cycle cost-based framework to obtain optimal design of yielding metallic devices is proposed. In Dyanati et al. (2017) the seismic performance and economic effectiveness of two prototype buildings utilizing self centering concentrically braced frames are assessed and compared with the not self centering ones.

2.5 Literature gap

For the sake of completeness in the literature review it is useful to more specifically describe the main literature gap with reference to previous works on the topic:

1. Focusing on the individual aspects concerning the design of wind-excited tall buildings, the methodologies proposed in the current literature are difficult to generalize since they deal with aspects of the design separately under specific conditions (Section 2.3). Consequently the applicability of a complete LCCA to real cases is not considered.

2. In the current works regarding wind engineering applications (Section 2.3), practical design issues are not included such as the geographical location, wind directionality effects (building orientation) or the choice of nonstructural elements (type, numbers, location).

3. The literature on this topic is largely conceptual in nature with a small amount of data referring to possible real applications and to how stakeholders can make a decision on the basis of a common decision variable. As a matter of fact cost analysis is often neglected since costs data are too commercially sensitive and are difficult to be quantified. Therefore, the possibility to choose the best solution over the project life-cycle of different suitable alternatives is not enough stressed.

4. The most literature studies concerning LCCA of wind-exposed tall buildings (Section 2.3), assume the intervention and repair cost to be directly associated with the probability of exceeding a pre-selected limit state at a global or floor level (Ciampoli et al. 2011; Cui and Caracoglia 2015; Spence and Kareem 2014). As a matter of fact the

wind-induced effects (especially for non-structural components) are often neglected because of the lack of extensive experimental tests in the wind-induced damage. The lack of experimental fragility data in the field of wind engineering confirms the need of further investigating these design approaches based on the estimation of the losses during the building lifetime.

5. Just a few works deal with a detailed examination of serviceability limit states, which are not exclusively associated with occupants' comfort or excessive displacements (Pozzuoli et al. 2013; Zhao and Yu 2013; Spence and Kareem 2014; Bernardini et al. 2015) but also with the damage on nonstructural elements .

6. Most of the literature works concerning the installation of control systems (Section 2.4) on high-rise buildings are aimed at optimizing the cost of the device. Indeed, it is a common opinion to associate relevant initial costs to the installation of a control device. The examination of the cost savings over time is not included in current works.

2.6 Innovative contributions

Though many research works are devoted to LCCA, its use is still far from being systematic and general in practical applications.
Capitalizing from the existing literature and from recent advancements of LCCA methods, the main objective of LCCWD is to provide a general and computationally efficient procedure for the design of tall buildings under wind loads. Cost accumulation over time is a measure of the optimal design, achieved by comparison of alternative solutions.
LCCWD has been developed with the aim of overcoming the main limitations in the current literature. The main features and novelties are summarized below:

1. LCCWD tries to develop a general framework (Section 4.1) identifying the important aspects that have to be taken into consideration in the design phase (literature gap 1). The LCCWD approach provides an automated tool that is easily adaptable to specific real applications in order to achieve the best design configuration.
   The possibility to compare different feasible alternatives is beneficial for designers and stakeholders because it allows taking into account simultaneously the needs of both.

2. LCCWD procedure focuses on the potential benefits of an automated life-cycle procedure (literature gap 1) with a certain number of INPUT data (Chapter 4):

- structural characteristics (materials, shape, etc);
- control system characteristics;
- wind load measurements;
- geographical location and consequent information about the probability distribution of mean-wind speed and direction;
- fragility curves related to nonstructural components;
- cost data

and an OUTPUT result (Chapter 4):

- expected life-cycle cost that represents a decision variable that allows to choose between the various design alternatives (Sections 4.10 and 6.6). The way in which the results are presented makes the approach comprehensive to both designers investors allowing a practical application(literature gap 3).

3. LCCWD procedure allows to account for (literature gap 2):
   - wind directionality
   - building's orientation with respect to the prevailing winds at a specific site (Sections 4.9.2 and 6.3).
   - design of outdoor and indoor distribution of non nonstructural elements (i.e. glass façades, partition walls and others), which are considered strictly dependent on the building's destination of use which in turn becomes an integral part of the design (Sections 4.9.4 and 6.5.1).
4. LCCWD allows to differentiate the approach proposed for wind engineering in comparison with the well-established approach in seismic engineering. Indeed, the transfer of the PEER equation (Equation 2.3) is not in general adaptable to wind engineering. The arrival of an earthquake is not predictable and can cause severe damages and the performance objectives are devoted to collapse prevention and life safety. LCCWD specializes the performance objectives in the case of wind engineering by considering the damage on secondary systems and nonstructural elements while the main structural system remain linear (literature gap 5).
5. The fundamental sources of uncertainty are considered: those associated with aerodynamic loads, wind load intensity, directionality and fragility models. Uncertainty

in the wind load estimation is examined and used to assess the probability distributions of the damage-related response components by splitting the wind tunnel records in several segments corresponding to independent realizations of the stochastic load process (Section 4.4). The procedure is computationally efficient since wind tunnel records are used and converted to generalized forces along with their uncertainty, enabling the analysis in the frequency domain.
The mean-wind speed intensity and direction randomness can be taken into account in the computation of the expected life-cycle cost by using experimental data at a specific site or by using literature data. By accounting for the probability distribution of the wind direction, the life-cycle cost is evaluated as a function of both time and building's orientation angle.
Fragility models are represented with fragility curves (Section 4.6).

6. As concerns the structural analysis, the randomness of IP is indirectly taken into account by evaluating the peak response and the corresponding value of the selected EDP parameters for each one of the N segments of wind tunnel data (Section 4.4) which allows the calculation of the PDF of EDP. This approach and the frequency domain analysis allows to overcome one of the main disadvantage related to the application of a life-cycle cost approach: the high required computational time and the extended data processing.
It is worth noticing that structural modeling uncertainty might include other variables such as frequencies, modal damping ratios, mode shapes and other variables that are non-deterministic. For the purpose of this thesis the uncertainty characterization is primarily concentrated on the fundamental source of uncertainty in tall buildings, the wind load, but the approach is general and allows to include in the models all the uncertain variables.

7. In the LCCWD approach, the cost is indirectly related to the probability of exceeding a damage state obtained by incorporating specific structural fragility functions at the component level (Section 4.6). The proposed LCCWD emphasizes the need for considering realistic experimental models for the characterization of nonstructural wind-induced damages (literature gap 4).

8. Intervention and repair costs related to structural elements are accumulated along both principal lateral deformation planes of the building by considering the torsional effects (Section 5.3).

9. LCCWD procedure allows accounting for the presence of structural auxiliary damping devices (Section 4.9.3) and overcomes the traditional preconception for which the installation of the control device significantly increases the required investment (literature gap 6).
   An improvement of the proposed LCCWD procedure, compared to the existing methods, is related to the capability of accounting for the control system in the lifetime damage probability estimation and cost assessment (Sections 4.8 and 4.7).
   The LCCWD approach emphasizes the need to evaluate the ratio costs/benefits over time through the estimation of the long-term investment costs for the installation of the control system.

10. Since LCCA for wind-excited tall buildings is not largely used, to date, no acronyms have been identified. The proposed approach in this thesis is named LCCWD in order to globally characterize the framework (Section 1.1).

Chapter 3

Response of tall buildings to dynamic wind loading

3.1 Introduction

Before entering into the discussion, it is appropriate to recall some basic concepts on the characterization of the dynamic response of tall buildings under wind loads.
There is no absolute definition of what constitutes a tall building because it depends on the height relative to the context, the proportions between height and width and the embedded technologies.
From the structural design point of view, a building can be considered tall when the structural analysis and consequently the structural design is primarily affected by the swing caused by lateral loads (wind/earthquake) (Taranath 1998).
Figure 3.1 shows the average height of the tallest 100 buildings in the world and the average height of all buildings higher then 200 m. From the figure it can be noted that in the last decade the average height of the tallest structures continues to rise into the sky, constantly introducing new challenges in structural engineering.
As a matter of fact these modern tall buildings can be classified as wind-sensitive struc-

tures since they usually are light in weight, slender, and could have relatively low damping ratios.

Wind can be defined as air circulation on the Earth's surface linked to the air mass and to the atmospheric pressure. In the atmosphere, the air masses move from a high pressure

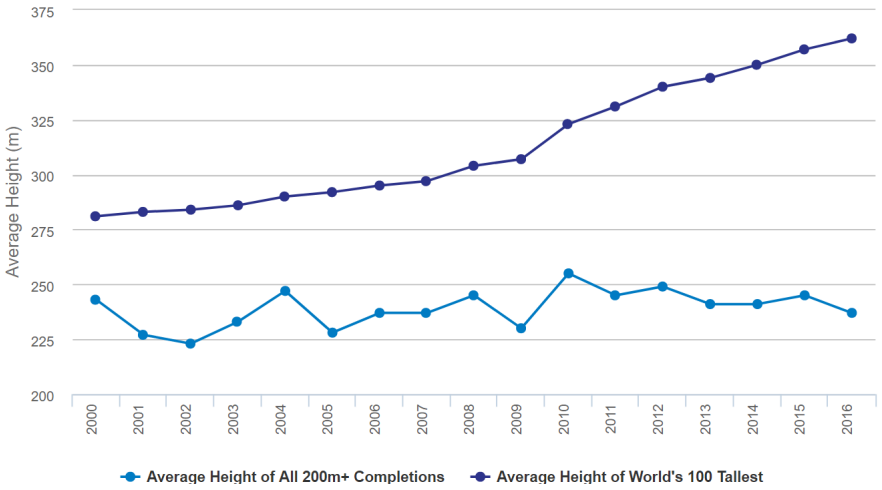

Fig. 3.1: World's tallest buildings average heights (*Council on Tall Buildings and Urban Habitat, CTBUH*).

zone to a low pressure zone, forming the wind. The movement is regulated by complex thermodynamic and mechanical phenomena that change over time and space.

Wind can be weak, strong and moderate and a classification called *Beaufort Wind Scale* was devised by Sir Francis Beaufort in 1805 (Table 3.1), which explains the wind's intensity based on it's effects on land. Several higher categories were added in time to better account for hurricane winds.

Table 3.1: Sir. Francis Beaufort (1805) wind scale

Beaufort number	Wind speed [m/s]	Seaman's term	Effects on land
0	<0.3	Calm	Calm, smoke rises vertically
1	0.3-1.5	Light Air	Smoke drift indicates wind direction, still wind vanes
2	1.6-3.3	Light Breeze	Wind felt on face, leaves rustle, vanes begin to move
3	3.4-5.5	Gentle Breeze	Leaves and small twigs constantly moving, light flags extended
4	5.6-7.9	Moderate Breeze	Dust, leaves, and loose paper lifted, small tree branches move
5	8.0-10.7	Fresh Breeze	Small trees in leaf begin to sway
6	10.8-13.8	Strong Breeze	Larger tree branches moving, whistling in wires
7	13.9-17.1	Moderate Gale	Whole trees moving, resistance felt walking against wind
8	17.2-20.7	Fresh Gale	Twigs breaking off trees, generally impedes progress
9	20.8-24.4	Strong Gale	Slight structural damage occurs, slate blows off roofs
10	24.5-28.4	Whole Gale	Seldom experienced on land, trees broken or uprooted, "considerable structural damage"
11	28.5-32.6	Storm	Very rarely experienced; accompanied by widespread damage
12	32.7	Hurricane Force	Violence and destruction

In this Chapter, the characterization of wind effects on tall buildings is briefly reviewed, along with a synthetic discussion on the control solutions for wind-excited high-rise structures. It is emphasized that this chapter does not intend to present a complete discussion on wind response of tall buildings but it focuses on the topics and on the analytical models needed to understand the research work presented in Chapters $4-5-6$.
The following Sections are organized as follows:
Section 3.2 reports an introduction on the effects on tall buildings with a particular attention on turbulence and vortex shedding phenomena.
Section 3.3 is devoted to characterize the dynamic response of wind-excited tall buildings by considering aerodynamic effects.
Section 3.4 briefly presents the most used experimental wind tunnel tests techniques.
Section 3.5 introduces the structural control methodologies for wind-excited tall buildings focusing in particular on Tuned Mass Damper (TMD).

3.2 Wind load characterization

3.2.1 Wind turbulence

With the aim to characterize the wind action, Figure 3.2 reports the variability of wind power spectral density over different frequencies/timescales (Hoven 1957). From the figure two peaks can be noted in the low frequency zone and a third peak is evident in the high frequency area. The first peak corresponds to about 4 days and represents the typical development of a storm. The second peak corresponds to the daily (day/night) wind period, representing variable breezes with a period of about 12 hours. The third peak at about 1-2 minutes is due to the atmospheric turbulence. In the center of the graph, the spectral power density displays a minimum within a time range of 10 minutes to 1 hour. This area, called *spectral gap*, provides information for the experimental evaluation of the wind load: since the variance is small and constant, the speed of the wind can be calculated by averaging recordings over a period of 10 minutes to 1 hour. The gap allows to separate macro-meteorological (storm) and micro-meteorological effects (turbulence).
On the basis of the previous considerations it is possible to clearly distinguish the stationary components of the wind $\bar{V}_u$, $\bar{V}_v$ and $\bar{V}_w$ (which does not experience large changes from hour to hour) and the turbulent components v_u, v_v, v_w. The directions u, v (horizontal) and w (vertical) are specified in Figure 3.3. Consequently it is possible to define the wind velocity V in the three principals directions as the sum of the average value ($\bar{V}$) obtained over a

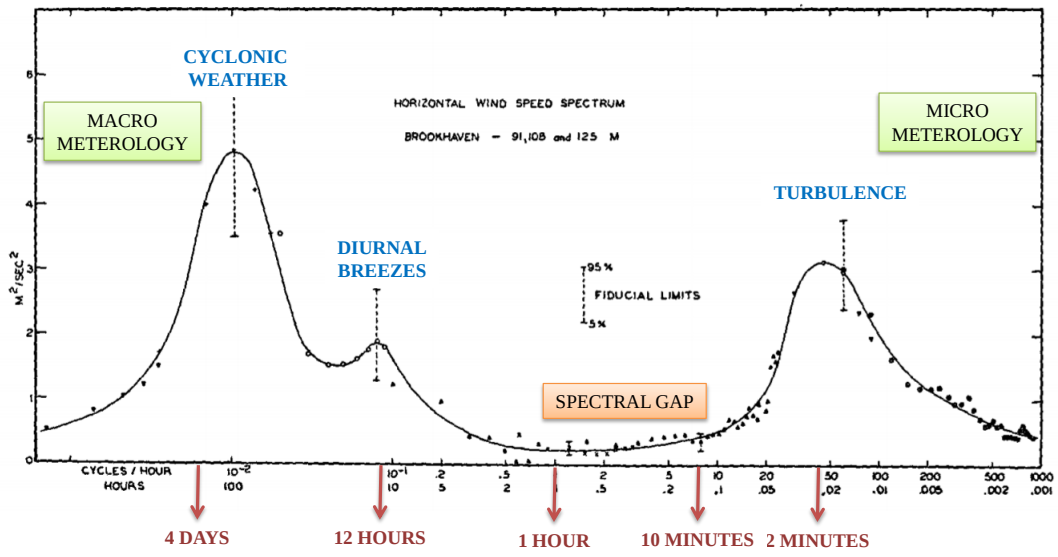

Fig. 3.2: Horizontal wind speed spectrum at Vrookhaven National Laboratory at about 100-m height in synoptic conditions (Hoven 1957).

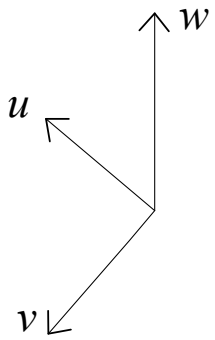

Fig. 3.3: Principal directions u, v, w of wind velocity and of wind turbulence.

period of 10-60 and of the fluctuating turbulent component:

$$V_u(z,t) = \bar{V}_u + v_u(z,t) \tag{3.1}$$

$$V_v(z,t) = \bar{V}_v + v_v(z,t) \tag{3.2}$$

$$V_w(z,t) = \bar{V_w} + v_w(z,t) \tag{3.3}$$

The mean component characterizes the steady nature of wind. Typical profile of the mean-wind speed in the earth's atmospheric boundary layer is shown in Figure 3.4. The friction force derived from the earth's surface influences the air movement with a consequent decrease of the mean wind speed close to the ground. This effect is reduced with height up to a certain z called gradient height (δ_{gr}), known as the height of the atmospheric boundary layer. Above δ_{gr} the speed of the wind follows the isobars (Gradient velocity V_{gr}).

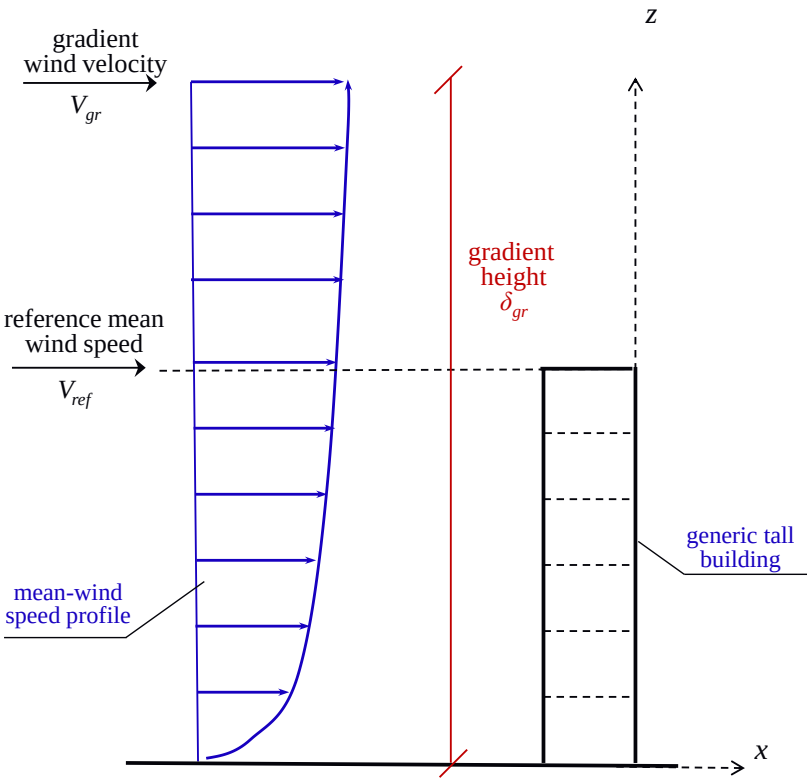

Fig. 3.4: a schematic representation of the mean wind speed of a generic tall building.

Two models can be used to describe the mean wind profile: the power law and the logarithmic law. For the sake of simplicity the two models are reported for the u component. The first model used is the power law, given by:

$$\bar{V_u}(z) = \bar{V_u}(z_{ref})(\frac{z}{z_{ref}})^{\alpha} \tag{3.4}$$

where $\bar{V_u}(z_{ref})$ is the mean-wind speed at the reference height z_{ref} and α is the power law exponent which depends on the terrain type. The second model (logarithmic law) is described by:

$$\bar{V_u}(z) = \frac{1}{\kappa} v_* \ln \frac{z}{z_0} \tag{3.5}$$

where $\kappa \approx 0.4$ is the Von Karman constant, z_0 is the soil roughness and $v_* = \sqrt{\tau_0/\rho}$ is the friction velocity depending on the surface shear stress τ_0 and on the air density ρ.
Fluctuating components of wind velocity v_u, v_v and v_w show gustiness of the wind. The turbulence is considered as a random process and needs to be studied with appropriate statistical models. In many cases it is justified the simplification that the wind turbulence is an ergodic and stationary Gaussian process and the first two statistical moments allow to characterize it completely. However, many research studies are devoted the evaluation of the structural response by considering the wind non-Gaussianities (Blaise et al. 2016).
A physical description of the turbulence is given by the characterization of the following quantities (Borri and Pastò 2006):

1. turbulence intensities;
2. integral and time scales of turbulence;
3. power spectral density.

1. The turbulence intensities I, corresponding to the fluctuating components of the wind velocity v_u (longitudinal), v_v (lateral), v_w (vertical), can be computed as follows:

$$I_u(z) = \frac{\sigma_u(z)}{v_u} \tag{3.6}$$

$$I_v(z) = \frac{\sigma_v(z)}{v_v} \tag{3.7}$$

$$I_w(z) = \frac{\sigma_w(z)}{v_w} \tag{3.8}$$

where $\sigma_u(z)$, $\sigma_v(z)$, $\sigma_w(z)$ are the root mean square (RMS) of the fluctuating components. The term $\sigma_u(z)$ can be evaluated as (Holmes 1987):

$$\sigma_u(z) = E[u(z)^2]^{0.5} \tag{3.9}$$

The lateral and vertical turbulence components are generally lower in magnitude than the corresponding longitudinal value and, for well-developed boundary-layer

winds, can be evaluated in a simple manner as a function of the friction velocity u_* (Holmes 1987).

$$\sigma_v(z) \approx 2.2u_* \tag{3.10}$$

$$\sigma_w(z) \approx 1.3 - 1.4u_* \tag{3.11}$$

2. Obtaining the average sizes of eddies in a turbulent wind flow is important both for experimental and numerical simulations. The average sizes of eddies is described by a quantity known as the integral length scale (Simiu and Scanlan 1996). Corresponding to each of the fluctuating components of the wind velocity (v_u, v_v, v_w), there are three integral lengths scales corresponding to the coordinates (x, y, z) with a total of 9 scales. Considering the longitudinal component, the integral time scale can be computed as the area under the auto-correlation curve $R_{v_{u1},v_{u1}}$ of the fluctuating components of the velocity:

$$L^x_{v_u} = \frac{1}{\sigma^2_u(z)} \int_0^\infty R_{v_{u1},v_{u2}}(x, \tau = 0)dx \tag{3.12}$$

where τ is the time lag and $v_{u1}(x_1, t_1)$ is the turbulence at the point 1 and $v_{u2}(x_1 + \Delta x, t_1 + \tau)$ is the turbulence at the point 2. Considering the Taylor's hypothesis (Taylor 1938) that the flow disturbance v_u travels with mean velocity $\bar{V}$, $L^x_{v_u}$ can be written:

$$L^x_{v_u} = \frac{\bar{V}}{\sigma^2_u(z)} \int_0^\infty R_{v_u}(\tau)d\tau \tag{3.13}$$

Considering the wind flow in a certain time interval, the average time taken for the fluctuating components of the wind speed is described by a quantity known as the integral time scale:

$$T_{v_u}(z) = \int_0^\infty R_{v_u}(z, \tau)d\tau \tag{3.14}$$

3. The turbulent nature of wind flow creates eddies of variable sizes which overlap with different frequencies and energies. The turbulence spectrum gives information about the vortex frequency content. Several empirical equations have also been suggested by different researchers for computing the longitudinal and transverse components of the wind velocity of which some examples are given (Borri and Pastò 2006):

- Von Karman (longitudinal)

$$\frac{nS_{v_u,v_u}(z,n)}{v_*^2} = 4\frac{nL_{v_u}^x}{V(z)}\frac{1}{\left[1+70.8\left(\frac{nL_{v_u}^x}{V(z)}\right)^2\right]^{(}5/6)} \tag{3.15}$$

- Davenport (longitudinal)

$$\frac{nS_{v_u,v_u}(z,n)}{v_*^2} = 4\left(\frac{1200n}{V_{10}}\right)^2\frac{1}{\left[1+\left(\frac{1200n}{V_{10}}\right)^2\right]^{4/3}} \tag{3.16}$$

- Kaimal (longitudinal)

$$\frac{nS_{v_u,v_u}(z,n)}{v_*^2} = \frac{200n}{(1+50n)^{5/3}} \tag{3.17}$$

- Kaimal (transverse)

$$\frac{nS_{v_v,v_v}(z,n)}{v_*^2} = 15\frac{nz}{V(z)}\frac{1}{\left[1+9.5\frac{nz}{V(z)}\right]^{5/3}} \tag{3.18}$$

- Lumley and Panofsky (transverse)

$$\frac{nS_{v_w,v_w}(z,n)}{v_*^2} = 3.36\frac{nz}{V(z)}\frac{1}{\left[1+10\frac{nz}{V(z)}\right]^{5/3}} \tag{3.19}$$

3.2.2 Vortex shedding

In aerodynamics, a bluff body is the one which has a length in the flow direction close or equal to that perpendicular to the flow direction. Most of the man-made structures are bluff bodies. A principal feature of the flow around bluff bodies structures is the formation of large vortices in their wakes, which strongly affect the wind loading and the structural response. The investigation, the analysis and the understanding of bluff bodies aerodynamics are complex since the flow around bluff bodies depends not only on the shape of the body, but on many factors, such as the Reynolds number and the characteristics of the turbulence (Irwin 2008). The Reynolds number is the ratio of inertial fluid forces to viscous fluid forces:

$$R_e = \frac{\rho VL}{\tilde{\mu}} = \frac{VL}{\tilde{\nu}} \tag{3.20}$$

where ρ is the air density, V is the wind velocity, $\tilde{\mu}$ is the air dynamic viscosity and $\tilde{\nu}$ is the air kinematic viscosity. At low Reynolds numbers, viscous forces are dominant, flow is laminar and it is characterized by smooth, constant fluid motion. At high Reynolds numbers the inertial forces dominate and tend to produce chaotic eddies, vortices and other flow instabilities. The latter effect depends also on the shape of the body (Figure 3.5). The inspection of the figure suggests that the aerodynamic profiles (wing profiles) are designed in such a way that they do not present flow separation along the section, but only in correspondence of the last part where the vortices are small and the wake region is thin. Bodies with sharp edges present separation of the fluid stream especially in correspondence of the edges with the consequent formation of vortices.

The effect of the vortex shedding is strongly affected by the Reynolds number and it is

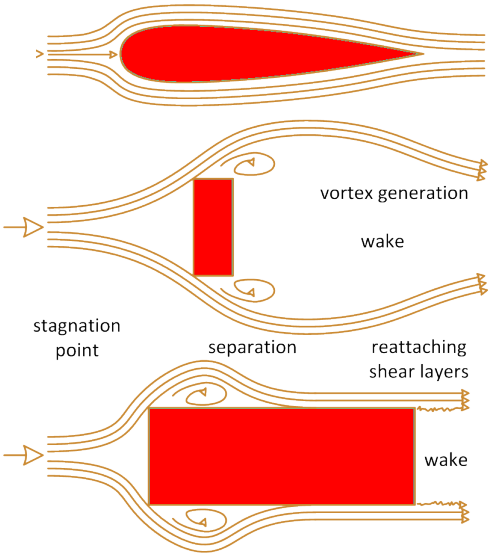

Fig. 3.5: Flow around bluff bodies (*Bluff-body aerodynamics*).

more dangerous as R_e increases. This phenomenon is shown in Figure 3.6 (Lienhard 1996). It is worth stressing that the way in which the vortices are detached determines the loads that force the structure. Moreover the size of the wake region depends on the shape of the body (Borri and Pastò 2006).

The process of vortex shedding induce movements in the across-wind direction when the natural frequency of the structure coincides with the frequency of the vortex shedding (n_{vs})

which is described by the Strouhal law:

$$n_{vs} = S_t \frac{V}{D} \tag{3.21}$$

wherein S_t is the Strouhal number. Hence it is possible to evaluate the critical velocity V_{cr} around which there is the full synchronization of the vortex shedding:

$$V_{cr} = \frac{n_0 D}{S_t} \tag{3.22}$$

At critical velocity, the high-rise building is *locked-in*. The flow of the wind and the motion of the building adversely affect each other and largest amplitude oscillations occur.
The effect of synchronization is a complex aeroelastic phenomenon and if the acrosswind response is found exclusively from the turbulence (lift forces), it is likely to underestimate the response since the *lock-in* will intensify the building's motion (Cheng et al. 2002). Wind tunnel measurements allow to consider the effect of vortex shedding.

3.3 Dynamic response of wind-excited tall buildings

Civil structures subjected to wind load can vibrate in different directions (Holmes 2007; Lin et al. 2005):

- in the wind direction (alongwind response) as a result of turbulence;
- in the orthogonal direction to the flow (acrosswind response) induced by the phenomenon of the vortexes shedding;
- around the central principal vertical axis (torsional response).

Also, within a certain speed range called synchronization interval, structures can resonate. (Figure 3.7) shows the directions of motion of a generic prismatic tall building subjected to wind load.

3.3.1 Literature background

Wind effects on tall buildings have been widely studied during the last decades. Both analytical and experimental methods have been adopted in the research. In the early 1960s, approaches for simulating the dynamic response of buildings under wind excitations started

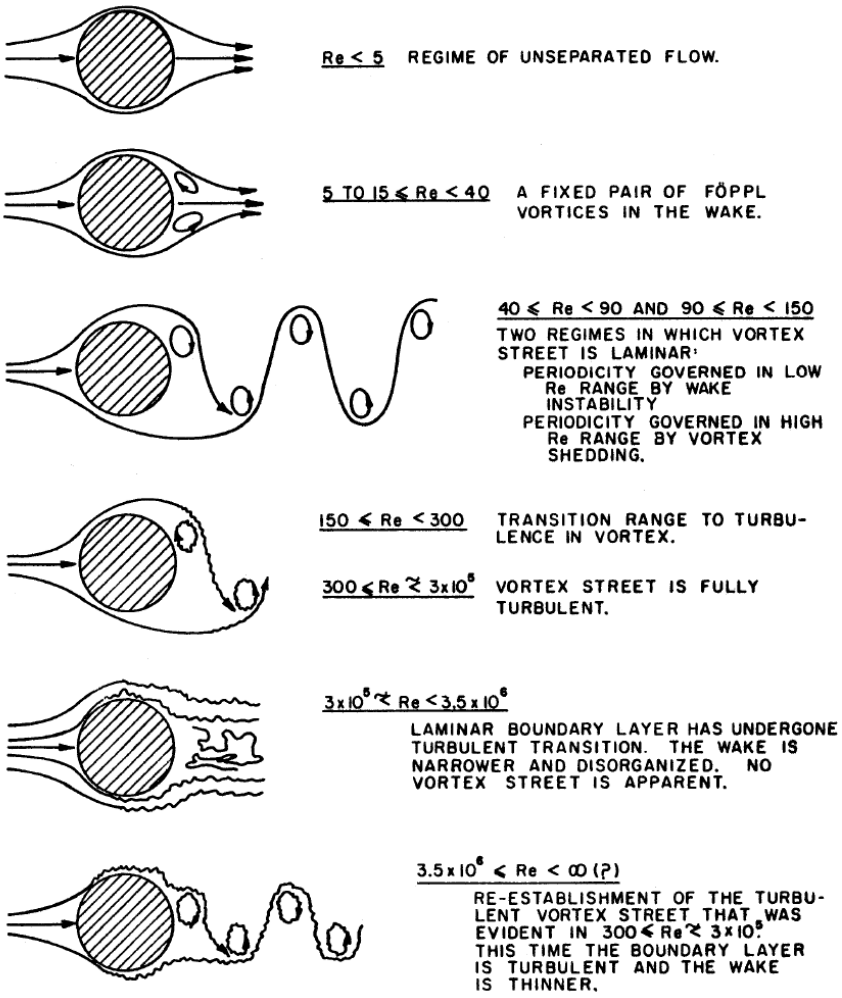

Fig. 3.6: Regimes of fluid flow across smooth circular cilinders (Lienhard 1996).

to be investigated. The turbulent wind flow is considered as a locally stationary random process and the structural response is evaluated in statistical terms (Davenport 1961; Davenport 1964; Davenport 1967; Davenport 1971). Figure 3.8 illustrates the elements of the spectral approach (Davenport 1964). In the first row the response is evaluated in the time domain and in the second one it is evaluated in the frequency domain. In the second approach the structural response due to the fluctuating component is evaluated from the RMS of the response power spectral density (response spectrum). This spectrum is evaluated from the spectrum of the aerodynamic forces (wind/structure interaction) which is in turn calculated from the wind forces associated to the turbulence or from the gust spectrum. The mechanical admittance, frequency-dependent, forms the links between the

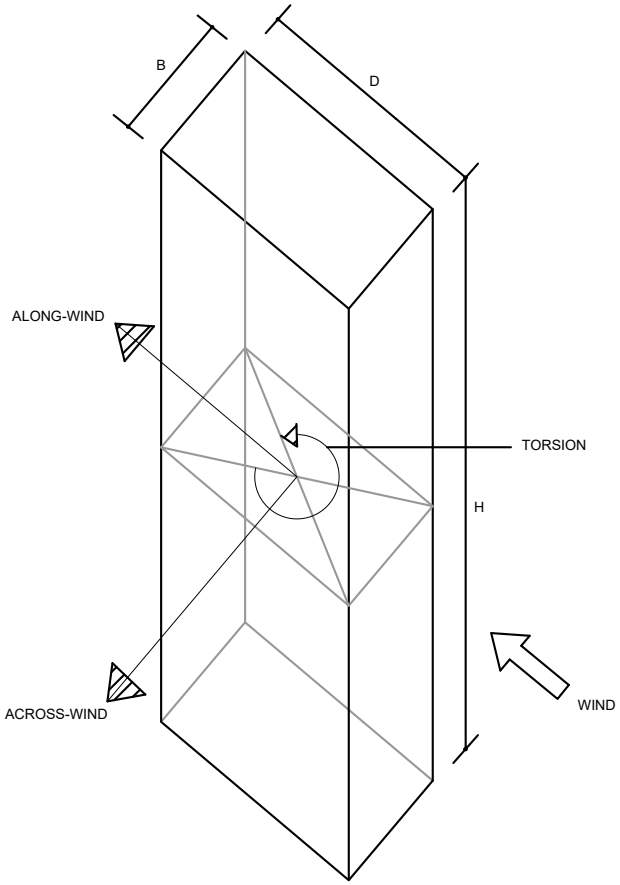

Fig. 3.7: Tridimensional view of a generic tall building with the indication of alongwind, acrosswind and torsional response.

spectra (Holmes 1987).

From Davenport's theory on, wind effects on structures have been deepened investigated and a large amount of researches can be found in the literature. The torsional and the unsteady wake excitation are introduced in Kareem (1981) and Kareem (1982), emphasizing the use of wind tunnel data. In Solari (1982) a close form solution for alongwind response is proposed.

Since tall buildings are not limited to movement only in the alongwind direction but also

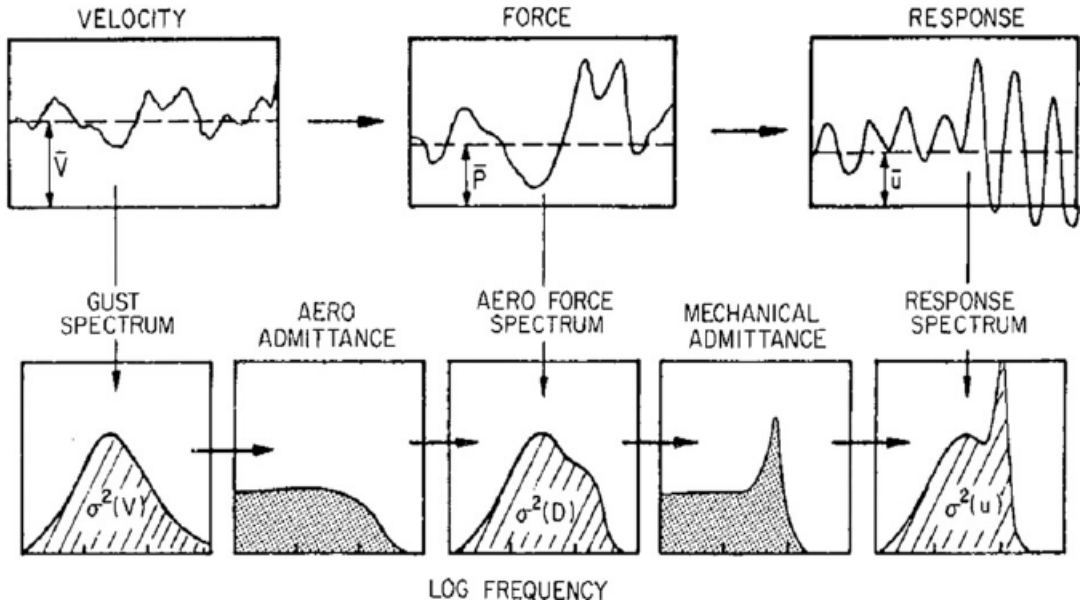

Figure 3.8: Davenports wind load chain (Davenport 1964).

in acrosswind and torsional directions, subsequent studies have led to the formulation of general frameworks for gust-excited vibrations of structures considering coupled and uncoupled three dimensional modes (Solari 1987; Solari 1994; Chen and Kareem 2005). Non linear mode vibration can be readily included (Holmes 1987; Xu and Kwok 1993).
Simiu and Scanlan (1996) presents an up-to-date coverage of new methods and standards for wind-resistant structures. The need for considering accurate models for acrosswind response is emphasized in Cheng et al. (2002), Matsumoto (1986), and Gu and Quan (2044). In Piccardo and Solari (2000), a three-dimensional closed-form solution for the evaluation of the dynamic response of slender structures is developed. The need to refer to as realistic as possible models is highlighted in Kareem and Zhou (2003). The possibility of including non-Gaussian processes is explored in (Chen and Huang 2009).
Technological advances in the experimental modeling of wind loads (wind tunnel tests) allow an accurate estimation of the preliminary design wind forces by testing scaled models of tall buildings in a simulated atmospheric boundary layer (Lin et al. 2005; Chen and Kareem 2005).

3.3.2 Frequency-domain response of tall buildings

The fundamental equations of the LCCWD procedure are derived from a standard frequency-domain approach (widely used in the wind engineering literature) which relates the wind-induced vibrations of a structure with the random vibration theory (Holmes 2007). Averaged quantities like standard deviations and spectra are used to describe the main features of both the exciting forces and the structural response. Wind speeds, pressures and the resulting structural response have been treated as stationary random processes in which the time-averaged or mean component is separated from the fluctuating component. The following discussion refers to the models presented in Solari (1994).
Under the assumption of uncoupled principal vibration modes, the components of motion in the three main directions (x, y, ψ) can be separately studied (Solari 1987). The equation of motion of a generic structure in a turbulent flow for a generic degree of freedom can be written as:

$$\tilde{m}\ddot{q}(t) + \tilde{c}\dot{q}(t) + \tilde{k}q(t) = F_r(t) \tag{3.23}$$

wherein $q(t), \dot{q}(t), \ddot{q}(t)$ are the degrees of freedom and $\tilde{m}, \tilde{c}, \tilde{k}$ are the mass per unit length, the damping and the stiffness associated to a generic degree of freedom. $F_r(t)$ is the vector collecting the forces per unit length which is in general defined by the sum of three components:

$$F_r(t) = F(t) + F_a(t) + R(t) \tag{3.24}$$

in which $F(t)$ is the external forces vector linearly dependent on the turbulence components and on the wake coefficients, $F_a(t)$ is the vector collecting the aeroealastic forces, R(t) takes into account non linearity. Under the hypothesis that the aeroealastic effects are neglected (absence of fluid-structure interaction) and under the hypothesis of small displacements and turbulence, $F_r(t)$ in Equation (3.23) coincides with $F(t)$:

$$\tilde{m}\ddot{q}(t) + \tilde{c}\dot{q}(t) + \tilde{k}q(t) = F(t) \tag{3.25}$$

Dividing both sides of the previous equations by $\tilde{m}$ the equation of motion becomes:

$$\ddot{q}(t) + 2\xi(2\pi n_0)\dot{q}(t) + (2\pi n_0)^2 q(t) = F(t)/\tilde{m} \tag{3.26}$$

where ξ and n_0 are the structural damping coefficient and the fundamental frequency in the generic x, y, ψ direction. The external force $F(t)$, considering the Equation (3.1) is:

$$F(t) = \bar{F} + F'(t) \tag{3.27}$$

wherein $\bar{F}$ is the mean value and $F'(t)$ is the fluctuating component:

$$F'(t) = F'_{ut}(t) + F'_{vt}(t) + F'_{vw}(t) \tag{3.28}$$

In the previous equation subscripts ut, vt indicate the turbulence components and vw is due to the vortex wake.
Consequently the generic displacement (or rotation) can be expressed by:

$$q(t) = \bar{q} + q'(t) \tag{3.29}$$

where $\bar{q}$ is the mean value of $q(t)$:

$$\bar{q} = \frac{\bar{F}}{K} = \frac{\bar{F}}{M(2\pi n)^2} \tag{3.30}$$

and $q'(t)$ is the nil mean fluctuation of $q(t)$ around $\bar{q}$ and can be solved in time domain by using Equation (3.25) with $q(t) = q'(t)$ or in frequency domain taking advantage of the stationarity of the processes $F'(t)$ and $q'(t)$ as follows:

$$S'_q(n) = |H_q(n)|^2 S_{F'_q(n)} \tag{3.31}$$

$$S_{F'_q} = S^{(u)}_{F'_q} + S^{(v)}_{F'_q} + S^{(w)}_{F'_q} \tag{3.32}$$

$$|H_q(n)|^2 = \frac{1}{\tilde{m}^2(2\pi n_0)^4[(1-(\frac{n}{n_0})^2) + 4\xi^2(\frac{n}{n_0})^2]} \tag{3.33}$$

In previous equations $S'_q(n)$, $S_{F'_q(n)}$, $S^{(u)}_{F'_q(n)}$, $S^{(v)}_{F'_q(n)}$, $S^(w)_{F'_q(n)}$ are the one-sided power spectral densities of q', F', F'_u, F'_v, F'_w while the term $|H_q(n)|^2$ is the absolute value of the standard transfer function.
Considering that $q'^{(k)}(t)$ derived k-times follows the laws: $q'^{(0)} = q'$,$q'^{(1)} = \dot{q}'$, $q'^{(2)} = \ddot{q}', ...$, the power spectral density of the process can be written as:

$$S_{q'^{(k)}}(n) = (2\pi n)^{2k} S'_q(n) \tag{3.34}$$

Therefore the variance of $q'^{(k)}$ results:

$$\sigma^2_{q^{(k)}} = \int_0^\infty (2\pi n)^{2k} S'_q(n) dn \tag{3.35}$$

Assuming that the time interval T coincides with the period on which is calculated the mean

wind speed (Section 3.2.1), i.e. 600-3600 s, applying the Davenport's theory (Davenport 1964), the peak response (or rotation) $q_{\max}$ can be evaluated as the maximum probable value of q during T:

$$q_{\max} = \bar{q} + g_q \sigma_q \tag{3.36}$$

where σ_q is the standard deviation of $q(t)$ and g_q is the peak factor:

$$g_q = \sqrt{2\ln(\nu_q T)} + \frac{0.5772}{\sqrt{2\ln(\nu_q T)}} \tag{3.37}$$

wherein ν_q is the expected frequency of $q(t)$.

$$\nu_q = \frac{1}{2\pi}\frac{\sigma_{\dot{q}}}{\sigma_q} \tag{3.38}$$

In a similar manner, the maximum acceleration can be computed as:

$$\ddot{q}_{\max} = \bar{q} + g_{\ddot{q}} \sigma_{\ddot{q}} \tag{3.39}$$

where $\sigma_{\ddot{q}}$ is the standard deviation of $\ddot{q}(t)$ and $g_{\ddot{q}}$ is the acceleration peak factor:

$$g_q = \sqrt{2\ln(\nu_{\ddot{q}} T)} + \frac{0.5772}{\sqrt{2\ln(\nu_{\ddot{q}} T)}} \tag{3.40}$$

wherein $\nu_{\ddot{q}}$ is the expected frequency of $\ddot{q}(t)$.

$$\nu_{\ddot{q}} = \frac{1}{2\pi}\frac{\sigma_{\dddot{q}}}{\sigma_{\ddot{q}}} \tag{3.41}$$

On the basis of the previous formulations, it is in principle possible the evaluation of the alongwind, acrosswind and torsional responses as discussed in the following subsections.
It is worth noticing that in the case of flexible structures the vector collecting the aeroealastic forces $F_a(t)$ in Equation (3.24) cannot be neglected. As a consequence, according to Solari (1994), the equation of motion is modified in order to take into account the aeroelastic phenomena (related to the vortex-induced vibration) which modifies the damping and the frequency of the system (Mannini et al. 2011; Huang et al. 2013; Marukawa et al. 1996; Vickery and Steckley 1993; Hayashida et al. 1992).

3.3.2.1 Alongwind response

The alongwind response (Figure 3.7) is the response in a parallel direction with respect to the wind and it depends on the total alongwind force that is the sum of the forces acting on the windward and leeward faces of the structure. As shown in Figure 3.5, the wake recirculation region in the leeward face is highly turbulent but has low velocities, and in turn low pressures. Thus the alongwind response can be evaluated by applying the quasi-steady theory and the component associated to the vortex wake $F'_{vw}(t)$ in Equation (3.28) can be neglected.

3.3.2.2 Acrosswind and torsional response

The acrosswind response (Figure 3.7) is the response in an orthogonal direction with respect to the wind incidence angle while the torsional response is due to the non-symmetric pressure distribution around the bluff body. Whereas alongwind oscillations (induced by turbulence) can be reasonably estimated using quasi-steady theories, across-wind and torsional oscillations (partially caused by separation of the wake flow and vortex shedding) cannot (Kwok and Melbourne 1981; Cheng et al. 2002). In this case the term $F'_{vw}(t)$ represents the vortex shedding component which has often a dominant role. It is worth noticig that $F'_{vw}(t)$ in the case of the acrosswind response is different from $F'_{vw}(t)$ in the case of alongowind. The first one is related to the vortex shedding, the latter to the vortex wake (Figures 3.5 and 3.6). Even if a number of researches have been conducted in this area, more general approaches to determine the acrosswind and torsional response need to be developed and incorporated into current design codes (Chen and Kareem 2005). For this reason it is essential the reconstruction of the wind loads by means of experimental tests by using wind tunnel measurements.

3.4 Wind tunnel tests

As it was discussed in the previous section, aerodynamic wind tunnel tests are the most common experimental techniques used for civil structures with the aim to characterize the wind loads. The basic idea is to reproduce the real prototype in a scale model. Air movement is produced by a fan system (Figure 3.10b).
Once determined a set of dimensional parameters that govern and completely define the physical problem, the correct reproduction of the scaled phenomenon requires the fulfillment of some similitude requirements (Borri and Pastò 2006) based on the Buckingham's

theorem. This allows to maintain the same parameters for the two models. Carpet or roughness blocks are used to generate the required velocity and turbulence profiles. Figure 3.9 shows a photograph of a typical wind tunnel set up.

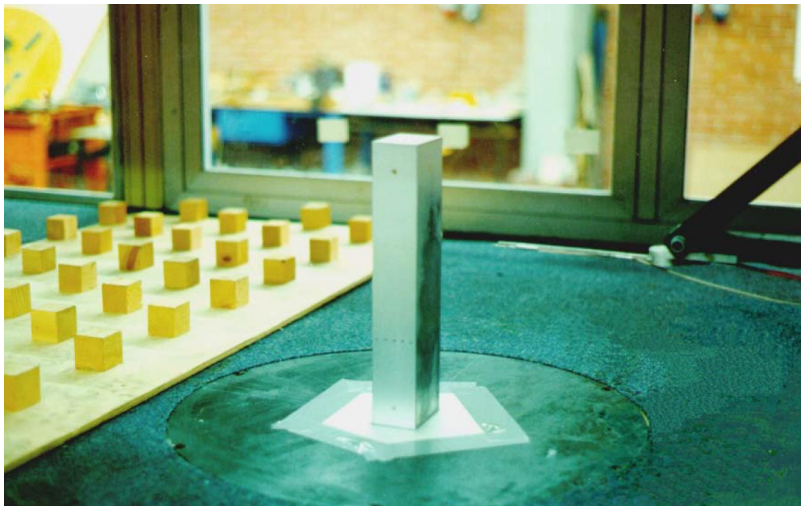

Fig. 3.9: An example of an experimental set up in a boundery layer wind tunnel (*Azioni ed effetti del vento su edifici alti*).

Commonly, two groups of wind tunnel tests are used in practice:

- aerodynamic tests, where only geometry of the building is modeled and the model is rigidly grounded;
- aeroelastic tests, where, in addition to the building geometry also dynamic properties are modeled. The model is considered flexible in order to estimate the aeroelastic effects.

One of the main advantage related to the aerodynamic tests is the fact that the test results depend only on the building geometry. Hence the structural properties could be optimized during the design process without repeating the tests.
Two types of aerodynamic tests are commonly conducted:

1. High Frequency Force Balance (HFFB) tests;
2. synchronous wind pressure measurements.

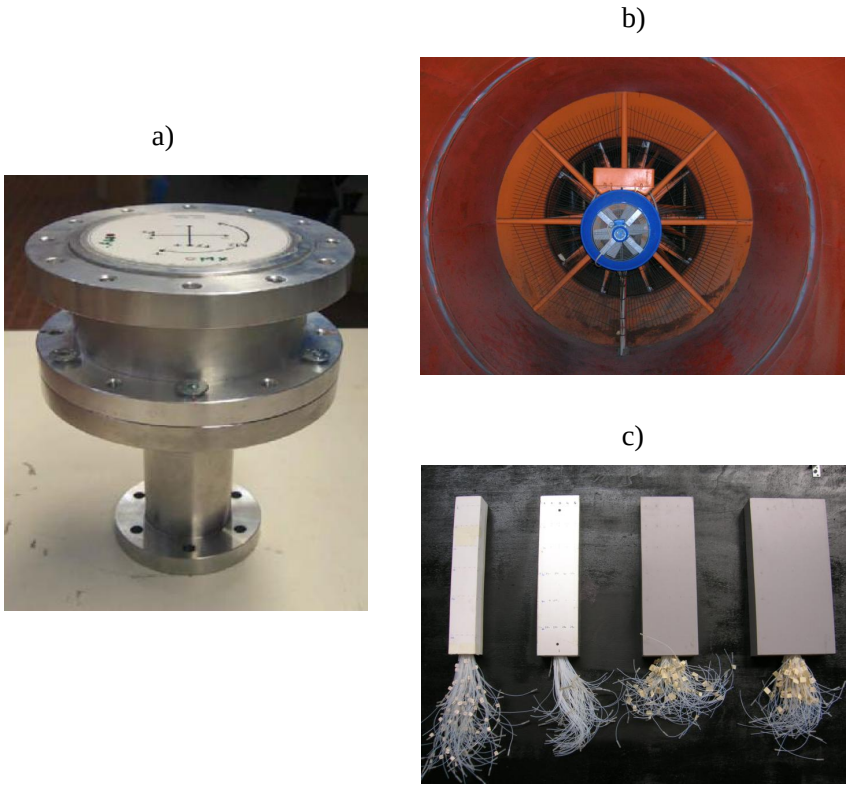

Fig. 3.10: Wind tunnel test: a) An example of force balance (*Azioni ed effetti del vento su edifici alti*), b) Wind tunnel blades (courtesy of Prof. I. Venanzi), c) pressure taps on scaled models (courtesy of Prof. I. Venanzi).

The use of HFFB is dated to the early 1970's (Whitebread 1975). The base balance technique is described in Tschanz and Davenport (1983). In this kind of test, the model is mounted on a force balance (Figure 3.10a) connected to the base of the model. In the HFFB test the base overturning and the torsional moments as well as the base shears can be measured. The basic principle behind the HFFB test is to assume the wind-induced responses to come primarily from the fundamental vibration modes with the assumption of ideal mode shapes. The experimental wind loads are represented as time-dependent generalized forces (base moments and forces). In order to consider the effect of more realistic non-ideal mode shapes, correction coefficients are proposed in several research works (Holmes et al. 2003; Tallin and Ellingwood 1985; Zhou et al. 2002).
The use of wind pressure measurements has developed since the 1980's (Kareem 1982). With this type of test the wind pressure on the model surface is measured using a synchronous multi-pressure sensing system in which pressure taps are installed at several

locations on the model surface (Figure 3.10c). These taps are connected to pressure transducers which are capable of recording the pressure fluctuations over a period of time. Using the tap pressures it is possible to evaluate the dimensionless pressure coefficient C_p:

$$C_p(t) = \frac{P(t) - P_0}{0.5\rho\bar{V}_{ref}^2} \tag{3.42}$$

wherein P is the surface pressure, P_0 is the mean static pressure at the reference height and V_{ref} is the mean-wind speed at the reference height (for example the building's height). To convert these combined pressure coefficients into floor forces, $f_x(z,t)$, $f_y(t,z)$ and base torque $f_\psi(t,z)$, acting on the three main directions of the full-scale building, the following equations are used:

$$f_x(t,z) = \sum_x 0.5\rho\bar{V}^2 C_{p,x}(t,z)A(z) \tag{3.43}$$

$$f_y(t,z) = \sum_y 0.5\rho\bar{V}^2 C_{p,y}(t,z)A(z) \tag{3.44}$$

$$f_\psi(t,z) = \sum_x 0.5\rho\bar{V}^2 C_{p,x}(t,z)Ab_t(x) + \sum_y 0.5\rho\bar{V}^2 C_{p,y}(t,z)Ab_t(y) \tag{3.45}$$

In the previous equations A corresponds to the single tap influence Area, b_t is the tap coordinate.

3.5 Control methodologies for wind-excited tall buildings

Flexible structures may experience excessive vibrations under the wind action. Hence high-rise buildings are often equipped with control devices with the aim to reduce wind-induced movements. According to Kareem et al. (1999) the methodologies to suppress vibrations can be (Figure 3.11):

1. aerodynamic design;
2. structural design;
3. auxiliary damping devices adoption.

The aerodynamic design regards the modification of the cross-sectional shape of the building in order to reduce wind loads. The most widespread solutions are: slotted and chamfered corners, fins, setbacks, buttresses, horizontal through-building openings and variations of the cross-section with height (tapering) (Kim et al. 2008). The purpose is to

Means	Type	Method & Aim	Remarks
Aerodynamic Design	Passive	Improving aerodynamic properties to reduce wind force coefficient	chamfered corners, openings
Structural Design	Passive	Increasing building mass to reduce air/building mass ratio	Increased Material Costs
		Increasing stiffness or natural frequency to reduce non-dimensional windspeed	Bracing Walls, Thick Members
Auxiliary Damping Device	Passive	Addition of materials with energy dissipative properties, increasing building damping ratio	SD, SJD, LD, FD, VED, VD, OD
		Adding auxiliary mass system to increase level of damping	TMD, TLD
	Active	Generating control force using inertia effects to minimize response	AMD, HMD, AGS
		Generating aerodynamic control force to reduce wind force coefficient or minimize response	Rotor, Jet, Aerodynamic Appendages
		Changing stiffness to avoid resonance	AVS

SD: *Steel Damper;* SJD: *Steel Joint Damper;* LD: *Lead Damper;* FD: *Friction Damper;* VED: *Visco-Elastic Damper;* VD: *Viscous Damper;* OD: *Oil Damper;* TMD: *Tuned Mass Damper;* TLD: *Tuned Liquid Damper;* AMD: *Active Mass Damper;* HMD: *Hybrid Mass Damper;* AGS: *Active Gyro Stablilizer;* AVS: *Active Variable Stiffness*

Fig. 3.11: Means to suppress wind-induced response of buildings (Kareem et al. 1999).

confuse the effect of the vortices by reducing the dangerous effects (Section 3.2.2).
The increase of the building mass or stiffness to reach a selected performance level could lead to disproportionate increase of the construction cost.
The use of auxiliary damping devices has the main goal of reducing the structural vibrations due to both wind or earthquake (Chen et al. 2017). Suppression of wind-induced vibrations or seismic vibrations towards occupants' comfort and safety. For the hazard mitigation and risk reduction, structural control has proved its efficacy in the past few decades. The control devices allow the modification of the structural behavior during an extreme event and reduce excessive displacements or accelerations. According to different types of devices, the control systems can be classified in:

1. passive control systems;
2. active control systems;

3. semi-active control systems.

The passive control systems (Soong and Dargush 1997) include a wide range of devices which are able to change the mechanical characteristics of the structure, such as the stiffness, the mass and the damping, in order to have a smaller response of the structure with respect to the uncontrolled case. The main advantage is the total absence of an external source of power (this ensures the effectiveness even in emergency cases). The main drawback is that passive control is not adaptive to the actual conditions.
The active control systems (Soong 1990) include the set of devices with the ability to monitor the dynamic state of a structure at a given moment and with the capacity to apply the feedback to adjust more favorably the dynamic process to which they are subject. Unlike the passive control systems, these devices use external power to carry out the control action.
The semi-active control (Chu et al. 2005) makes use of devices able to adjust, in real time, the mechanical parameters of the protection devices which passively interact with the structure without introducing large amount of energy.

3.5.1 Tuned Mass Damper

Tuned Mass Damapers (TMDs) are the most widespread passive control devices for the mitigation of tall buildings vibrations. The TMDs are devices consisting of a mass connected to the structure through a mechanical apparatus that emulates the behavior of a spring and a dashpot in parallel. This system is adjusted (tuned) to the fundamental frequency of the building. If optimally tuned, the movement of the mass counterbalances the displacement of the structure, with a consequent reduction of accelerations, displacements and vibrations (Soong and Dargush 1997). Figure 3.12 shows the schematic view of a SDOF (single degree of freedom) system to which a TMD is applied. The equations that describe the motion of a two degrees of freedom (system SDOF + TMD) system subject to an external force $F(t)$, can be written in the following form (Constantinou et al. 1998):

$$m_1\ddot{x}_1(t) + c_1\dot{x}_1(t) + k_1x_1(t) = k_2z(t) + c_2\dot{z}(t) + F(t) \tag{3.46}$$

$$m_{\mathrm{TMD}}\ddot{z}(t) + c_{\mathrm{TMD}}\dot{z}(t) + k_{\mathrm{TMD}}z(t) = -m_{\mathrm{TMD}}\ddot{x}_1(t) + g(t) \tag{3.47}$$

where x_1 is the the main structure displacement, $z(t)$ is the relative displacement of the added mass with respect to the structure, m_1 is the mass of the structure and m_{TMD} is the TMD's mass. The TMD damping and stiffness coefficients are denoted by c_{TMD} and

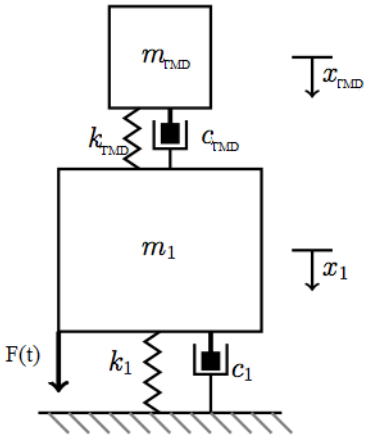

Fig. 3.12: A schematic representation of a system equipped with a TMD (*Tuned Mass Damper Applet*).

k_2 and c_1 and k_1 refers to the structure. The term $g(t)$ is nil in the case of wind excitation. By denoting the auxiliary device with the subscript TMD and the structure with subscript s, summation of Equations (3.46) and (3.47) leads to:

$$(m_{\mathrm{TMD}} + m_s)\ddot{x}_s(t) + c_2\dot{x}_s(t) + k_{\mathrm{TMD}}x_{\mathrm{TMD}}(t) = F(t) - m_{\mathrm{TMD}}\ddot{z}(t) \tag{3.48}$$

An important aspect in the study of TMD systems is to quantify the mass, useful for the proper operation of the TMD and compare it with the mass of the building to determine what increase in load the structure can handle. The mass of the TMD with respect to the total mass of the structure is commonly called mass ratio μ. The optimization of TMDs parameters is a topic extensively studied in literature. Den Hartog (1956) showed the dynamic effect of the TMD compared with the static deflection by applying the maximum force to the structure statically. Considering a sinusoidal force with frequency ω the dynamic amplification factor for an undamped structural system R is:

$$R = \frac{x_{\max}}{x_{\mathrm{st}}} = \sqrt{\frac{(\alpha^2 - \beta^2) + (2\xi\alpha\beta)^2}{[(\alpha^2 - \beta^2)(1 - \beta^2) - \alpha^2\beta^2\mu]^2 + (2\xi\alpha\beta)^2(1 - \beta^2 - \beta^2\mu)^2}} \tag{3.49}$$

wherein $\alpha = \omega/\omega_0$ is the forced frequency ratio, $\beta = \omega_{\mathrm{TMD}}/\omega_0$ is the frequency ratio, $\omega_{\mathrm{TMD}} = \sqrt{k_{\mathrm{TMD}}/m_{\mathrm{TMD}}}$ is the natural frequency of the TMD, $\omega_0 = \sqrt{k_s/m_s}$ is the natural frequency of the structural system and $\xi_{\mathrm{TMD}} = c_{\mathrm{TMD}}/2m_{\mathrm{TMD}}\omega_{\mathrm{TMD}}$ is the damping ratio of TMD. In Figure 3.13 the amplification factor R as a function of β and ξ_{TMD} is

shown for $\alpha = 1$ (tuned case), $\mu = 0.05$. From Figure 3.13 it can be noted that in absence

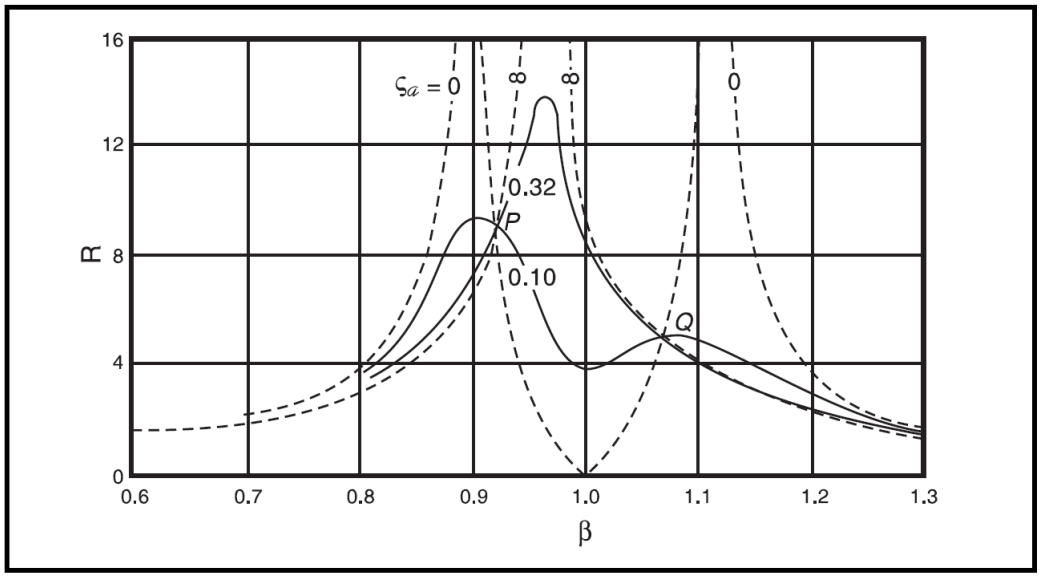

Fig. 3.13: Amplification factor as a function of $\beta = 0.05, \alpha = 1$ (Constantinou et al. 1998).

of structural damping, the response of the structure with TMD has infinite values in correspondence of the two resonant frequencies. When instead the TMD has infinite damping, the advantage of having installed the device fails and there is again a resonant condition. Between these conditions there are optimum values that make the peaks minimal.
The traditional approach for the TMD design seeks for the minimum TMD mass that guarantees the desired performance of the structure under random loading such as wind forces (Warburton 1982; Hoang et al. 2008). In Figure 3.14 the optimum absorbers parameters according to Warburton (1982) are shown. The main disadvantage of these devices is the fact that the control response is only obtained for the fundamental vibration modes, while, for the others, a slight reduction or even an amplification of the response can occur. This problem is solved by the introduction of more than one tuned masses MTMD (Multiple Tuned Mass Dampers). Numerous studies have been conducted to verify the actual efficiency of such systems compared to the TMDs (Patil and Jangid 2011; Huang et al. 2010; Moon 2010).
More recently, uncertainties in the dynamic properties of the structure have been consid-

Case	Excitation		Optimized Response		Optimized Absorber Parameter	
	Type	Applied to	Parameter Optimized (R)	R_{opt}	α_{opt}	ζ_{opt}
1	Force $P_o e^{i\omega t}$	Structure	$\frac{K y_1}{P_o}$	$\left(1+\frac{2}{\mu}\right)^{1/2}$	$\frac{1}{1+\mu}$	$\sqrt{\frac{3\mu}{8(1+\mu)}}$
2	Force $P_o e^{i\omega t}$	Structure	$\frac{M y_1}{P_o}$	$\left(\frac{2}{\mu(1+\mu)}\right)^{1/2}$	$\left(\frac{1}{1+\mu}\right)^{1/2}$	$\sqrt{\frac{3\mu}{8(1+\mu/2)}}$
3	Acceleration $\ddot{X}_g e^{i\omega t}$	Base	$\frac{\omega_s^2 y_1}{\ddot{X}_g}$	$\left(\frac{2}{\mu}\right)^{1/2}(1+\mu)$	$\frac{(1-\mu/2)^{1/2}}{1+\mu}$	$\sqrt{\frac{3\mu}{8(1+\mu)(1-\mu/2)}}$
4	Acceleration $\ddot{X}_g e^{i\omega t}$	Base	$\frac{\ddot{X}_g+\ddot{y}_1}{\ddot{X}_g}$	$\left(1+\frac{2}{\mu}\right)^{1/2}$	$\frac{1}{1+\mu}$	$\sqrt{\frac{3\mu}{8(1+\mu)}}$
5	Random Force	Structure	$\frac{<y_1^2>K^2}{2\pi S_o \omega_s}$	$\left(\frac{1+3\mu/4}{\mu(1+\mu)}\right)^{1/2}$	$\frac{(1+\mu/2)^{1/2}}{1+\mu}$	$\sqrt{\frac{\mu(1+3\mu/4)}{4(1+\mu)(1+\mu/2)}}$
6	Random Acceleration	Base	$\frac{<y_1^2>\omega_s^3}{2\pi S_o}$	$(1+\mu)^{3/2}\left(\frac{1}{\mu}-\frac{1}{4}\right)^{1/2}$	$\frac{(1-\mu/2)^{1/2}}{1+\mu}$	$\sqrt{\frac{\mu(1-\mu/4)}{4(1+\mu)(1-\mu/2)}}$

Notes: $<y_1^2>$ is the mean-square value of $y_1(t)$
S_o is force intensity in case 5 and acceleration intensity in case 6

Warburton, 1982

Fig. 3.14: Optimum absorbers parameters (Warburton 1982).

ered for the robust optimization of TMDs (Marano et al. 2013; Venanzi and Materazzi 2013; Venanzi 2015).

Chapter 4

The proposed Life-Cycle Cost Wind Design (LCCWD)

4.1 Introduction

The LCCWD approach, developed in its entirety to take full account of the major needs associated with the design of tall buildings under wind loads, provides the most cost-effective design solution. In this chapter the procedure is explained step-by-step. Each step of the procedure can be easily tailored with the aim to extend its applicability to different case studies.
The outline of the LCCWD procedure, schematically presented in Figure 4.1, can be summarized as follows:

1. Select the structural model (Section 4.9.1) and, eventually, the control system model (Section 4.3).
2. Select the wind hazard model (Section 4.4): wind tunnel measurements, mean-wind speed annual maximum and wind direction probability distributions.
3. Evaluate the structural response (Section 4.5).

4. Select the damage states associated to nonstructural components and evaluate the corresponding complementary cumulative distribution function (CCDF), i.e. the fragility curve (Section 4.6).

5. Compute the annual damage probability (Section 4.7).

6. Calculate the expected life-cycle cost (Section 4.8).

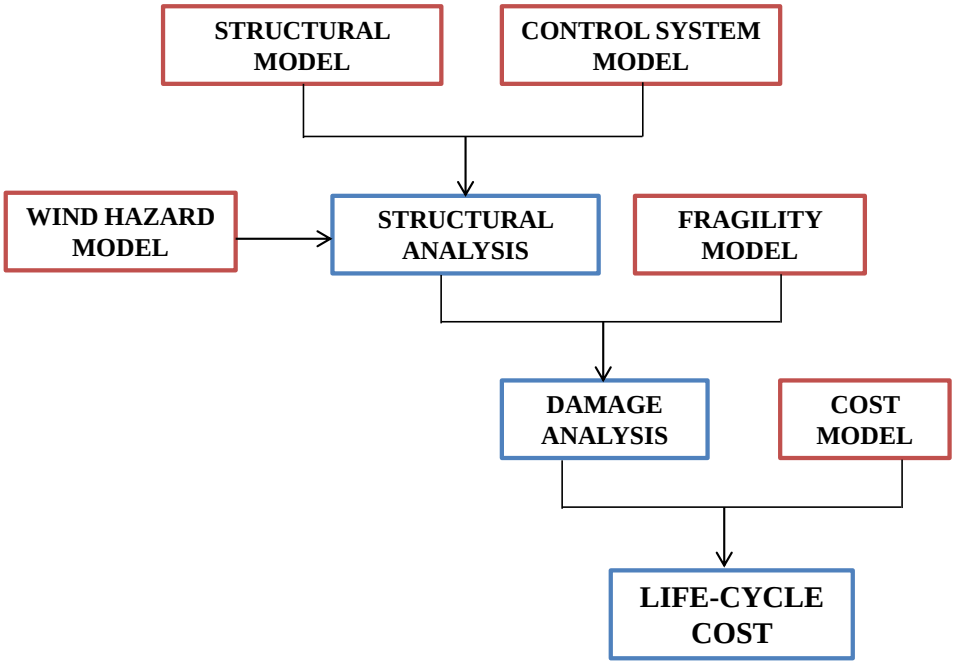

Fig. 4.1: Outline of the LCCWD procedure.

Differently from existing literature and previous studies, LCCWD is targeted at design purposes and it takes into account the long-term economical consequences and benefits for different design configurations. The key goal is to reach the best design solution by considering at the same time the structure of the building and all the boundary conditions that can compromise the correct fruiting.
As shown in Figure 4.2, in order to find the best design solution, different aspects of the design have to be investigated, like structural system, building orientation, type of control system, non structural elements. In order to compare the different solutions, for each

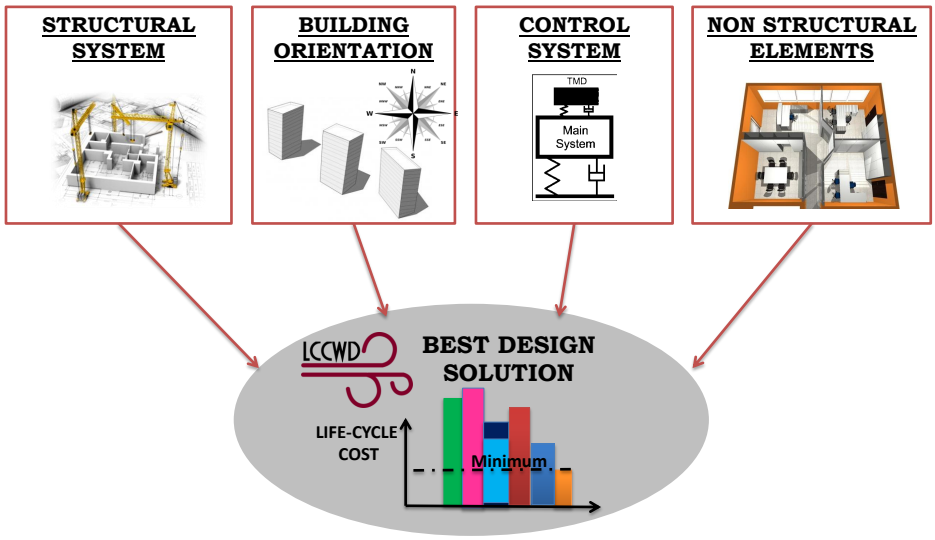

Fig. 4.2: Design alternatives flowchart.

design alternative of Figure 4.2, the LCCWD procedure (Figure 4.1) needs to be executed. With reference to Figure 4.2 the following aspects of the design can be addressed by LCCWD:

- The structural system, with reference to the shape, the materials and the geometry of the building.
- The building orientation considering the wind exposure with respect to the geographical location.
- The structural control system in order to reduce undesirable movements.
- The nonstructural elements (number, location and typology) which are considered as integrated elements of the design process since they are damage-sensitive.

The chapter is organized as follows:
Sections 4.2 to 4.8 present the necessary steps and equations for the comprehensive application of LCCWD as briefly summarized in Figure 4.1.
Section 4.9 reports some indication about the choice of the design solutions that can be

investigated and compared in order to achieve the best design solution with reference to Figure 4.2.
Section 4.10 describes how to summarize all the obtained results.

4.2 Structural model

In order to predict the full-scale behavior of the building a finite element model needs to be developed. Such aspects like the structural damping, the translational and torsional natural frequencies and the associated mode shapes define the dynamic characteristics of the structure. These information are crucial since they are used to predict equivalent static wind loads (through wind tunnel testing) to be applied to the building model (Section 4.4) and, consequently, are also used in the analyses to evaluate the structural response in terms of displacement or acceleration (Section 4.5).
As concerns the structural modeling, particular attention needs to be devoted to the soil–foundation–structure interaction. Indeed the soil deformability can modify the modal proprieties (natural periods/modal shapes) of the structure. Therefore under the hypothesis of high soil-structure inter-facial stiffness, the building can be modeled as fixed at the base. Alternatively, the soil can be described with elastic, nonlinear elastic, fully inelastic elements or hypoplastic macroelements (Venanzi et al. 2014).
In order to clarify the meaning of the symbols used in the following equations, Figure 4.3 illustrates a schematic view of the plan of a generic tall building. The angle δ denotes the building orientation with respect to the North-South direction. The angle θ characterizes the relative mean-wind incidence angle measured from the reference building axis x of the local coordinate system. The angle ψ refers to the torsional rotation.
The angle θ is used as a reference measure of direction, compatible with the building model orientation in standard wind tunnel experiments. A clockwise rotation is considered positive for δ and θ. The angle ψ is considered positive according to an anticlockwise rotation. The angle δ is evaluated with respect to the global coordinates system, i.e. X-axis facing South and Y-axis facing East. The angles θ and ψ are evaluated with respect to the local coordinates system which rotate firmly to the building plan. Hence the mean-wind direction angle is defined as the summation between the building orientation angle δ and the angle θ, in the global reference system:

$$(\theta+\delta) = \begin{cases} (\theta+\delta) & \text{if } (\theta+\delta) < 360^o, \\ (\theta+\delta) - 360^o & \text{if } (\theta+\delta) \geq 360^o. \end{cases} \tag{4.1}$$

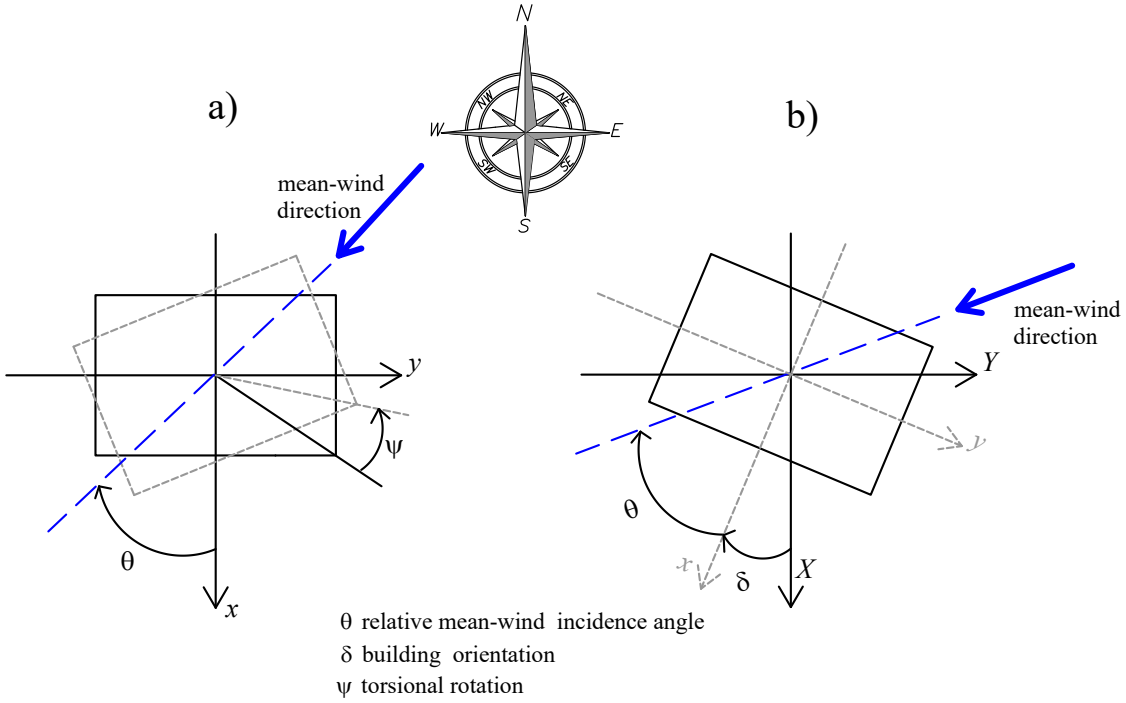

Fig. 4.3: Schematic view of the tall building denoting: (a) building orientation angle δ, relative mean-wind incidence angle θ; (b) torsional rotation ψ.

For the sake of clarity with reference to Figure 4.3, $(\theta+\delta) = 0°$ corresponds to a Northerly wind (wind which blows from the North).

4.3 Structural control system

The dynamic nature of the wind can cause discomfort to building occupants and can pose serious serviceability issues. As explained in Section 3.5, the performance of a tall building can be improved in many ways. In order to validate the procedure, LCCWD focuses on the use of passive auxiliary damping devices (TMD). The following information are required for the numerical application of LCCWD:

- mechanical and dynamic characteristics of the device to use them in the frequency domain formulation. In order to guarantee an optimal behavior, the TMD needs to be tuned to the fundamental frequencies of the structure (Den Hartog 1956).
- relative cost with respect to the total construction cost. Usually cost data are not

available in literature but they can be provided by the companies.

It is worth noticing the fact that the LCCWD formulation is general and can include different types of structural control.

4.4 Wind hazard model

This phase of the procedure is devoted to the accurate modeling of the wind load with respect to the structure and to the construction site (geographical location). Therefore, in order to meet target safety and performance levels during the design process, the LCCWD procedure requires the following input data:

1. wind tunnel simultaneous pressure measurements or alternatively HFFB records (Section 3.4) by considering specialized atmospheric boundary layer. These features can accurately represent the wind speed and turbulence profile acting on the structure. Wind tunnel tests provide the necessary design pressure measurements for the dynamic analysis of the building;

2. joint PDF of the reference mean-wind velocity at the building top V_{ref} and of the mean-wind direction angle θ. Indeed, since LCCWD is based on a probabilistic approach, the geographic site with its climate can greatly change the design conditions. Hence the wind in a certain place can be characterized by the mean speed value of the maximum annual distribution and by the incidence angle relative the prevailing winds.

4.4.1 Wind load time histories

The wind loads are represented as time-dependent generalized forces. The generalized loads of the fundamental lateral modes, associated with the turbulent wind pressure loads on the building's surface, are needed. These quantities can be directly evaluated from wind tunnel data via conventional HFFB tests or can be obtained by integrating synchronous wind pressure measurements (see Section 3.4). The evaluation of the time-dependent experimental aerodynamic forces is different if the wind tunnel test is performed according to the HFFB or the pressure integration techniques (Section 3.4).
A key point of the procedure relies on the indirect estimation of wind loading uncertainty by exploiting information derived from the time histories of the experimental pressure loads. In order to examine the measurement uncertainty, a long record of the total base bending

moments and base torque is divided in $i = 1, .., N$ segments of equal time duration Δt. Each i^{th} segment is treated as an independent realization of the generalized force which is labeled as $F_{Q_{i,k}}(t)$. The quantity t indicates time ($0 \leq t \leq T$) and $k = \{x, y, \psi\}$ is the index denoting the three principal response components (the displacements of the floors geometric centers in directions x and y and the torsional rotation ψ around the vertical axis z). The generalized forces and moments (with their appropriate units) $F_{Q_{i,k}}(t)$, from which the structural response is evaluated, can be written as:

$$F_{Q_{i,k}}(t) = \int_0^H f_{i,k}(z,t)[\Phi_k(z)]\mathrm{d}z \tag{4.2}$$

In the previous equation H is the building height, $f_{i,k}(z,t)$ is the i^{th} realization of the experimental aerodynamic force per unit height in the k direction calculated at height z (for example by local pressure integration); $\Phi_k(z)$ is the fundamental mode shape in the k direction. The mode shapes $\Phi_k(z) = \frac{z}{H}$ can be assumed to vary linearly along the height or it is possible to consider the general form, by adopting the following exponential formulation $\left[\frac{z}{H}\right]^{\gamma}$ with $0.5 \leq \gamma > 2$ (Holmes 1987). This leads to the following expression of the generalized forces and torsional moment:

$$F_{Q_{i,k}}(t) = \int_0^H f_{i,k}(z,t) \left[\frac{z}{H}\right]^{\gamma_k} \mathrm{d}z \tag{4.3}$$

By following standard approaches (Section 3.3.2), after removal of the mean load component from the fluctuating aerodynamic loads and some manipulation, the previous equation may be converted to frequency domain to obtain the generalized force spectrum. It is worth noticing that the spectral analysis is commonly used for structures under random vibrations (Denöel 2014). In particular the Welch's averaged modified period-gram method of spectral estimation is used to evaluate the power spectral density of the experimental realization of the generalized force (Welch 1967). The vector $F_{Q_{i,k}}(t)$ is segmented into K sections $(X_1, ..., X_K)$ of equal length L, each with 50% overlap. Each segment is windowed with a Hamming window $W(j), j = 0, .., L-1$. For each windowed segment the finite Fourier transform $A_1(n), A_K(n)$ is calculated:

$$A_k(n) = \frac{1}{L} \sum_{j=0}^{L-1} X_K(j) W(j) e^{-2kijn/L} \tag{4.4}$$

where $i = \sqrt{-1}$. Then, the K modified period-grams are evaluated:

$$I_k(f_n) = \frac{L}{U} |A_k(n)|^2 \tag{4.5}$$

where $k = 1, .., K$, $f_n = n/L$ with $n = 0, .., L/2$ and U is evaluated as follows:

$$U = \frac{1}{L} \sum_{j=0}^{L-1} W(j)^2 \tag{4.6}$$

The set of modified period-grams is averaged on all K segments to form the spectrum estimate.
The following normalized generalized force spectrum is adopted in the numerical analysis:

$$nS_{\hat{F}_{Q_{i,k=\{x,y\}}}}(n) = \frac{nS_{F_{Q_{i,k=\{x,y\}}}}(n)}{(1/2\rho V_{ref}^2 HD)^2} \tag{4.7}$$

where $S_{F_{Q_{i,x}}}$ and $S_{F_{Q_{i,y}}}$ are the one-sided dimensional power spectra of the i^{th} experimental realization of the generalized force in the x and y directions. The normalized-dimensionless power torque spectral density is similarly defined as follows:

$$nS_{\hat{F}_{Q_{i,\psi}}}(n) = \epsilon \cdot \frac{nS_{M_{i,\psi}}(n)}{(1/2\rho V_{ref}^2 HD^2)^2} \tag{4.8}$$

In the previous expression $S_{F_{Q_{i,\psi}}}$ is the dimensional power spectrum of the i^{th} experimental realization of the base torque (moment); ϵ is a correction factor, depending on the exponent of the power-law γ_k (Holmes et al. 2003; Tallin and Ellingwood 1985), used to correctly adjust the experimental evaluation of the uniformly distributed base torque along the height.
Wind tunnel tests are performed considering a rigid connection to the floor and aeroelastic effects are neglected. However it must be pointed out that in the case of tall structures exposed to wind flow, the interaction between inertial, structural and aerodynamic forces, particularly in the acrosswind direction can cause several undesirable phenomena (see Section 3.3.2). One of the main advantage of the LCCWD is the fact that the approach is general and adaptable and allows to specialize the models used over time. Therefore it is possible to incorporate aeroelastic models in the evaluation of the wind-induced response.

4.4.2 Joint probability distribution of mean-wind velocity and direction

To estimate the joint PDF of the yearly maxima of the mean-wind speed and of the mean-wind direction $f(V_{ref}, \theta)$, different approaches can be used. First, it is necessary to establish the geographical location of the building. In the case of available continuous experimental data on the mean-wind speed and on the direction for several years, the statistic correlation between the two variables can be matched. In terms of the strength of correlation, the value of the correlation coefficient can vary between 1 and -1. Only in the case of the correlation coefficient value lies around 0, the two variables can be considered uncorrelated and $f(V_{ref}, \theta) = f(V_{ref}) \cdot f(\theta)$.
Alternatively, if the variables cannot be considered uncorrelated it is possible to reconstruct the joint PDF from information provided by experimental data or literature. For example in Johnson and Wehrly (1978) parametric models are proposed for the numerical reconstruction of a general joint distribution considering bivariate random variables when one variable is directional and one is scalar. In Carta and Ramirez (2008) the previous method is specified in the field of wind energy including wind speed and direction. A statistical model is presented in Basile et al. (2015). An empirical method is also proposed in Chen and Zhang (2009). The importance of considering wind directionality effects related to the geographical location is emphasized in Yi and Li (2015).

4.5 Structural analysis

In order to limit the computational effort required by a life-cycle cost approach while still preserving adequate estimation accuracy, the structural analysis is carried out in the frequency domain by assuming that the response is dominated by the three fundamental lateral vibration modes (Cui and Caracoglia 2016b), two lateral bending modes and one torsional mode. The three modal components (mode shapes) are assumed as uncoupled (Caracoglia 2014). Hence the response can be determined independently in each direction. Three-dimensional mode shapes are not considered in this study but may be readily included without any loss of generality, also considering any inter-modal dependence for modes with closely-spaced frequencies.
The assumptions are made that both wind force and structural response are stationary multi-variate Gaussian processes and that the effects may be approximately cumulated using the SRSS (square root of the sum of the squares) approach. By combining flexural and torsional response, the peak lateral displacements at the top floor $D_{i,x,H}$ and $D_{i,y,H}$ ($z = H$) can be computed, for the i^{th} wind tunnel realization of the load, as:

$$D_{i,x,H} = (\bar{D}_{i,x} \pm \bar{D}_{i,\psi,x}) + \sqrt{(g_{i,x}\sigma_{i,x})^2 + (g_{i,\psi}\sigma_{i,\psi,x})^2} \tag{4.9}$$

$$D_{i,y,H} = (\bar{D}_{i,y} \pm \bar{D}_{i,\psi,y}) + \sqrt{(g_{i,y}\sigma_{i,y})^2 + (g_{i,\psi}\sigma_{i,\psi,y})^2} \tag{4.10}$$

In the previous equations $\bar{D}_{i,x}$ and $\bar{D}_{i,y}$ are the mean responses in x and y directions, $\bar{D}_{i,\psi,x}$ and $\bar{D}_{i,\psi,y}$ are the x and y components of the mean torsional response:

$$\bar{D}_{i,x} = \frac{mean[F_{Q_{i,x}}(t)]}{(2\pi n_{0,x})^2 \cdot M_x} \tag{4.11}$$

$$\bar{D}_{i,y} = \frac{mean[F_{Q_{i,y}}(t)]}{(2\pi n_{0,y})^2 \cdot M_y} \tag{4.12}$$

$$\bar{D}_{i,\psi} = \frac{mean[F_{Q_{i,\psi}}(t)]}{(2\pi n_{0,\psi})^2 \cdot M_\psi} \tag{4.13}$$

where M_x, M_y, M_ψ are the generalized masses corresponding to the three fundamental modes. The terms $g_{i,x}$, $g_{i,y}$, $g_{i,\psi}$ are the peak factors computed in accordance with the structural response spectrum and Davenport's theory for the three generalized displacements (see Section 3.3.2). In Eqs. (4.9)-(4.10), the terms $\sigma_{i,\psi,x}$ and $\sigma_{i,\psi,y}$ are the x and y components of the standard deviation and $\sigma_{i,\psi}$ pertains to the rotation. The standard deviations of the response components are computed for each i^{th} wind tunnel load realization from:

$$\sigma_{i,k}^2 = \int_0^{+\infty} S_{Q_{i,k}}(n)\mathrm{d}n \tag{4.14}$$

where $S_{Q_{i,k}}(n)$ is the one-sided response power spectral density obtained as:

$$S_{Q_{i,k}}(n) = |H_k(n)|^2 S_{F_{Q_{i,k}}}(n) \tag{4.15}$$

$|H_k(n)|$ is the absolute value of the modal transfer function defined from:

$$|H_k(n)|^2 = \frac{1}{(2\pi n_{0,k})^4 (M_k)^2 [(1 - (\frac{n}{n_{0,k}})^2)^2 + 4\xi_{0,k}^2 (\frac{n}{n_{0,k}})^2]} \tag{4.16}$$

In the previous expression, $n_{0,k}$ is the k^{th} natural frequency, $\xi_{0,k}$ is the structural damping ratio and M_k is the k^{th} modal generalized mass $M_k = \int_0^H m(z)\Phi_k^2(z)\mathrm{d}z$, where $m(z)$ is the mass per unit height of the building, H is the building height and $\Phi_k(z)$ is the k^{th} mode shape. No uncertainty in the physical building properties is assumed in this implementation, whereas variability in the wind loads and their spectrum is considered

through index i.
By considering the mode shapes, it is also possible to compute the peak displacements at a generic floor, identified through vertical coordinate z:

$$D_{i,x}(z) = (\bar{D}_{i,x}\Phi_x(z) \pm \bar{D}_{i,\psi,x}\Phi_\psi(z)) + \sqrt{(g_{i,x}\sigma_{i,x}\Phi_x(z))^2 + (g_{i,\psi}\sigma_{i,\psi,x}\Phi_\psi(z))^2} \quad (4.17)$$

$$D_{i,y}(z) = (\bar{D}_{i,y}\Phi_y(z) \pm \bar{D}_{i,\psi,y}\Phi_\psi(z)) + \sqrt{(g_{i,y}\sigma_{i,y}\Phi_y(z))^2 + (g_{i,\psi}\sigma_{i,\psi,y}\Phi_\psi(z))^2} \quad (4.18)$$

The choice of + or − sign in Equations (4.9)-(4.10)-(4.17)-(4.18) depends on the relative position of the considered point within each cross-section (or floor) of the building, as explained in Section 5.3.
Similarly, the peak acceleration at the building top floor is evaluated by combining the flexural and torsional accelerations as:

$$a_{i,H} = \sqrt{(g^a_{i,x}\sigma^a_{i,x})^2 + (g^a_{i,\psi}\sigma^a_{i,\psi,x})^2 + (g^a_{i,y}\sigma^a_{i,y})^2 + (g^a_{i,\psi}\sigma^a_{i,\psi,y})^2} \quad (4.19)$$

where $g^a_{i,k}$ is the acceleration-related peak factor. The standard deviations of the acceleration responses are:

$$[\sigma^a_{i,k}]^2 = (2\pi)^4 \int_0^{+\infty} n^4 S_{Q_{i,k}}(n)\mathrm{d}n \quad (4.20)$$

By considering the mode shapes, the acceleration at the generic floor (height z) is:

$$a_i(z) = \sqrt{(g^a_{i,x}\sigma^a_{i,x}\Phi_x(z))^2 + (g^a_{i,\psi}\sigma^a_{i,\psi,x}\Phi_\psi(z))^2} + \sqrt{(g^a_{i,y}\sigma^a_{i,y}\Phi_y(z))^2 + (g^a_{i,\psi}\sigma^a_{i,\psi,y}\Phi_\psi(z))^2} \quad (4.21)$$

In presence of a generic bidirectional TMD, intended to reduce one of the two fundamental modal responses ($h = x, y$), the response power spectral densities are modified as follows:

$$S_{Q_{i,h}}(n) = |H^{cs}_h(n)|^2 S_{F_{Q_{i,h}}}(n) \quad (4.22)$$

where the term $|H_h^{cs}(n)|$ is the transfer function (mechanical admittance) accounting for the presence of the control system which can be written as (Xu et al. 1992):

$$|H_h^{cs}(n)|^2 = \frac{(\chi^2 - \lambda^2)^2 + 4\chi^2\lambda^2\xi_h^2}{2\pi n_{0,h}^4 M_h^2(a^2 + b^2)} \tag{4.23}$$

In the previous expression μ is the mass ratio of the TMD and χ and λ are the frequency ratios (Equations (4.24) and (4.25)), $\xi_{\mathrm{TMD},h}$ is the reference damping ratio (Equation (4.26)), $n_{\mathrm{TMD},h}$ is the TMD's frequency.

$$\chi = \frac{n_{\mathrm{TMD},h}}{n_{0,k}} \tag{4.24}$$

$$\lambda = \frac{n}{n_{0,h}} \tag{4.25}$$

$$\xi_{\mathrm{TMD},h} = \frac{c_{\mathrm{TMD},h}}{(2\sqrt{m_{\mathrm{TMD},h}k_{\mathrm{TMD},h}})} \tag{4.26}$$

$$n_{\mathrm{TMD},h} = 1/2\pi\sqrt{k_{\mathrm{TMD},h}/m_{\mathrm{TMD},h}} \tag{4.27}$$

The coefficients a and b in the Equation 4.23 are given by:

$$a = \lambda^4 - \lambda^2(1 + \chi^2 + \mu\chi^2 + 4\xi_{0,h}\xi_h\chi) + \chi^2 \tag{4.28}$$

$$b = 2\lambda[\xi_h\chi(1 + \lambda^2 - \mu\lambda^2) + \xi_{0,h}(\chi^2 - \lambda^2)] \tag{4.29}$$

The optimum parameters of the TMD are evaluated according to Warburton (1982) equations for random force according to Figure 3.14.

4.6 Fragility model

Wind-exposed tall buildings can experience damage to non-structural components during their lifetime. Serviceability limit states are often underestimated during the preliminary design of a tall building but can cause local damages which may reduce the durability of the structure. Unacceptable deformations can affect the efficient use or the appearance of structural or nonstructural elements or the functioning of equipment and excessive vibrations can cause discomfort to people. An efficient and economical tall building cannot be designed without considering the damage probability over time of nonstructural components.

As confirmed by forensic engineering investigations after extreme wind hazards, adequate initial design usually avoids altogether such a problem in the case of engineered tall buildings; consequently, most attention is devoted to nonstructural damage. Therefore, the choice of the type of nonstructural elements is an important issue and, among the various factors, it is strictly related to the destination of use of the building.
In this context, the destination of use of the building is integrated in the design process. A single-function office tall building is chosen for the LCCWD approach since, as statistically reported in Figure 4.4, tall buildings are principally commissioned for office use. Therefore the economic interest associated with a high-rise buildings is an important issue that needs to be taken into consideration.

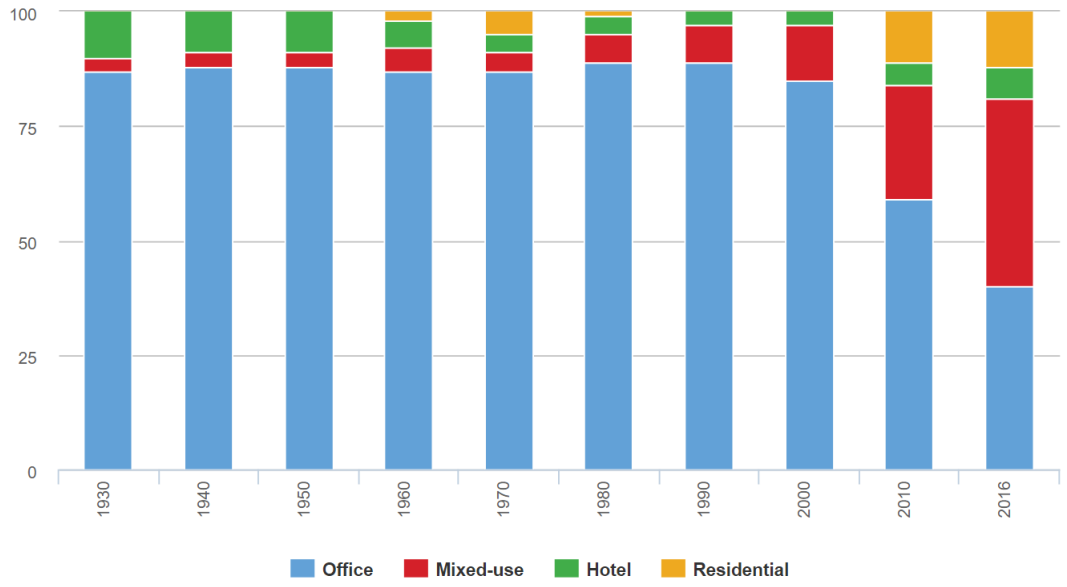

Fig. 4.4: World's 100 tallest classified by function (*Council on Tall Buildings and Urban Habitat, CTBUH*).

Nonstructural components can be traditionally classified into two main categories: (i) drift-sensitive elements where the risk damage is primarily a function of the interstory drift ratio (ii) acceleration-sensitive elements where the maximum sustainable damage depends on the peak floor acceleration.
Examples of drift-sensitive components are ceiling-high partitions, gypsum board partition,

curtain walls and façades. As these components are integrated with the main structure at different locations and heights of the building, the deformation follows the deflection profile.
In contrast, acceleration-sensitive elements are connected to the building floor (or wall) at single locations. Examples of acceleration-sensitive components are acoustical ceilings, vertical piping, mechanical-electrical components (boilers, pressure vessels, transformers, generators and air-conditioners). Others building's contents like heavy furniture items or library book shelves are also acceleration-sensitive components.
According to the probabilistic PBD approach the probability of damage to nonstructural elements is represented by fragility functions (Section 2.2.2). A fragility curve shows the relationship between the input excitation (such as interstory drift ratio or acceleration) and the probability of exceeding a certain damage state threshold. Fragility functions of nonstructural components are commonly modeled using a log-normal cumulative distribution function as follows:

$$P(D > d_i|X = x) = \Phi\left(\frac{1}{\beta_d} ln(x/\theta_d)\right) \tag{4.30}$$

In the previous equation D is the uncertain damage, d is a certain value of D, X is the uncertain EDP, x is a particular value of X, Φ represents the standard normal cumulative distribution, θ_d is the median and and β_d is the standard deviation. Both θ_d and β_d refer to d.

Different methods can be used to create Fragility functions (Porter et al. 2007):

- *Empirical method.* Fragility curves can be created by exploiting experimental tests or by real world observations. Since PBD is well established in earthquake engineering for the seismic performance assessment of buildings, an accurate database (PACT), which includes a collection of fragility and consequence data for the most common structural systems and building occupancies, is available online (FEMA-P-58 2012a). Most of the fragility functions are derived from post-earthquake observations or experimentally. Furthermore in Hazus (2017) statistical parameters for fragility functions of generic nonstructural drift and acceleration-sensitive components are presented as a function of the damage level that the building can experience: slight, moderate, extensive and complete (see Tables 4.1 and 4.2). The standard deviation values are calibrated considering the uncertainty in the damage state threshold but also the variability in the capacity properties of the building and in the ground motion. For completeness it should be noted that some modification to these fragility

Table 4.1: Drift ratios used to define median values of damage for nonstructural drift-sensitive components (Hazus 2017).

Damage level	IDR_m %	σ_{IDR}
DS1-IDR: slight	0.4	0.5
DS2-IDR: moderate	0.8	0.5
DS3-IDR: extensive	2.5	0.5
DS4-IDR: complete	5.0	0.5

Table 4.2: Peak floor accelerations used to define median values of damage for nonstructural acceleration-sensitive components (Hazus 2017).

Damage level	a_m %	σ_a
DS1-a: slight	0.25	0.6
DS2-a: moderate	0.5	0.6
DS3-a: extensive	1.0	0.6
DS4-a: complete	2.0	0.6

curves can be considered in order to take into account the uncertainties associated to the experimental nature of these curves (Kiani et al. 2016; Yamin et al. 2017).

- *Numerical method.* Fragility curves can be numerically reconstructed through Equation (4.30) by making use of numerical simulations of specific elements on the basis of the material resistance (Filliben et al. 2002).

- *Expert opinion-based method.* In this case fragility curves can be derived from the judgment of experts who have experience with the specific asset class. In many cases the empirical method and the expert opinion-based method can be considered complementary.

For the numerical simulations, the LCCWD procedure utilizes structural fragility curves, experimentally derived and available in literature. Because of the lack of experimental data for wind-induced damages, the seismic fragility curves are taken by the FEMA (Federal Emergency Management Agency) database (Chuang and Spence 2017). Such experimental curves are provided for unit elements, i.e. specific dimensions and characteristics related to each element. As introduced in Section 2.2.2, the fragility curves represent the CCDF

of a selected structural or non structural component as a function of a specific engineering demand parameter (EDP).
For the purpose of this thesis the following nonstructural elements are considered:

- glass façades (drift-related damages)
- partition walls (drift-related damages)
- suspended ceilings (acceleration-related losses)

It is worth noticing the fact that the procedure could easily incorporate different elements and types of damage.
For example, damage to façades can be induced by strong winds producing disproportionate lateral interstory drifts, accelerations, large pressures loads at specific locations of the structural envelope or by impact of wind-borne debris. Only in the case of occurrence of very strong wind events like tornadoes, the building can experience structural damage and collapse of structural members (LaFave et al. 2016). Recent studies (Verma et al. 2013) aimed at the experimental evaluation of pressure coefficients on the surfaces of a square plan tall building model. The wind pressures on the surface are in this phase neglected but they can be incorporated in the LCCWD analysis. Indeed, starting from the pressure distribution on the façades, the pressure coefficients C_p can be used as an EDP parameter. Further investigations must be done to estimate the fragility curves that relate the probability of damage to the pressure coefficient considering a specific technology of glass façades.
Also occupants discomfort-related losses can be taken into account, especially in the case of office buildings. In this case fragility curves can not be evaluated on the basis of the repair/replacement costs but on the basis of downtime losses. In fact in this case losses do not emanate from property damage but to business downtime when occupants of the top floors have to leave their workplace or are not able to work because of the building oscillations.

4.7 Damage analysis

The core of the LCCWD procedure is the computation of the probability of exceeding a damage state (damage analysis), which is used for the cost evaluation (cost analysis).
The original formulation of the convolution integral as defined in Section 2.2.2 was formulated for computing the mean annual rate of a performance measure exceeding a specified

threshold. However, it has also been used for computing the probability that a performance measure will exceed a specified threshold during a given period of time (Kiureghian 2005). Hence Equation (2.3) is modified in this study to evaluate the annual damage probability in the k direction associated with the limit state j and accounting for the building orientation δ as follows:

$$P_j^h(\delta, z) = \int\int\int\int P[DS_j(z)|EDP] f[EDP|IM, SP, IP] \\ f(IP|IM, SP) f[IM(\delta)] f(SP) \mathrm{d}(EDP) \mathrm{d}(IP) \mathrm{d}(IM) \mathrm{d}(SP) \quad (4.31)$$

where DS_j is the j^th damage state; EDP is the vector collecting the engineering demand parameters (i.e. structural response components) inducing the damage; IM is the vector of the intensity measure; SP is the vector of the parameters characterizing the structural system; IP is the vector of the interaction parameters (aerodynamic and aeroelastic parameters); $P(DS_j(z)|EDP)$ is the structural fragility curve (i.e. the complementary cumulative distribution function of DS_j conditional on the occurrence of EDP at height z); $f(EDP|IM, SP, IP)$ is the probability density function (PDF) of EDP conditional on IM, SP and IP; $f(IP|IM, SP)$ are the joint PDFs of the IP components conditional on IM and SP, $f[IM(\delta)]$ are the joint PDFs of the components of the intensity measure vector as a function of the building orientation angle δ; $f(SP)$ are the joint PDFs of the components of the vector SP; z is the generic height within the building.

In a typical wind engineering application, the random components of the intensity measure vector IM are: the 10-minute average mean-wind speed at a reference elevation (i.e. the building's top floor, V_{ref}) and the mean-wind direction $(\theta+\delta)$ as defined in Equation (4.1). The joint PDF of the intensity measure vector is designated as $f(V_{ref}, \theta + \delta)$ and it refers to the mean-wind direction angle.

The vector of interaction parameters IP is composed of the aerodynamic coefficients, i.e. determined from the pressure data measured in the wind tunnel.

It is assumed that, without any loss of generality, SP (building mass, stiffness, damping) are deterministic and that the randomness of IP is taken into account as explained in Section 4.4.1. The integration is carried out considering the mean-wind direction angle $(\theta+\delta)$ as the integration variable, noting that $\mathrm{d}(\theta + \delta) = \mathrm{d}\theta$. Consequently, the convolution

integral in Eq. (4.31) becomes:

$$P_j^h(\delta, z) = \int\int\int P(DS_j(z)|EDP(\theta))f(EDP|V_{ref}, \theta) \\ f(V_{ref}, \theta + \delta)\mathrm{d}(EDP)\mathrm{d}(V_{ref})\mathrm{d}(\theta) \quad (4.32)$$

It is worth observing that, in the presence of a prevailing wind direction, the joint PDF of the IM vector, $f(V_{ref}, \theta + \delta)$ accounts for the building orientation angle δ. Moreover, the parameter EDP only depends on the relative mean-wind incidence angle θ since the structural analysis is conducted in accordance with the local coordinate system x, y.
In the case of a structure equipped with TMD, the annual probability of exceeding a damage state j depends on the specific choice of the control system. The control system is characterized by a vector CS collecting the parameters of the TMD (i.e. mass, stiffness and damping). The annual damage probability can be written as follows:

$$P_{j,cs}^h(\delta, z) = \int\int\int P(DS_j|EDP(IM, CS))f(EDP|IM, CS) \\ [f(IM, \delta)]\, f(CS)\mathrm{d}(EDP)\mathrm{d}(IM)\mathrm{d}(CS) \quad (4.33)$$

with the same meaning of symbols as in Eq. 4.31. The joint probability of EDP is conditional on V_{ref} and θ but it also depends on the selected control system CS, since the dynamic structural response is mitigated by the presence of the TMD. Although, in principle, the components of the vector CS could be considered random parameters, they will be assumed as deterministic in the following. By substituting the vector $IM = \{V_{ref}, \theta\}$, Eq. 4.33 is specialized as follows:

$$P_{j,cs}^h(\delta, z) = \int\int\int P(DS_j|EDP(V_{ref}, \theta, CS))f(EDP|V_{ref}, \theta, CS) \\ f(V_{ref}, \theta + \delta)\mathrm{d}(EDP)\mathrm{d}(V_{ref})\mathrm{d}(\theta) \quad (4.34)$$

In order to better clarified the previous equations, the damage probability is evaluated in each principal direction ($h = x, y$) and for each floor of the building, characterized by the variable z.

4.8 Cost analysis

The cost analysis evaluates the total expected repair and intervention costs over a time period t corresponding to the lifetime of a structure.
Without loss of generality, the ordinary maintenance and structural replacement costs are neglected, as well as the indirect business losses associated with activity interruption. Indeed, considering the ultimate purpose of comparing different design solutions, it is assumed that these costs do not vary much between different design alternatives.
The cost evaluation is based on the assumption that the structure is restored to its original condition after each occurrence of the wind-induced damage. For the sake of simplicity and as a first approximation in the absence of more-detailed design plans, the initial construction cost $C_{0,s}$ is assumed to be independent of the building orientation angle δ.
The total expected total life-cycle cost (Wen 2001; Wen and Kang 2001) is computed as the sum of the initial cost $C_{0,s}$ (deterministic) and the expected repair costs in each k direction in each floor of the building at a generic height z:

$$E[C^k(t,\delta,z)] = C_0 + E[\sum_{l=1}^{L}\sum_{j=1}^{K} C_j e^{-\lambda t_l} P_j^k(\delta,z)] \tag{4.35}$$

In the previous equation $E[.]$ denotes expected value; l is the loading occurrence number; L is the total number of loading occurrences between time 0 and time t; j is the damage state number; K is the total number of damage states under consideration; C_j is the cost of j^{th} damage state supposed as a deterministic quantity; λ is the discount rate per year; t_l is the loading occurrence time assumed as a uniform Poisson process between 0 and t. The arrival times of each storm, t_l, are simulated as uniformly distributed over the time interval by Monte Carlo sampling.
The quantity $P_j^k(\delta,z)$ is the probability of exceeding the j^{th} damage state given the mean arrival rate ν per unit time (i.e., number of events per year) (Mitropoulou et al. 2011) for a given building orientation δ:

$$P_j^k(\delta,z) = -\frac{1}{\nu t} log[1 - P_{tj}^k(\delta,z)] \tag{4.36}$$

where P_{tj}^k is the t-year probability of exceeding the damage state in the k direction, defined as follows:

$$P_{tj}^k(\delta,z) = 1 - [1 - P_j^k(\delta,z)]^t \tag{4.37}$$

where $P_j^k(\delta, z)$ is the annual damage probability evaluated through damage analysis, as explained in the previous Section 4.7, dependent on the building's floor at a generic height z. It is worth noticing that, with respect to the original formulation by Wen (Section 2.2.3) that considers the probability of limit state crossing, in Equation (4.35) the probability of exceeding a certain damage state is considered. The use of probability of exceeding a damage state (a level of damage) instead of a limit state (a response threshold) allows accounting for the randomness of damage occurrence given a specific value of the structural response.

Considering the presence of the TMD, the index cs is introduced and the initial construction cost C_0 can be defined as the summation of the initial building cost (without the TMD) $C_{0,s}$ and the initial cost of the passive control system $C_{0,cs}$ (installed during construction stage at $t = 0$), i.e. $C_0 = C_{0,s} + C_{0,cs}$. Therefore Equation (4.35) becomes:

$$E[C_{cs}(t, \delta, z)] = C_{0,s} + C_{0,cs} + E[\sum_{z=1}^{H} \sum_{k=x,y} \sum_{l=1}^{L} \sum_{j=1}^{K} \hat{n}_j^k(z) C_j e^{-\lambda t_l} P_{j,cs}^k(\delta, z)] \tag{4.38}$$

where $\hat{n}_j^h(z)$ is the number of units of nonstructural elements sensitive to the j^{th} type of damage at height z in the $h = x, y$ direction and C_j is the unit cost associated with the replacement or repair of the selected nonstructural element. $P_{j,cs}^k$ is computed as in Eq. 4.34. The summation terms in Eq. 4.38, with index z varying between 1 and H and index k, are employed to separately examine all the nonstructural elements in both principal directions and for each floor.

The previous expression implies that periodic maintenance of the control system is either accounted for in $C_{0,cs}$ or substantially absorbed by the standard maintenance building costs, which are not considered in the cost accumulation [since these cost items are substantially independent of wind damage occurrence and the primary use of Equation (4.38) is for the comparison among design scenarios].

It should be noted that, since the FEMA fragility curves are derived from the standard unit elements (Figure 5.13), the damage probability of each floor evaluated through Equation (4.34) is associated to the damage of the single unit element. For this reason, with the aim to evaluate the overall cost of the building according to Equation (4.38), it is necessary to introduce the number of unit elements at the floor level for each direction and for each type of nonstructural component $\hat{n}_j^h(z)$.

Considering in Eq. (4.36) and Eq. (4.37) the presence of the TMD with the index cs, a simplification is introduced below [Eq. (4.39)], which evaluates the expected value of the

relative intervention and repair cost $c_{cs}(t,\delta)$ normalized with respect to the initial construction cost $C_{0,s}$. The normalized cost $c_{cs}(t,\delta)$ represents the portion of the lifetime cost that is directly connected to the repair and maintenance induced by the wind damage and, contrary to other cost items, is a function of the building orientation δ. Consequently $c_{cs}(t,\delta)$ is exclusively needed to determine the optimal orientation. Eq. 4.38 is rewritten as:

$$c_{cs}(t,\delta) = E[\frac{C_{cs}(t,\delta,z) - C_{0,s}}{C_{0,s}}] = c_{0,cs} + E[\sum_{z=1}^{H}\sum_{k=x,y}\sum_{l=1}^{L}\sum_{j=1}^{K}\hat{n}_j(z)c_j \\ e^{-\lambda t_l}[-\frac{1}{\nu t}\log(1 - P_{tj,cs}(z))] \quad (4.39)$$

with normalized costs $c_j = C_j/C_{0,s}$, $c_{0,cs} = C_{0,cs}/C_{0,s}$ and $P_{tj,f,cs} = 1 - [1 - P_{j,f,cs}]^t$. This probability $P_{tj,cs}(z)$ may be different at each floor and for a given nonstructural element as a result of the nonlinear mode shapes. The quantity $c_{cs}(t,\delta)$ above is preferable to cross-examine various life-cycle investment scenarios and to evaluate the relative differences between wind-damage-induced intervention costs with and without installation of the control system.

4.9 Alternative design solutions

It is worth noting that comparative design solutions can be numerous and the designer has to select the most suitable alternative for the customer. The design can regard different aspects of the project (Figure 4.2) as detailed in the following section.

4.9.1 Structural configuration

The model should be designed considering the fact that structural system has the main objective of safely carrying gravity and lateral loads. The principal required functions are the structural safety and the serviceability. Hence the design criteria are strength, serviceability, stability and human comfort. As reported in Jayachandran (2009), the strength is satisfied by limit stresses, while serviceability is satisfied by drift limits in the range of $H/500$ to $H/1000$. Stability is satisfied by sufficient factor of safety against buckling and P-Delta effects. The human comfort aspects are satisfied by accelerations in the range of 10 to 25 milli-g, where g=acceleration due to gravity, about $9.81 m/sec^2$.

The aim of the structural engineer is to arrive at suitable structural schemes, to satisfy these criteria. It is worth noticing that there is not a single solution that meets at the same time all the required limits at the beginning. However, it is necessary that the fulfillment of the criteria is maintained over time. It is therefore appropriate to compare different life-cycle cost-based solutions.
Regarding the structural system carrying vertical and lateral loads, tall buildings can be classified as:

- steel structures: the main vertical/lateral structural elements and the floor systems are made of steel. Note that a building of steel construction with a floor system of concrete planks or concrete slab on top of steel beams is still considered a steel structure;
- concrete structures: the main vertical/lateral structural elements and the floor systems are made of concrete;
- mixed-structures: utilize distinct steel and concrete systems, one on top of the other. Steel/concrete indicates a steel structural system located on top of a concrete structural system, with the opposite true of concrete/steel.
- composite structures: a combination of both steel and concrete components are used together in the main structural elements. Examples include buildings which utilize: steel columns with a floor system of concrete beams; a steel structure with a concrete core; concrete-encased steel columns; concrete-filled steel tubes; etc.

The most commonly used are steel or composite structures (Taranath 2012; Günel and Ilgin 2014). For the numerical applications, as detailed in Chapter 5, a steel structure is chosen.
As the height of the building increases, the alternatives in the choice of the structural system become restricted. Structural systems involve horizontal and vertical systems. The role of steel members is principally devoted to carry gravity loads. Others elements like outriggers, megaframes, and interior super-diagonals have the function of resisting wind and seismic loads. Moreover there are a lot of lateral brace systems like: interacting system of braced and rigid frames (not exceeding 40–50 stories), outrigger and belt truss systems (40–50 stories), framed tubes (50–60 stories), trussed tubes (60–70 stories), bundled tubes (80–100 stories), high efficiency systems for super tall buildings (100–150 stories).
A composite construction is characterized by the interactive behavior between structural

steel and concrete components designed to take advantage of the best load-resisting characteristics and economy of each material. Lateral load resisting elements can be summarized in the following structural units: composite slabs, composite beams, composite columns, composite diagonals, composite shear walls.
The structural system is the main part of the building which carries and transfers the loads, both vertical and lateral, safely to the soil through the foundation. The selection of the structural system must meet different aspects such as economic resources or architectural requirements. Therefore it is a designer choice and it is based on personal experience considering the fact that different solutions are able to satisfied the required design criteria.

4.9.2 Building orientation

In the design of a tall building, particularly susceptible to the wind action, it can not be neglected the probabilistic investigation on the prevailing winds (intensity and direction) distribution related to the specific geographical location. The main objective is the reduction of the wind effects on the structure, by changing its orientation. The primary role of building orientation in a performance-based design setting has been clearly emphasized by researchers (Jain et al. 2001).
In this context the results of the LCCWD procedure provide useful information to the designers and assistance to the selection of the orientation that minimizes the total life-cycle cost.
It is worth noticing that the orientation of a tall building in an existing urban context could be significantly constrained by the presence of neighboring buildings or by architectural and functionality issues. These aspects are neglected in the numerical application of LCCWD, but they could be easily incorporated.

4.9.3 Structural control

As explained in Section 3.5, the performance of a tall building can be improved by using different control techniques. The LCCWD approach can include all the different types of structural control with the final aim to compare different cost-effective solution.
As underlined in Section 4.3, for the purpose of this thesis, the LCCWD procedure is validated by making use of a TMD (Section 3.5.1). Parametric analyses on the TMD's characteristics (mass ratio) and on the TMD's cost, offer the possibility to explore different cost-based design alternatives.

4.9.4 Nonstructural elements: indoor distribution

The management of the interior spaces is related to the destination of use of the building and it is generally established by developers and investors. There is the possibility to design for single use or mixed-use, which include different types of functions such as commercial, business, hotel, residential, recreational, parking and similar. The choice of appropriate internal layout of the building plays a fundamental role in the structural design as it:

- guarantees the correct usability of the spaces according to the destination of use by providing comfortable and convenient workplace or living space;
- allows the adequate selection and distribution of nonstructural elements.

This last aspects can not be underestimated for the overall design of the building because nonstructural elements are damage-sensitive.
LCCWD approach highlights the increasingly need for an integrated design that, on the basis of cost-dependent solutions, brings together different areas of design that, in the current practice, are separated.

4.10 LCCWD global results

On the basis of the stakeholder's requests and taking advantage of his personal experience, the designer must be able to provide design alternatives that are easily comparable and understandable. As a global result the LCCWD procedure proposes a final chart summarizing all the investigated solutions. The graphical representation of the results must contain the following information:

- a brief description of all the proposed solutions identified with the acronym DC (Design Configuration);
- the expected cost corresponding to a certain value of the lifetime (expressed in years);
- any parameters useful for comparing the different solutions.

Chapter 5

The case study

5.1 Description of the structure and the FE modeling

The case study is a steel tall building, 180 m high, with a rectangular floor plan (cross section) characterized by a side ratio $B/D = 1 : 1.5$ and an aspect ratio $H/B = 6 : 1$ (Figure 5.1). The well known CAARC building is used as a benchmark in this research. This prototype had been introducted in 1980 by the Commonwealth Advisory Aeronautical Research Council of Australia as a benchmark high-rise structure to be employed for studying the wind-induced dynamic (Melbourne 1980).

The main wind force resisting system is composed of columns, central square core, beams and cross-bracing in both directions. All the structural elements are made of steel with a specific weight corresponding to 7700 Kg/m^3. The columns have a square hollow sections with gradually decreasing dimensions along the building height (every ten floors). The geometrical characteristics are illustrated in Table 5.1 where t_3 is the outside depth, t_2 is the outside width, t_f is the flange thickness, t_w is the web thickness. A system of steel columns and cross-bracing characterize the internal core. A schematic representation of the internal core brace distribution along the two main directions is shown in Figure 5.2, i.e. square-based prism ($15x15\ m$) centered in the geometric centroid of the plan section of

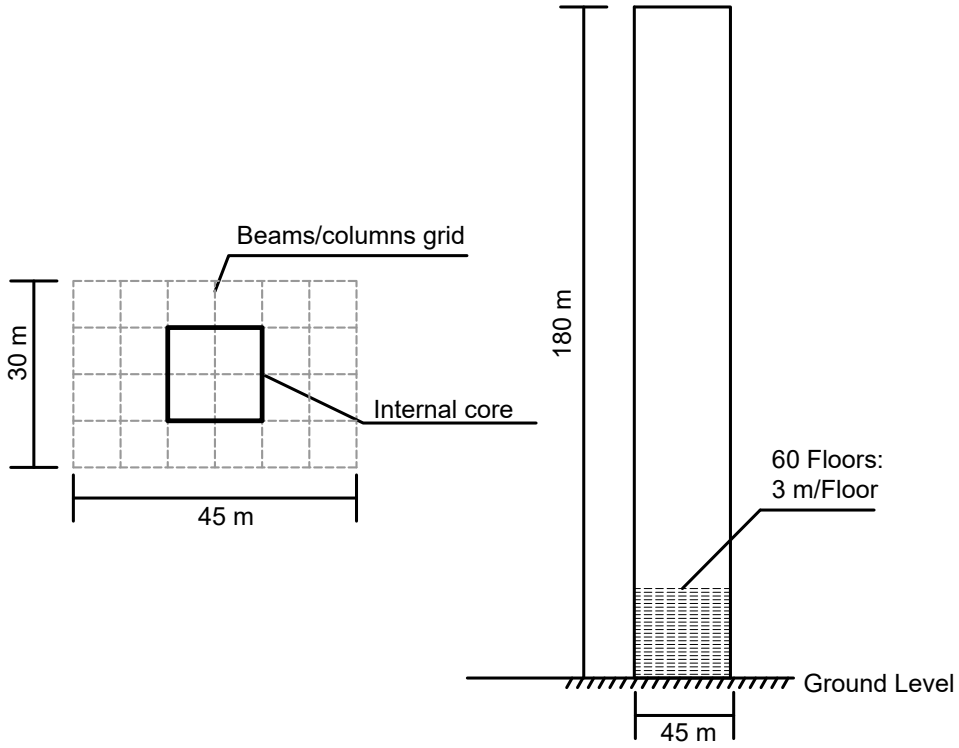

Fig. 5.1: Schematic view of the 60-stories building.

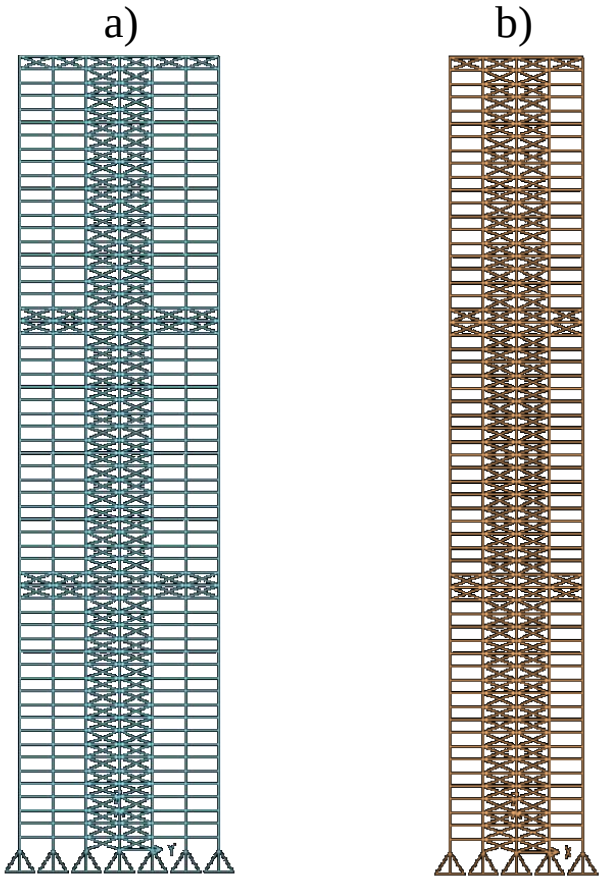

Fig. 5.2: Schematic view along the height of the central core in the two main directions.

the building (Figure 5.1). The bracings have a rectangular hollow section and have larger dimensions in the first 10 floors, an intermediate section between floor 11 and floor 40 and a reduced size for the last 20 floors (Table 5.2).

Structural hollow sections for columns and braces are chosen as they guarantee a higher resistance capacity with respect to an open section of a similar size and area. Indeed the radius of gyration is significantly higher with a much lower slenderness ratio for the same effective length.

The support of the concrete slabs is entrusted to beams characterized by an I-shaped cross-section. The I-beams of each floor have the same cross-section dimensions, as detailed in Table 5.3. It is worth noticing that the symbols used in this Table to describe the geometry

Table 5.1: Geometrical characteristics of the columns.

Columns	$t_3(m)$	$t_2(m)$	$t_f(m)$	$t_w(m)$
C1-10	0.7	0.7	0.05	0.05
C11-20	0.6	0.6	0.05	0.05
C21-30	0.6	0.6	0.04	0.04
C31-C40	0.6	0.6	0.03	0.03
C41-C50	0.5	0.5	0.02	0.02
C51-C60	0.4	0.4	0.015	0.015

Table 5.2: Geometrical characteristics of the diagonal cross-bracing.

Bracings	$t_3(m)$	$t_2(m)$	$t_f(m)$	$t_w(m)$
D1-10	0.5	0.3	0.015	0.015
D11-40	0.4	0.3	0.015	0.15
D41-60	0.3	0.25	0.012	0.012

of the section have the following meanings: t_3 is the outside height, t_2 is the top flange width, t_f is the top flange thickness, t_w is the web thickness, t_{2b} is the bottom flange width, t_{fb} is the bottom flange thickness.

A 3-D finite element model (Figure 5.3) is built for the preliminary sizing of the structural elements with respect to the static vertical and lateral loads. The Eurocode's standards are use for this first phase.

A simplified dynamic model of the system with rigid floor slabs and 3 DoF (degrees of freedom) for each floor is extracted from the full 3D model, which correctly reproduces the first three modes of the structure. The first two modes are translationals and the third one is torsional. The mass matrix is directly evaluated according to the steel sections defined previously. Unitary lateral loads and unitary torque moments have been inserted into all nodes of the central pillars. The stiffness matrix was calculated by inverting and combining the vector containing displacements and rotations due to unitary external

Table 5.3: Geometrical characteristics of the I-beams.

Beams	$t_3(m)$	$t_2(m)$	$t_f(m)$	$t_w(m)$	$t_{2b}(m)$	$t_{fb}(m)$
B1-60	0.24	0.12	9.8E-3	6.2E-3	0.12	9.652E-3

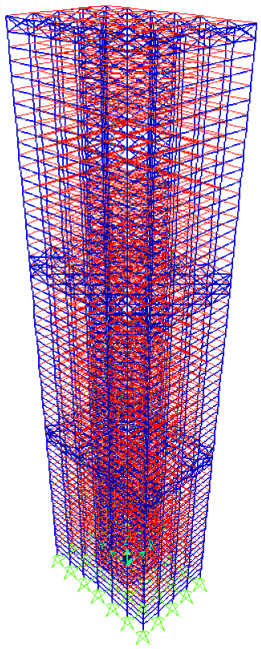

Fig. 5.3: 3D-view of the 60-story building.

loads. The principal modal characteristics of the building and the assumptions made for the simplified model are reported in Table 5.4. The vibration modes are assumed uncorrelated.

In order to select the coefficients γ_k $(k = x, y, \psi)$ used in Equation (4.3), the following functional is minimized:

$$Z = \sum_{k=x,y,\psi} (1 - \mathrm{MAC}_{kk}) \tag{5.1}$$

where MAC_{kk} is the Modal Assurance Criterion coefficient, the well-known estimator of the correlation between eigenvectors introduced by Allemang and Brown (1982). MAC coefficient allows to obtain information about the correlation between two mode shapes. Indeed the MAC coefficient describes the consistency between two mode shapes Φ and Φ^*. MAC takes values from 0, representing no consistent correspondence, to 1, representing a consistent correspondence. MAC is defined by Equation (5.2):

$$MAC = \frac{\|[\Phi]^T[\Phi^*]\|^2}{[\Phi]^T[\Phi][\Phi^*]^T[\Phi^*]} \tag{5.2}$$

In Figure 5.4 the discrete-model (FEM) modes and the continuous power-law function

Table 5.4: Modal characteristics of the simplified dynamic model of the building and coefficients of the power-law function mode shapes

Mode	Direction	n [Hz]	ξ [%]	γ_k	MAC_{kk}
1	x	0.228	1	1.24	0.9997
2	y	0.234	1	1.20	0.9996
3	ψ	0.237	1	0.75	0.9982

modes are compared.

5.2 Characterization of the wind load

5.2.1 Wind tunnel records

The aerodynamic loads are obtained from measurements on a scaled model of the building, tested in the boundary layer wind tunnel at the Inter-University Research Center for Building Aerodynamics and Wind Engineering (CRIACIV), in Prato (Italy).
A suburban terrain wind speed profile (boundary layer described by a power-law model with exponent approximately equal to 0.25) is used to numerically simulate the experimental conditions. Tests are conducted on the rigid model of the benchmark building (geometric scale 1:500) at various mean-wind directions between 0° and 360° with 22.5° step increments. The wind forces are determined over a set of 120 pressure taps, 30 taps on each vertical face, equally divided into 5 levels. The sketch in Figure 5.5 shows the repartition of the pressure taps along the building façades. The acquisition duration is 30 seconds with a corresponding acquisition frequency of 250 Hz. The wind tunnel set-up reproducing the suburban terrain conditions is shown in Figure 5.6.
As an example the pressure coefficients distribution for each principal façade of the building is shown in Figure 5.7 corresponding to 0° mean-wind direction. As explained in the previous Section 4.4.1, a key point of the approach is the estimation of the uncertainties related to wind tunnel measurements. To account for measurement variability (Section 4.4.1), the 30 s long wind tunnel pressure records are divided in 8 segments, having a duration corresponding to ten minutes at full scale. Each segment is treated as an independent realization of the generalized force, from which the structural response is independently evaluated. Figures 5.8a) and 5.8b) respectively illustrate the i^{th} realization of the normalized generalized force power spectra (PSDs) in the x and y directions as a function of the reduced frequency, at $(\theta + \delta = 0°)$. The normalized power torque spectral density is

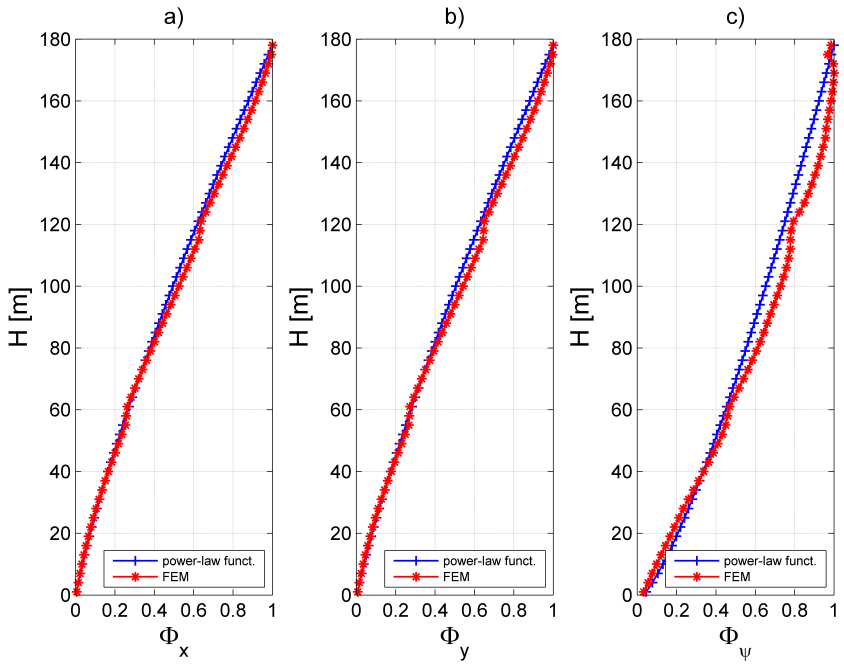

Fig. 5.4: Discrete-mode (FEM) vs continuous power-law function vibrations modes: a) flexural mode in direction x, b) flexural mode in direction y, c) torsional mode.

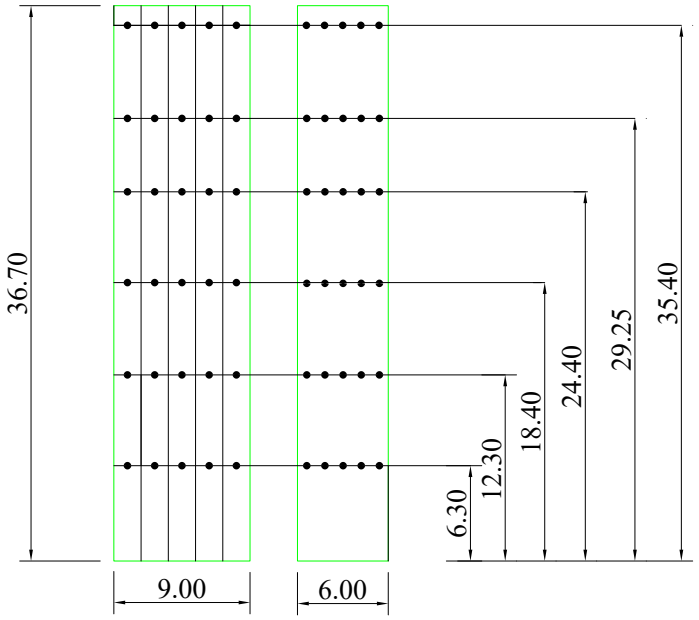

Fig. 5.5: Pressure taps location (measures in cm).

Fig. 5.6: Wind tunnel set-up, suburban terrain.

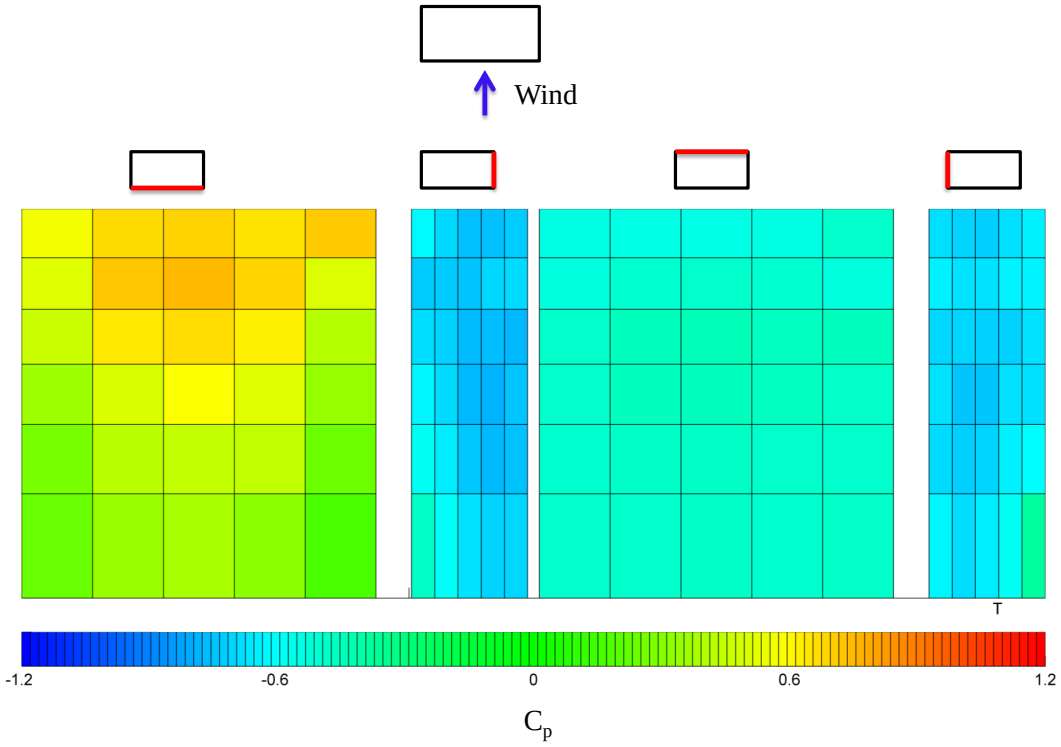

Fig. 5.7: i^{th} Pressure coefficient map corresponding to a wind tunnel realization and $\theta = 0°$.

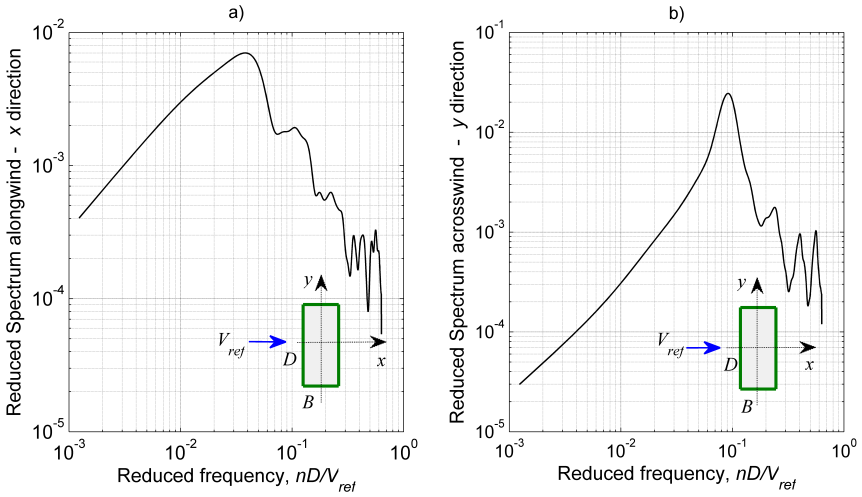

Fig. 5.8: A realization of the generalized force spectrum [Eq. (4.7)], experimentally measured for $(\theta + \delta) = 0°$.

plotted in Figure 5.9.

5.2.2 Joint PDF of the mean-wind speed and direction

In order to evaluate the joint probability distribution of the mean-wind velocity and direction (Section 4.4.2), the wind climate of the city of Boston (MA), along the Atlantic coast of the United States, is chosen as the site of the full-scale benchmark application in the numerical simulations. Boston is predominantly affected by extra-tropical synoptic winds and extremely rare hurricane events. Meteorological measurements available from the NERACOOS online database are used (*Northeastern Regional Association of Coastal and Ocean Observing Systems*). The data, recorded at the Station 44029 - Buoy A01 located in the Massachusetts Bay, are extracted from January 2001 to December 2016 and used to construct the PDF of θ (mean wind direction). The mean wind speeds, extracted from the records, are employed to examine the correlation between mean wind speed and direction. In fact, as described in Section 4.7, the vector IM collects two positive real-valued random variables: the mean reference wind speed V_{ref} and the relative wind incidence angle (angle of attack) θ.

First, the dependence between mean-wind speed and mean-wind direction θ is examined. To this aim the correlation coefficient is evaluated from the sample of the random variables, extracted from Buoy A01. Since the sample correlation is equal to 0.0948, the two random variables can be considered, as a first approximation, as uncorrelated. Therefore,

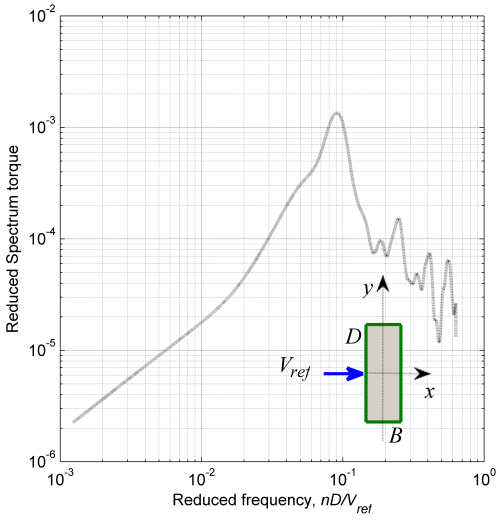

Fig. 5.9: Reduced torque spectrum.

the term $f(V_{ref}, \theta + \delta)$ of Eq. (4.32) can be simplified as $f(V_{ref}, \theta + \delta) = f(V_{ref})f(\theta + \delta)$. Consequently, the estimation of the PDFs of mean-wind speed and direction can be carried out separately and Equation (4.32) becomes:

$$P_j^k(\delta) = \int\int\int P[DS_j|EDP(\theta)]f[EDP|V_{ref}, \theta] \\ f(V_{ref})f(\theta + \delta)\mathrm{d}[EDP]\mathrm{d}(V_{ref})\mathrm{d}(\theta) \quad (5.3)$$

It is worth noticing that this result is not general and it depends on the specific geographical location chosen.

5.2.2.1 PDF of the mean-wind direction

Considering Equation (5.3), the quantity $f(\theta+\delta)$ is determined as follows: starting from the mean-wind direction with respect to the geographic North, taken from the database (*North-eastern Regional Association of Coastal and Ocean Observing Systems*), the experimental probability density function $f(\theta+\delta)$ of the mean-wind direction is evaluated (Figure 5.10). Since the probability distribution model is not known a priori, a non-parametric method is used to examine the data (Kernel density estimation) and to derive a suitable PDF. The PDF in Figure 5.10 is multi-modal; the wind predominantly blows from the South-West quadrant and the North-West quadrant. As underlined in the following section, the buoy

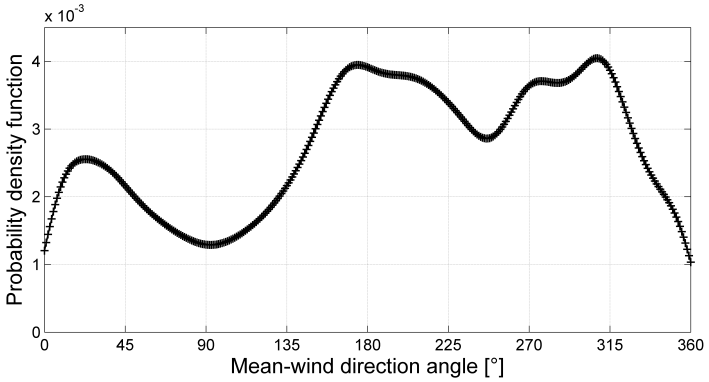

Fig. 5.10: Empirical marginal distribution of the mean-wind direction derived from the database. The angles are measured from the North direction.

data are only used for evaluating the PDF of the mean-wind direction and not for the PDF of the wind speed.

5.2.2.2 PDF of the mean-wind annual maximum

The PDF of the yearly maximum of the mean-wind speed, necessary to derive the annual extreme wind speed PDF of V_{ref} at the reference roof-top elevation $f(V_{ref})$, is reconstructed from information provided in the United States design standard (ASCE7-16 2017). This choice is justified by the necessity of having information with return times unreachable by experimentally accumulated results. Indeed the basic wind speeds (3-second gust at 10-meter elevation) of the wind maps (exposure C category) are extracted for different return periods: from 50 years to 1700 years (Figure 5.11). Basic wind speeds are adjusted from 3-second gust to obtain 10-minute average values at 10-meter elevation. The ratio between 3-second gust and 10-minute averages is approximately found as 1.45:1 using the approach described in ASCE7-16 (2017). In order to get mean wind speeds V_{ref}, the wind speed values are adjusted to the building's reference height (180 m) and to the Exposure B category by considering the change of roughness (from C to B category). Exposure B category is employed since it is compatible with the mean wind speed profile used in the wind tunnel (boundary layer power-law with exponent $\alpha = 0.25$) and representative of a suburban terrain roughness. The following relationship is used:

$$V_H^B = V_{10}^C \cdot \frac{(z_g^C/10)^{1/6.5}}{((z_g^B/180)^{1/4}} \cong V_{10}^C \cdot 1.394 \tag{5.4}$$

where z_g^i $(i = B, C)$ is the gradient height in meters, corresponding to each terrain category.

The exponents and gradients heights were estimated from ASCE tables.
The resultant distribution function, which can be adequately represented by a Gumbel model, is plotted in Figure 5.12.

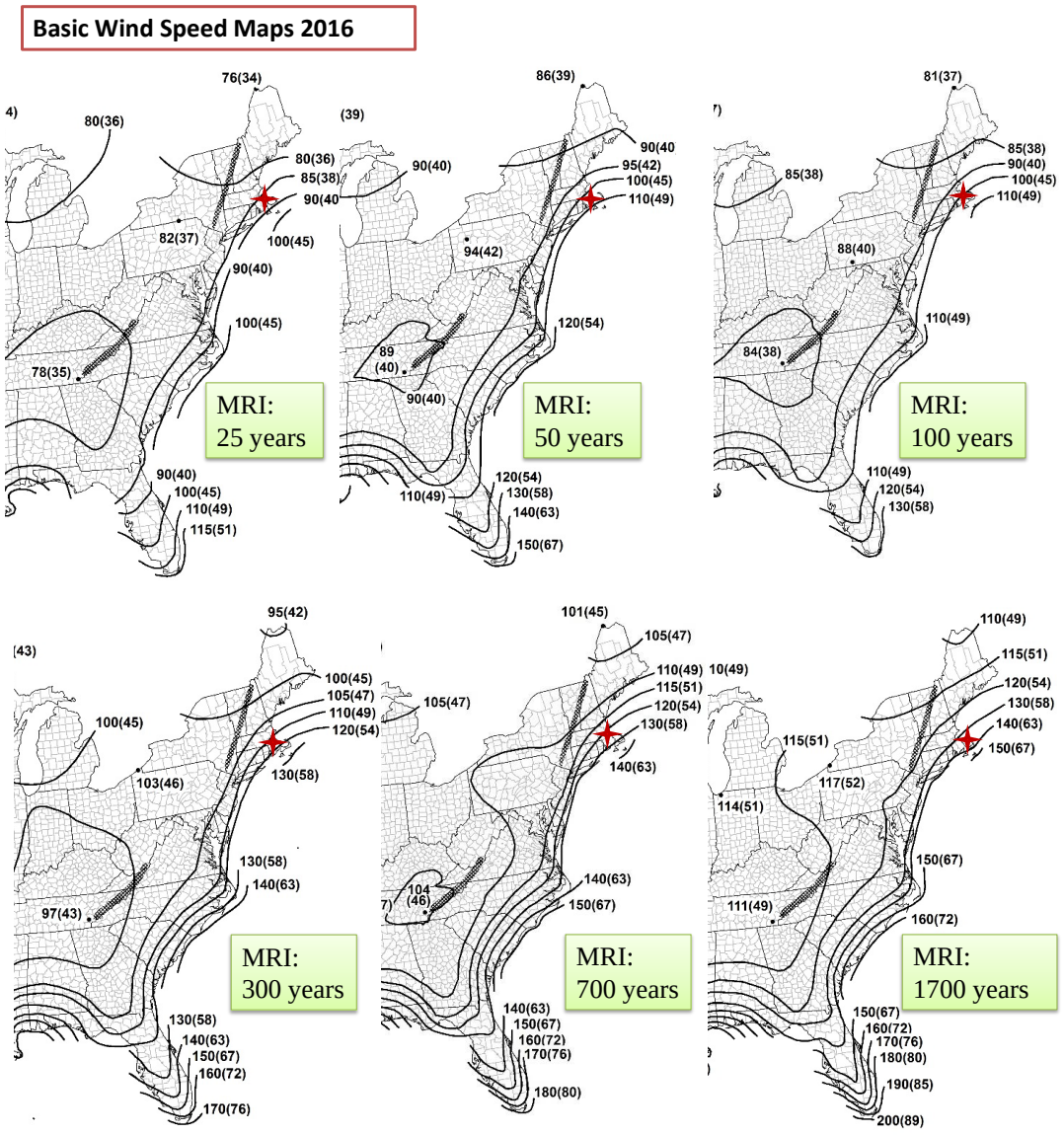

Fig. 5.11: 3-second gust wind-speed (in miles per hour) at 10 m above ground for Exposure category C and for different return periods ASCE7-16 (2017).

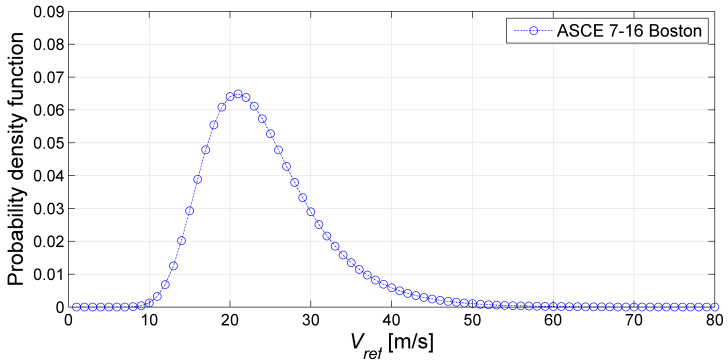

Fig. 5.12: Probability density function of the mean-wind speed annual maxima (10-minute averaging time) at the reference elevation, $f(V_{ref})$ for the city of Boston.

5.3 Non structural elements

As briefly introduced in Section 4.6, three different non-structural components are chosen for the application of the LCCWD procedure:

- glass façades (drift-sensitive)
- partition walls (drift-sensitive)
- suspended ceilings (acceleration-sensitive)

Fragility curves for the selected elements are derived from the FEMA pact database (see Section 4.6). The engineering demand parameters (EDPs) are the interstory drift ratio (IDR) and the peak floor acceleration (a), corresponding to the maximum absolute value of the peak response.
Figure 5.13a) shows the fragility curve for the partition walls. It refers to full-height partitions with slip track connections at the top and at the corners; the slip track connections restrict lateral motion of the element to in-plane displacements only. Damage occurs when the wall paper is warped and torn. Figure 5.13b) illustrates the case of the suspended ceilings, which run continuously over partitions with only vertical supports. Damage occurs when 5 % of tiles dislodge and fall. Figure 5.13c) presents the fragility curve associated with mid-rise stick built curtain walls systems laminated with annealed glass and with square cut corners glass windows; the installation details are unknown. The window systems is supported and contained within aluminum framing. Damage occurs when the panel cracked and need to be replaced. The damage model is derived for tall, slender, low-frequency structures which are primarily sensitive to dynamic resonant effects, such

as interstory drift or acceleration, rather than direct pressure loads or wind-borne debris (i.e., conceived for a first application example outside of the hurricane-prone regions in the United States).

For each nonstructural element ($f = 1, ..., F$) a unit is defined to which the fragility curve is referred: 100 linear feet (about 30 m) for the partition walls, 2500 square feet (about 230 square meters) for the suspended ceilings, a 1.8 panel height is considered with an aspect ratio corresponding to 6:5.

A high-rise building under wind excitation can experience at the same time translational vibrations in the horizontal x and y directions and torsional rotations ψ. The effect of torsion on the selected $EDPs$ (IDR and a) is twofold, as it contributes to both displacements and accelerations (Equations 4.9,4.10,4.19). In principle, each nonstructural element has a different torsional response, depending on its position within the floor and its distance from the floor's elastic center (Figure 5.14a). Moreover, the projection along the local axes of the torsional-induced displacement produces, on each side, an in-plane displacement and an out-of-plane displacement. This two-component motion is schematically represented in Figure 5.14a). Since the contribution of the component orthogonal to the wall axis is usually negligible compared to the in-plane one, only the latter, constant on each side, is considered in the cost analysis. Since the non-structural elements may be randomly distributed on each floor, torsional effects are evaluated in a simplified manner (Figure 5.14b) considering the border perimeter for the glass façades and a reference perimeter for internal nonstructural components built on the centroids of each of the quadrants identified by the local axes x and y. The displacements (Equations 4.9 and 4.10) are evaluated on each side of the perimeters and faces A,B,C,D and $\hat{\mathrm{A}}, \hat{\mathrm{B}}, \hat{\mathrm{C}}, \hat{\mathrm{D}}$ are identified (Figure 5.14b). Similar considerations can reasonably be made regarding the accelerations that are computed (Equation 4.19) for each quadrant at the reference points. Figures 5.15a) and b) report the spatial distribution of the non-structural components chosen for the numerical application. Partition walls are considered uniformly distributed at a distance of about 6 m from each other. Suspended ceilings are distributed continuously over the cross-section. Glass façades are considered uniformly distributed along the height. The same configuration is adopted for each floor of the building. Since the in-plane displacements are constant along each face it is sufficient to calculate the x and y displacements of the two diametrically opposed edges of each perimeter as represented in Figure 5.15.

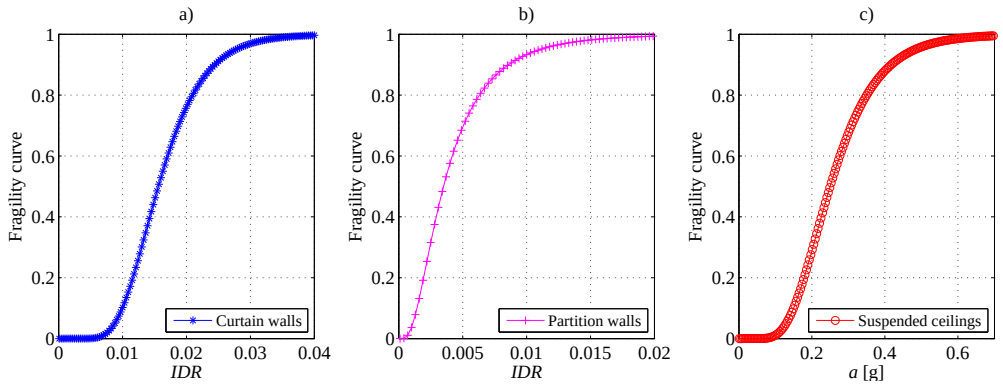

Fig. 5.13: Partition walls fragility curve as a function of *IDR* (a); Glass façade fragility curve as a function of *IDR* (b); Suspended ceiling fragility curve as a function of a (c).

5.4 Control systems characteristics

The considered control system is composed of a bidirectional TMD, located at the elastic center of the top floor of the building. The TMD controls the response along the two principal lateral directions of the building ($h = \{x, y\}$). The mass ratio of the TMD is $\mu = m_{\text{TMD}}/M_x = 2\%$.

The parameters of the TMD in each direction are tuned to control the response of the first two lateral modes. Without any loss of generality, the Warburton relationships (Warburton 1982), as shown in Figure 3.14, are adopted to compute the optimal stiffness and damping coefficient of the TMD:

$$k_{\text{TMD},h} = m_{\text{TMD}}\alpha_{WB}(2\pi n_{0,h})^2 \tag{5.5}$$

$$c_{\text{TMD},h} = 2m_{\text{TMD}}\gamma_{WB}(2\pi n_{0,h}) \tag{5.6}$$

where $\alpha_{WB} = \sqrt{1+\mu/2}/(1+\mu)$ and $\gamma_{WB} = \sqrt{\mu(1+3/4\mu)/[(1+\mu)(1+\mu/2)]}$.

5.5 Cost models

To compute the normalized lifetime costs, a cost model is needed. During the preliminary design stage the initial cost of the structure may be plausibly assumed as a percentage α_s of the mass of the structural steel elements M_s (Hasançebi 2017):

$$C_{0,s} = \alpha_s M_s \tag{5.7}$$

An average coefficient $\alpha_s = 1.07$ is computed by using the data reported in (Hasançebi 2017).

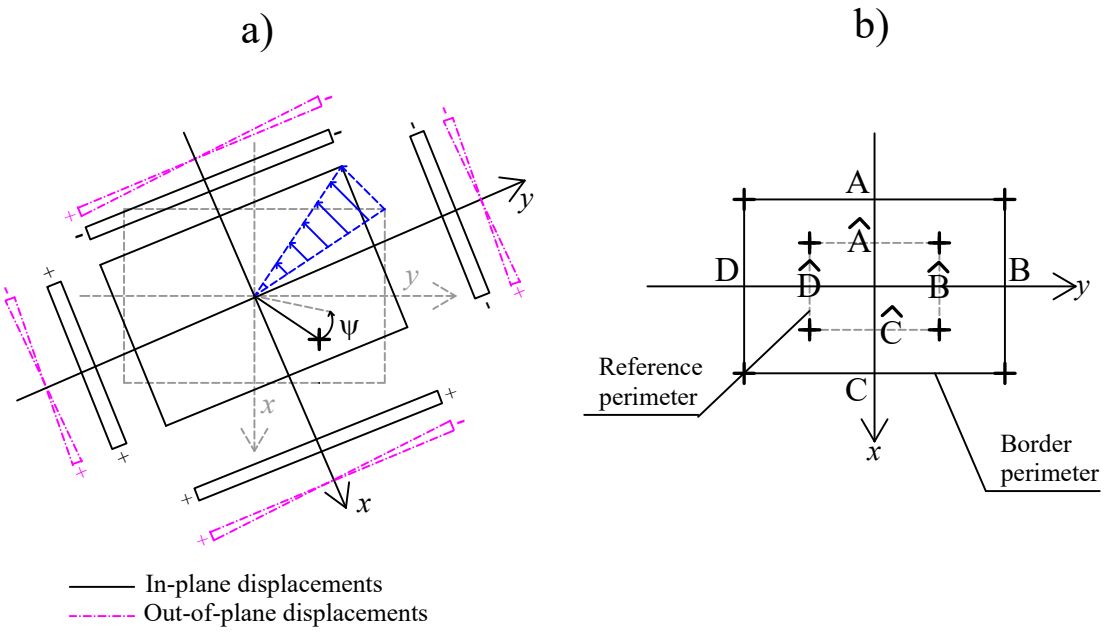

Figure 5.14: Schematic plan view of the building considering the torsional rotation ψ with the indication of torque-induced displacements along each side (a), reference and border perimeters (b).

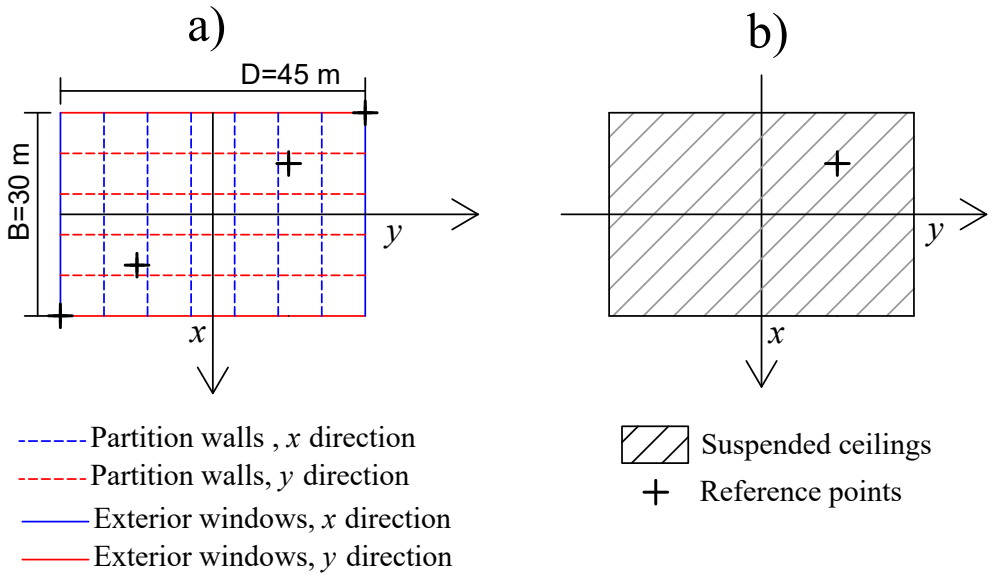

Figure 5.15: Plan view with selected locations of the partition walls (a), and the suspended ceilings (b).

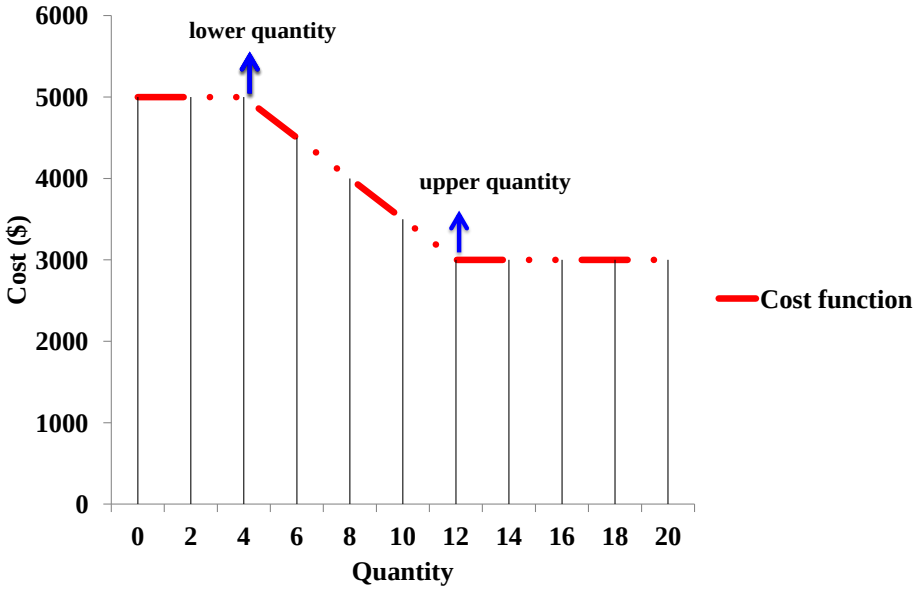

Figure 5.16: An example of a PACT graph showing upper and lower bound repair cost data.

The initial cost of the TMD may reasonably be assumed dependent on the initial construction cost $C_{0,s}$:

$$C_{0,cs} = \alpha_{cs} C_{0,s} \tag{5.8}$$

where $\alpha_{cs} = 0.2\%$ is adopted. In practical cases, the cost of the control device is known from the supplier. For the purpose of this analysis the cost value is chosen through a sensitivity analysis in order to recover the initial monetary capital spent in less than 10 years. Indeed, the repair cost over time due to the presence of the TMD decreases but at time 0 (construction time) the TMD installation cost increases the invested capital.
For each nonstructural element a unit cost is defined to which the fragility curve is referred. The unit costs C_j in Equation (4.38) are taken by FEMA (FEMA-P-58 2012a). In (FEMA-P-58 2012a), a lower and an upper bound for the unit repair costs of each nonstructural element are suggested. The lower bound is usually adopted when a significant number of elements must be repaired while the upper bound is selected when a limited number of elements must be repaired (FEMA-P-58 2012d). Figure 5.16 illustrates an example of the repair cost associated to a specific nonstructural components, as a function of different units. In the present application, given the large number of units present throughout the building, the upper bounds are chosen. The unit cost values correspond to: $C_j = 2200\,\text{USD}$

Table 5.5: Number of units and normalized unit costs for non-structural elements

Element	$\hat{n}_x(z)$	$\hat{n}_y(z)$	$\hat{n}_a(z)$	$c_j[10^{-4}]$
Partition walls	3	3	–	2.3
Suspended ceilings	–	–	5.9	3.5
Glass façades	31	46	–	1.7

Table 5.6: Parameters adopted for the cost analysis

PARAMETER		VALUE
Mean arrival rate per unit time	ν	1
Discount factor	λ	0.05
Number of Monte-Carlo samples	N_s	10000

(US dollars) for drift-dependent damage to partition walls, $C_j = 3300\,\text{USD}$ for acceleration-dependent damage to suspended ceilings and $C_j = 1700\,\text{USD}$ as concerns drift-dependent damage to glass façades. The number of interior walls and suspended ceilings units ($\hat{n}_x(z)$, $\hat{n}_y(z)$, $\hat{n}_a(z)$) and the corresponding costs c_j normalized with respect to the cost of the structure $C_{0,s}$ are presented in Table 5.5. The unit numbers are differentiated for the two main directions to take into account the side ratio of the building. The cost estimation described in Section 4.8 is carried out by Monte-Carlo sampling. The parameters that are employed for the cost analysis are summarized in Table 5.6 (Cui and Caracoglia 2015).

Chapter 6

Numerical results

6.1 Introduction

This section shows the main results of the numerical simulations obtained by using the LCCWD approach. All the results are illustrated separately for each face of the building, as described in Section 5.3. For the sake of simplicity, direction x refers to face B as concerns the glass façade or $\hat{B}$ for partition walls, direction y refers to face A (glass façade) or $\hat{A}$ (partition walls). The faces distinction is clarified in the plan view of the building in Figure 5.14. Moreover all the intermediate results from here onwards are associated with one of the N^{th} wind tunnel data segments (see Section 4.4.1).
According to Section 4.9, this Chapter summarizes all the investigated design alternatives and it is organized as follows:
Section 6.2 refers to the preliminary design configuration. Some results in terms of structural response (IDR and a) are shown. Some parametric analyses are developed in order to assess the influence of the building's natural frequencies.
Section 6.3 explores different building orientations and summarizes the results in terms of damage probabilities and life-cycle cost for each design solution.
Section 6.4 compares the uncontrolled solution (w/o TMD) and the controlled solution

(with TMD) in terms of structural responses, damage probabilities and cost analyses. Section 6.5 investigates different design configurations for indoor nonstructural elements. The cost-based results highlight the importance of choosing the destination of use of the building and, consequently, the distribution of nonstructural elements. Section 6.6 presents the chart of the LCCWD final results.

6.2 Preliminary design configuration

As described in Chapter 5, the initial nonstructural elements configuration is characterized by: glass façades, which are considered uniformly distributed along the height of the building; interior partition walls and suspended ceilings, which are considered uniformly distributed on each floor. The choice of materials, the shape of the building, the destination of use and the height of the building are considered as input data.
The uncertainties related to the experimental load, as described in Section 4.4.1, are taken into consideration by evaluating the term $f[EDP|V_{ref}, \theta]$ in Equation (4.32). This term represents the PDF of the selected EDP, i.e. the interstory drift ratio (IDR) or the acceleration (a), conditional on the reference mean-wind speed (defined within the hazard intensity interval), on the relative mean-wind incidence angle θ and depending on the building orientation. As an example, Figure 6.1a) presents the probability density functions of the IDR in x direction with reference to the partition walls (face $\hat{B}$) evaluated for $V_{ref} = 40m/s$ and the building orientation $\theta + \delta = 0°$ (wind that blows from the North). The corresponding fragility curve is also plotted in the figure. Figure 6.1b) illustrates the comparison between the numerical PDF, postulated from a log-normal distribution model, and the experimental PDF, found from the wind tunnel experimental loads by data parsing, at $V_{ref} = 40m/s$. The close proximity between the interpolated probability curve and the experimental points validates the adoption of the log-normal distribution model for the variable IDR. This choice possibly best fits the N peak responses, obtained from the corresponding N generalized fluctuating force spectra, which are evaluated by sampling the pressures and load time histories from the wind tunnel experiments, as described in Section 4.4.1. In order to validate the LCCWD procedure (presented in Chapter 4), some intermediate results are computed. First results are shown in terms of maximum peak acceleration and maximum displacement. First, Figure 6.2 illustrates an example of top floor IDR for all relative incidence angles θ for $\delta = 0$. The reference axes and the rotation angles are consistent with Figure 4.3. As expected, the figure suggests the symmetry of the structural response in terms of IDR, given the rectangular floor plan of the building. Very

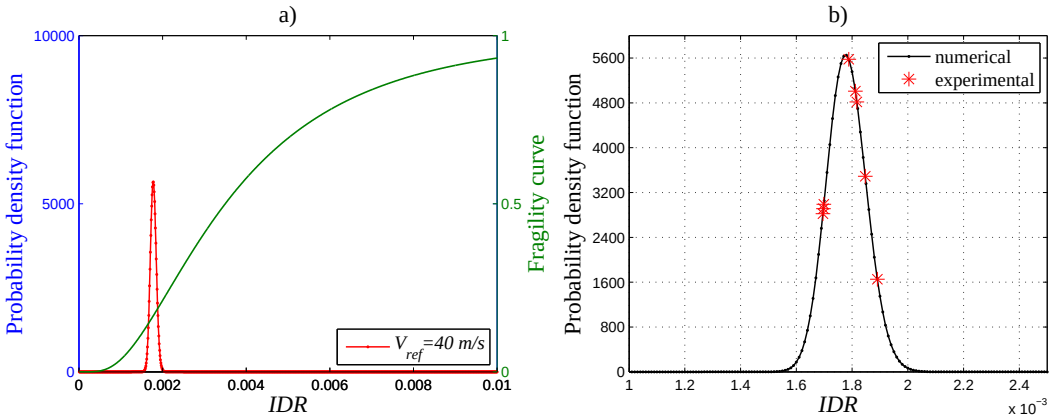

Fig. 6.1: $f(EDP, V_{ref,\theta})$ for direction x in the case of $(\theta + \delta = 0°)$: a) $f[EDP|V_{ref} = \{40\}$ m/s] and partition walls fragility curve; b) numerical PDF, $f[EDP|V_{ref} = 40$ m/s], vs. experimental points.

small differences between symmetrical angles are possibly related to small experimental wind tunnel measurement inaccuracies. By considering the mode shapes, as specified in

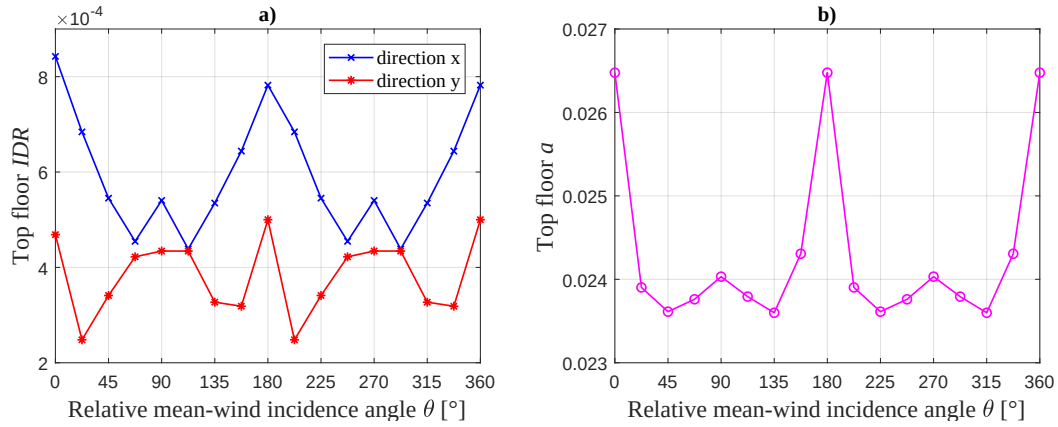

Fig. 6.2: Peak top floor IDR (a) and a (b) for directions x, y (local coordinate system) with $V_{ref} = 40$ m/s, as a function of the relative mean-wind incidence angle $(0° \leq \theta < 360°)$.

Equations (4.17), (4.18) and (4.21), Figure 6.3 shows the IDRs and the accelerations at a generic floor identified through the vertical coordinate z. Figures 6.3a)-b) refer to the interstory drift of glass façades (IDR_{gf}) and partition walls (IDR_{pw}), respectively. Figure 6.3c) refers to the acceleration of suspended ceilings (acc_{sc}).

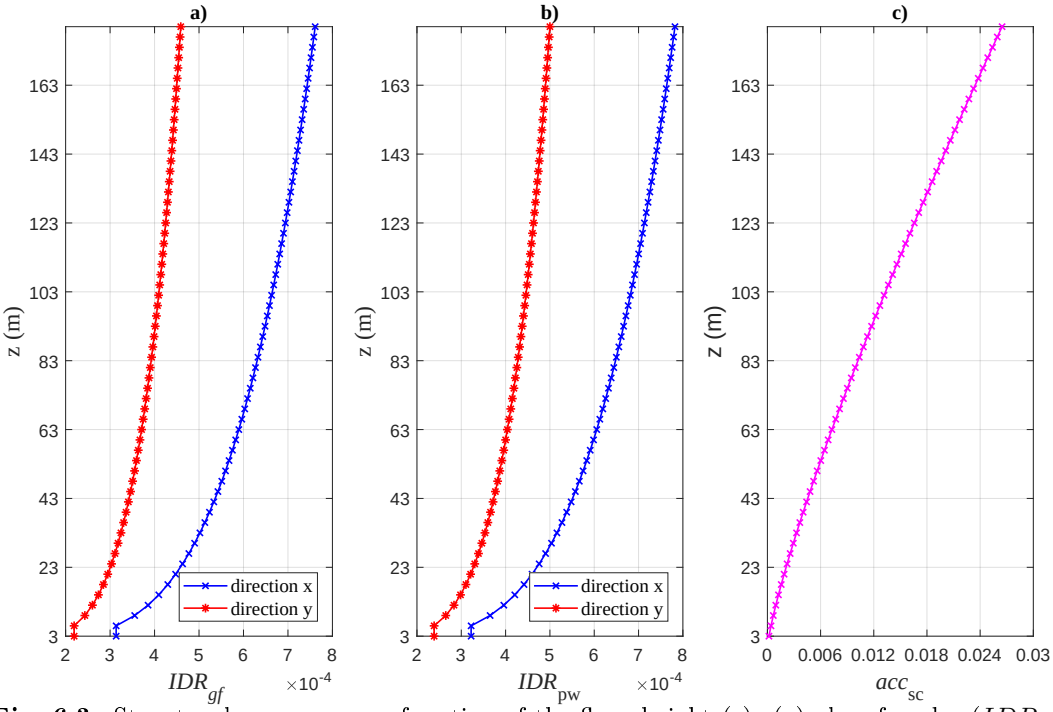

Fig. 6.3: Structural response as a function of the floor height (z): (a) glass façades (IDR_{gf}) and (b) partition walls (IDR_{pw}) for directions x, y (local coordinate system) and (c) suspended ceilings (acc_{sc}) with $V_{ref} = 40$ m/s and building orientation $\theta + \delta = 0°$ (wind that blows from the North).

6.2.1 Parametric analysis on building's natural frequencies

The design configuration procedure involves the assumption of the fixity at the base of the foundation and therefore, both the flexibility of the foundation and the compressibility of the sub-soil are neglected. In principle, the superstructure-foundation-soil interaction and the uncertainties related to the modeling of the building may give rise to possible variation in terms of structural and dynamic properties.

In this context a parametric analysis is carried out by modifying the fundamental frequencies of the tall building maintaining constant the ratio between the principal natural frequencies in x and y directions $\bar{n} = n_x/n_y$. Hence the frequency n_h $(h = x, y)$ is modified with a multiplicative coefficient α_n from 0.8 to 1.2, with step increments of 0.1. Figures 6.4 and 6.5 present the results in terms of peak top floor IDR and a for each V_{ref} within the hazard interval for different fundamental frequencies of the structure, i.e. different α_n. The building orientation is set to $\theta + \delta = 0°$ (wind that blows from the North). In this specific case the axis x corresponds to the alongwind direction while axis y to the acrosswind one.

It can be noted that a more flexible structure leads to larger values of the IDR, as clearly shown in Figure 6.4a). Hence, larger values of damage probabilities and costs are expected to reach a selected performance level. Instead, in the acrosswind direction, within certain values of V_{ref} (approximately between 30 and 50 m/s), the phenomenon is less pronounced (Figure 6.4b). This trend is confirmed in Figure 6.5(a) where the variation of the top floor acceleration with the principal lateral frequencies, suggests that the maximum value of a does no correspond to the larger flexibility. This effect is highlighted in Figures 6.5b),d) and it is probably due to the fact that specific values of the mean-wind velocity intensifies the vortex shedding phenomenon (see Section 3.2.2) in the acrosswind direction.

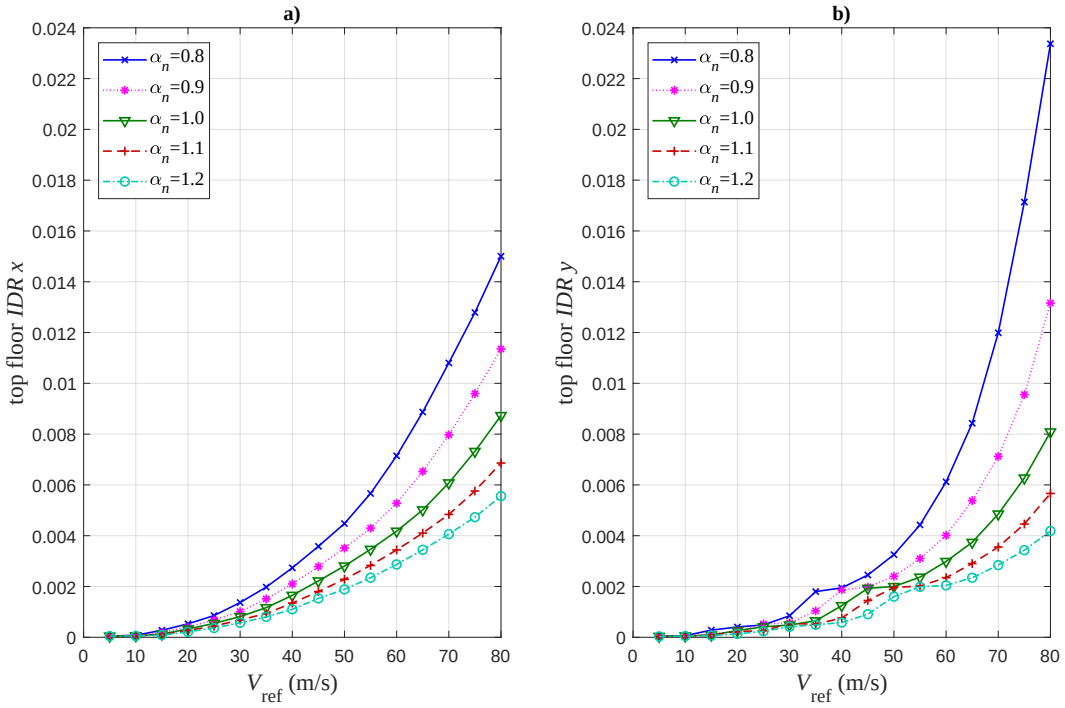

Fig. 6.4: Peak top floor IDR for directions x (a) and y (b) as a function of α_n and V_{ref}.

Aeroelastic effects are approximately accounted for by the quasi-steady formulation. Nevertheless unsteady theory may be necessary to account for non-linear effects due to severe vortex shedding, i.e., modification in the aerodynamic damping (Mannini et al. 2011; Pozzuoli et al. 2013; Huang et al. 2013; Marukawa et al. 1996; Vickery and Steckley 1993; Hayashida et al. 1992). These effects may become important for super-tall buildings with low mass and low frequency.

In addition, the procedure mainly addresses experimental errors in the wind load spectra

(Section 4.4.1). It is worth noticing that uncertainty may also consider measurement errors in the static aerodynamic coefficients, which may be used to adjust the aerodynamic damping effect, beneficial or detrimental in some cases (Le and Caracoglia 2017). In this respect, the results in terms of peak response are probably conservative. However, results are acceptable from the point of view of the life-cycle cost assessment whose goal is the comparison between different solutions.

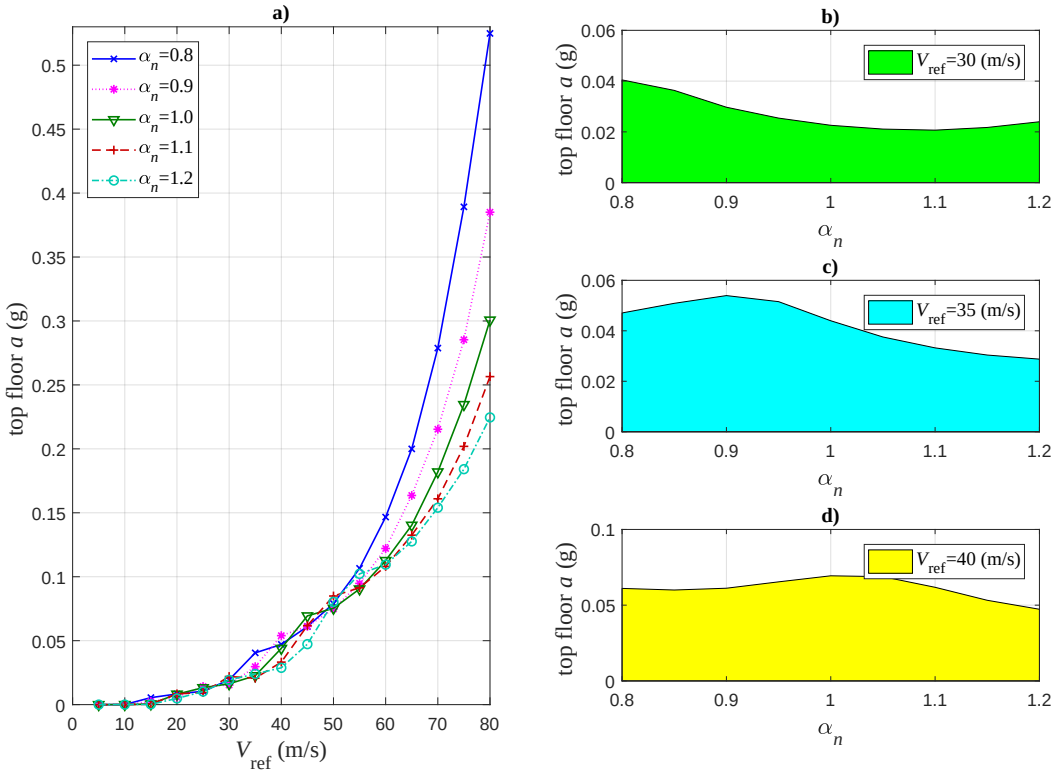

Fig. 6.5: Peak top floor a with respect to α_n and V_{ref} a), Peak top floor a by varying α_n for: $V_{ref} = 30m/s$ b), $V_{ref} = 35m/s$ c), $V_{ref} = 40m/s$ d).

Figure 6.6 shows the top floor annual damage probability as a function of α_n for the selected nonstructural elements. From the figure it can be noted that, both for drift-dependent (Figures 6.6a,b) and acceleration-dependent elements (Figure 6.6c), the annual damage probability decreases as the stiffness of the structure increases.

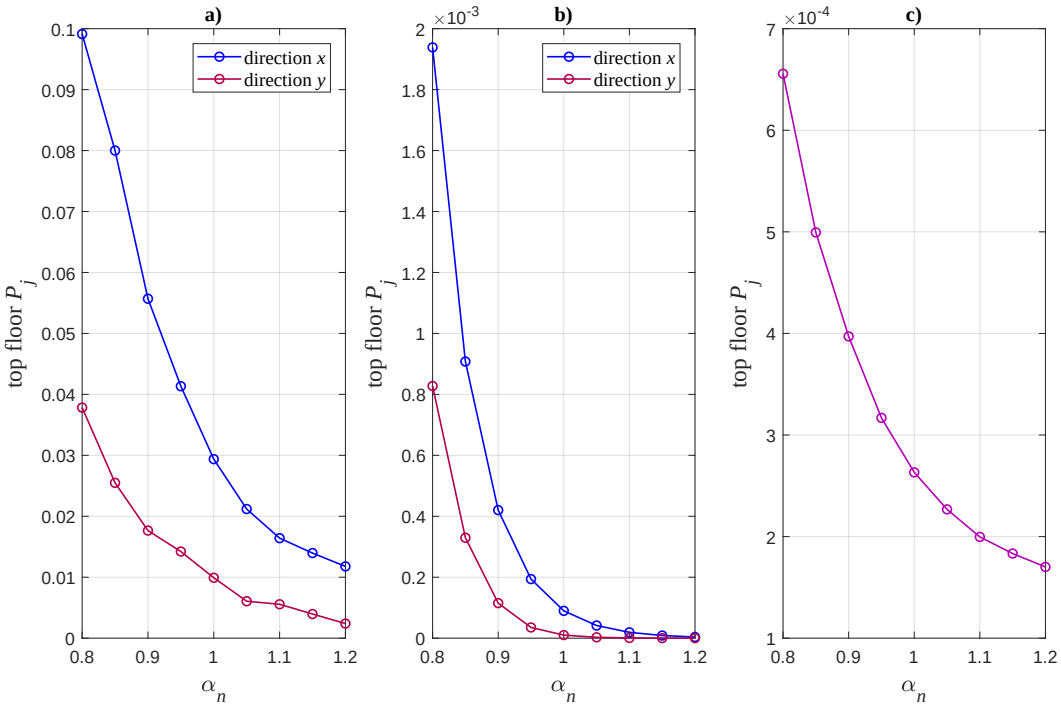

Fig. 6.6: Top floor annual damage probability P_j associated with $V_{ref} = 40$ m/s as a function of α_n: (a) partition walls (x,y direction); (b) glass façades (x,y direction); (c) suspended ceilings.

6.3 Choice of the building orientation

The site wind exposure is an important aspect that should not be neglected. Hence, by accounting for the probability distribution of the wind direction, the life-cycle cost is evaluated as a function of both lifetime and building's orientation angle. The results of the LCCWD procedure could provide useful information to the designers and assistance to the selection of the orientation that minimizes the total life-cycle cost. Without loss of generality the influence of wind exposure of a specific site on building's design is examined in order to find the best cost-saving structural solution.

6.3.1 Damage probability results

It is convenient to decompose the calculation of the damage probability by separately considering each relative wind incidence angle θ.

Figure 6.7 shows the top floor annual damage probability P_j for each unit of the selected

nonstructural element with $V_{ref} = 40$ m/s, as a function of the relative mean-wind incidence angle $0° \leq \theta < 360°$. Inspection of the results in Figure 6.7 confirms the symmetry of the damage as already seen with regard to the structural response as a function of θ. A considerable difference is noted between the damage along the two principal axes of the

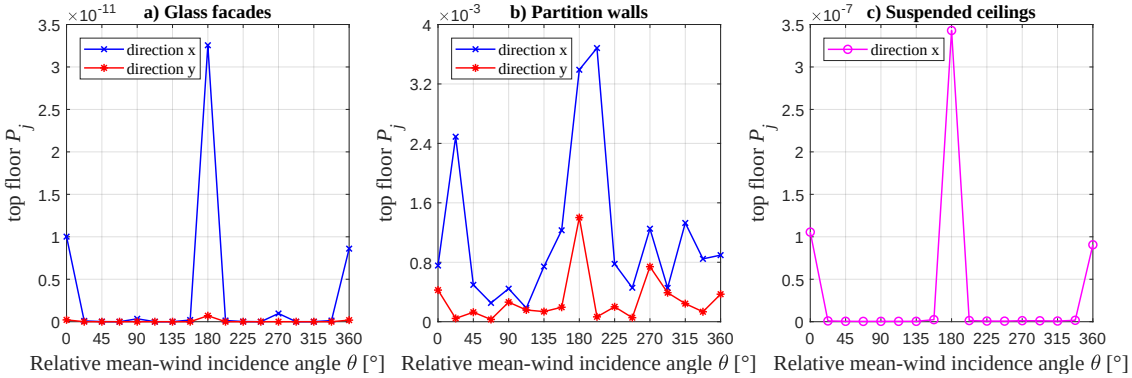

Fig. 6.7: Top floor annual damage probability P_j associated to each unit element with $V_{ref} = 40$ m/s as a function of the relative mean-wind incidence angle $0° \leq \theta < 360°$: (a) glass façades (curtain walls) for direction x (face B) and direction y (face A);(b) partition walls for direction x (face $\hat{B}$) and direction y (face $\hat{A}$); (c) suspended ceilings.

building, with higher annual damage probability values observed along the shorter side (principal building axis x) due to larger values of the associated IDR. Moreover partition walls are the more relevant damage-sensitive elements. This result depends on the fragility characteristics chosen for each type of nonstructural element (Section 5.3).
Subsequently, the building orientation can be introduced and the annual damage probability is evaluated according to Equation (4.32); results are plotted in the polar graphs of Figure 6.8. From the examination of this figure, it is concluded that:

- in Figures 6.8 a),b) the annual damage probability is larger along the principal building axis x. This is due to the fact that drift-dependent damage (Eq. 4.32) is more relevant for the x direction, as exhibited in Figure 6.2;
- in Figure 6.8 c) the dependence on the building orientation is highlighted (different values of the damage probability by varying δ).

6.3.2 Orientation-dependent damage cost accumulation results

As described in Section 4.8 the damage cost accumulation is assessed by simulating the number of wind storm events as a Poisson process between time 0 and the time t (in years).

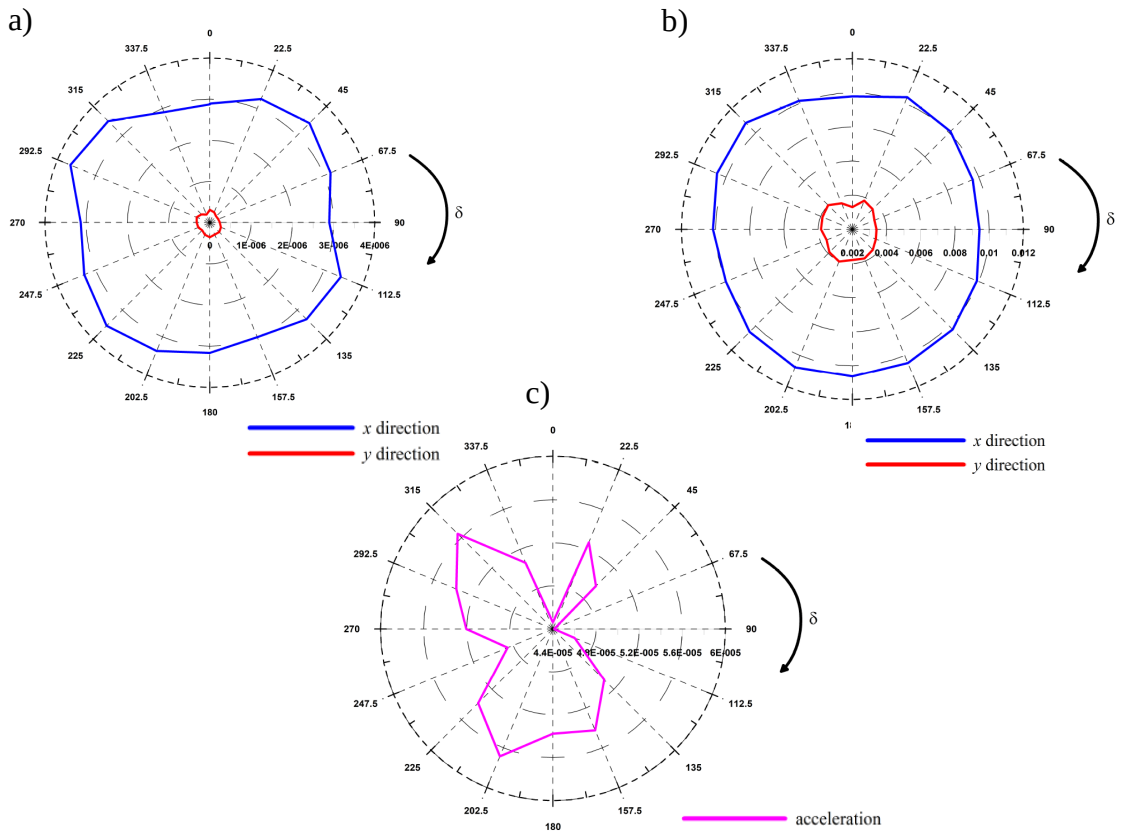

Fig. 6.8: Top floor annual damage probability for glass façades (a), partition walls (b) for direction x and direction y and suspended ceilings (c) as a function of the building orientation angle δ.

The arrival times of each storm, t_l, are simulated as uniformly distributed over the time interval by Monte-Carlo sampling. The parameters that are employed for the cost analysis are described in Section 5.5.

Figure 6.9 illustrates the numerical results of the cost analysis. The expected normalized intervention and repair cost (i.e. $t = 50$) is separately presented for the two principal building axes (directions) for each damage state under investigation. Consistently with the damage analysis, larger damage probabilities along the x principal axis induce higher values of the expected life-cycle cost and more significant variations depending on the building orientation angle δ. In order to determine the best building orientation, the total combined cost is evaluated by cumulating the effects in the x and y directions for all the faces, for each damage state and for each floor. Figure 6.10 illustrates the total life-cycle

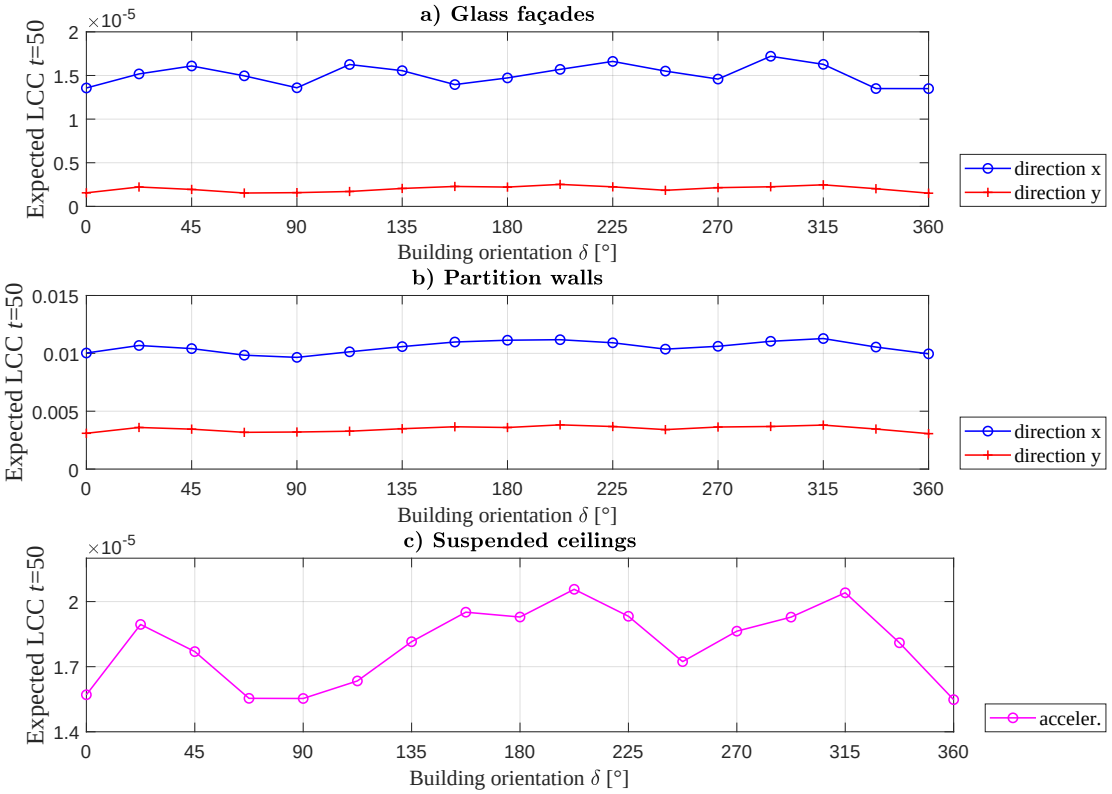

Fig. 6.9: Expected value of the life-cycle cost as a function of the building orientation δ for $t = 50$ years, along the two principal axes: (a) galss façades ;(b) partition walls; (c) suspended ceilings.

cost, cumulating the costs along both building axes, for various lifetimes (return periods in years): 1, 20, 50, 100. As expected, the cost increases with time even though the curves maintain the same shape as a function of building orientation angle δ, according to Equation (4.35). The three dimensional graph in Figure 6.11 shows the total life-cycle cost as a function of time and building's orientation.

According to Equations (4.35)- (4.37), the probability of exceeding a given damage state is the same and, consequently, the curves presented in Figure 6.10 are qualitatively the same at various years t, since the curves are simply translated along the vertical axis because of accumulation of damage over time. This aspect is more clearly clarified in Figure 6.11. As reported in Section 4.8, this is consistent with the hypotheses used by Wen (2001) and Wen and Kang (2001) in the original model.

Considering all damage states and the specific case study, it is quite clear that the total expected cost has a minimum value at $\delta = 90°$, as confirmed in Figures 6.10 and 6.11. This result clearly depends on the selection of the geographical location and, consequently, on the wind exposure of the site, which is influenced by the empirical reconstruction of the probability density function of the mean-wind direction. The cost variations observed in the previous figures are influenced by the relative differences in the damage probability, which in turn depend on δ and on the empirical PDF of the mean-wind direction, $f(\theta + \delta)$ in Equation (4.32).

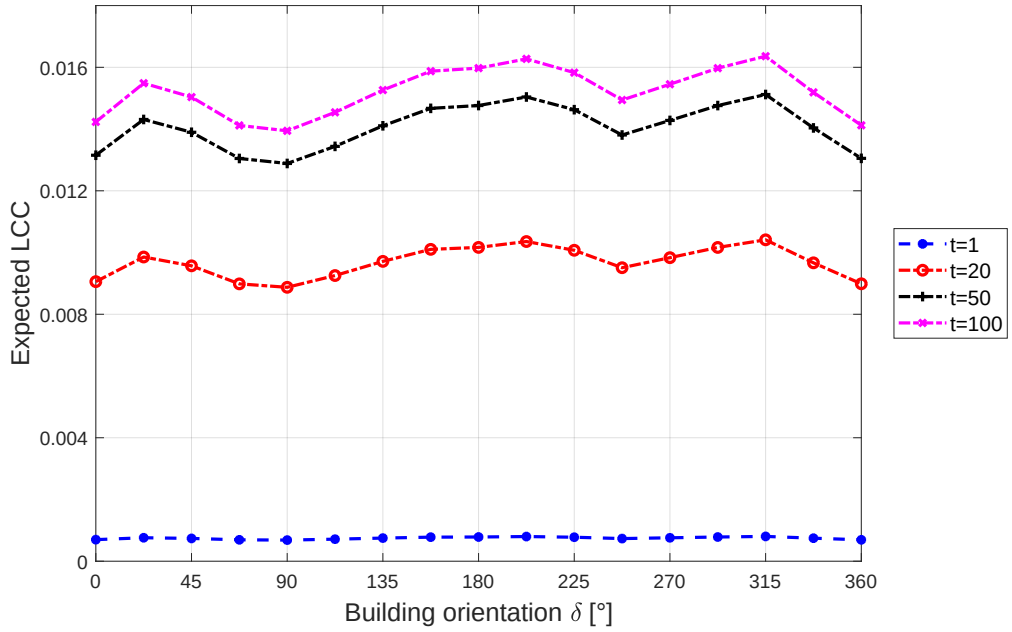

Fig. 6.10: Expected total life-cycle cost, normalized according to Equation (4.39), as a function of the building orientation angle δ and for various lifetimes t (years).

6.4 Design of the structural control systems

As introduced in Section 5.4, the considered control system is composed of a bidirectional TMD, installed at the building's top floor.

Comparative numerical results are reported in this section by considering the controlled configuration (with TMD) and the uncontrolled case (w/o TMD) for the best building orientation. According to the previous Section, the best building orientation is assumed

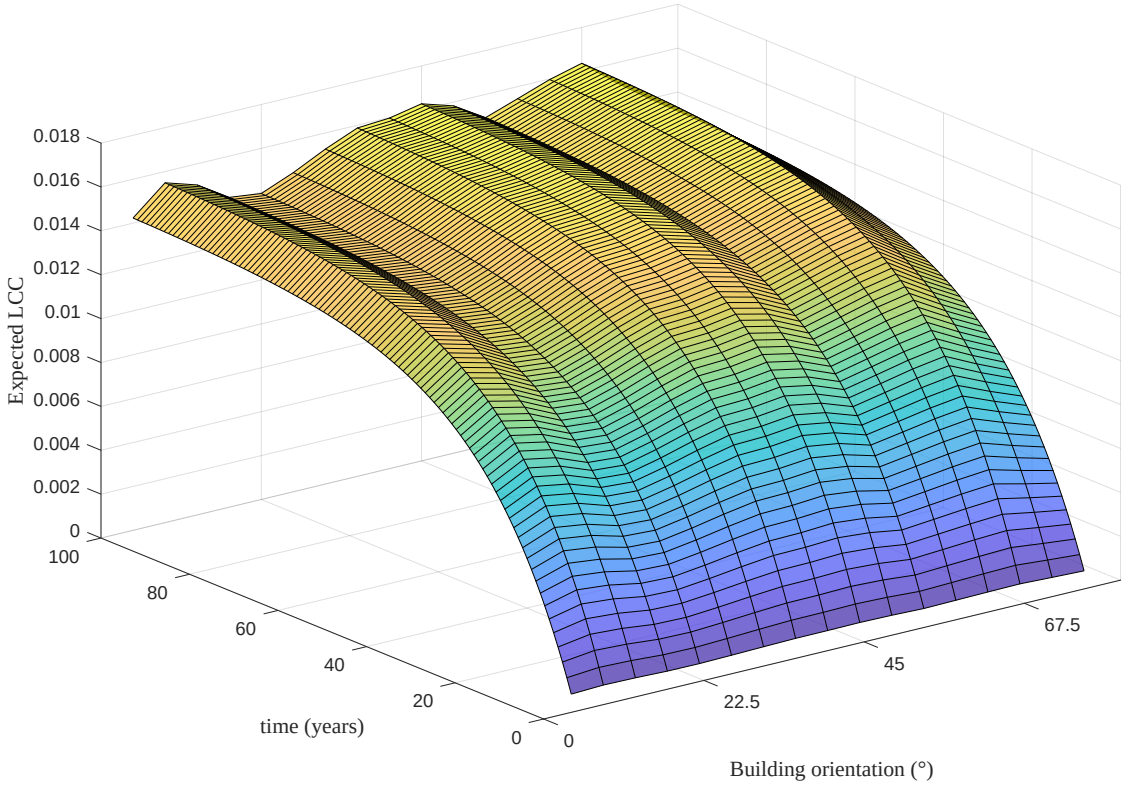

Fig. 6.11: 3D plot of the expected total life-cycle cost, normalized according to Equation (4.39), as a function of the building orientation angle δ and for various lifetimes t (years)

equal to $\delta = 90°$. The TMD characteristics are defined in Section 5.4.

6.4.1 Uncontrolled and controlled building response

Figure 6.12 illustrates an example of the top floor peak lateral displacements and accelerations obtained with a single wind tunnel load realization $i = 1$, normalized with respect to the uncontrolled case. Results correspond, at full scale, to the reference mean wind speed $V_{ref} = 40\ m/s$ and to the direction $\theta = 0°$, orthogonal to the building face of dimension $D = 45\ m$ and parallel to the local horizontal axis x (Figure 4.3). In presence of TMD, the peak response components are reduced by about 20% to 40%. Similar results have been found at other V_{ref} but are not reported for the sake of brevity. As expected, the TMD

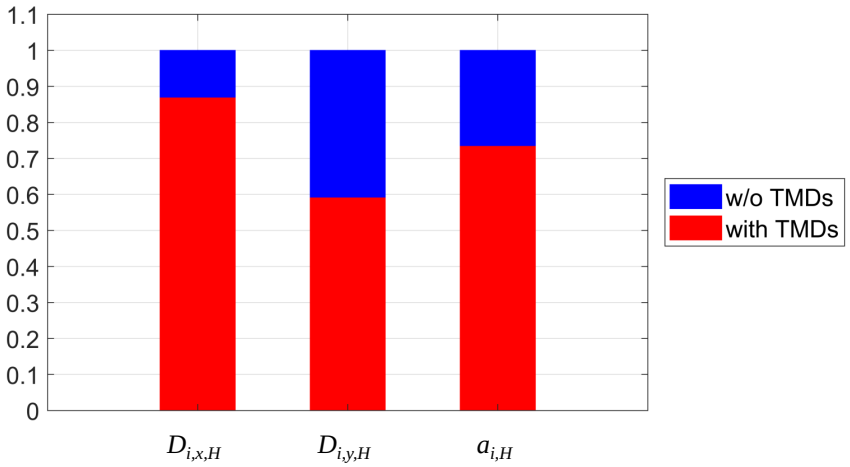

Fig. 6.12: Top floor peak response (x-displacements, y-displacements, acceleration) obtained for $i = 1$, $V_{ref} = 40\ m/s$ (at full scale) mean-wind incidence angle $\theta = 0°$ and building orientation 90°, normalized with respect to the uncontrolled case.

devices are very efficient in eliminating both the buffeting load and wake excitation effects.

6.4.2 Damage probability results

Figures 6.13, 6.14 show the annual damage probabilities for a unit element of partition walls, glass façades (separately analyzed along x and y lateral directions) and suspended ceilings. The annual damage probabilities are computed by accounting for the local wind climate probability distributions (joint PDF of mean wind speed and direction) at the site of the structure (data are reported in Section 5.2). The results are presented as a function of the height above ground z and compared for the cases in presence and in absence of the TMD. Damage probabilities are the same for all elements located on the same floor. In general, the annual damage probabilities increase with floor elevation (height z), as they are linked to the trends of both interstory drifts and accelerations which become more pronounced at higher z due to the power-law mode shapes. The annual damage probabilities are significantly reduced by the presence of TMDs. Reductions of about 60% and 50% are noticeable for the damages to the partition walls (Figures 6.13a-b) and glass façades (Figures 6.14a-b) of the upper floors in the x and y directions, respectively. A strong reduction can be also observed for acceleration-induced damages at the top floor

(Figures 6.14c).

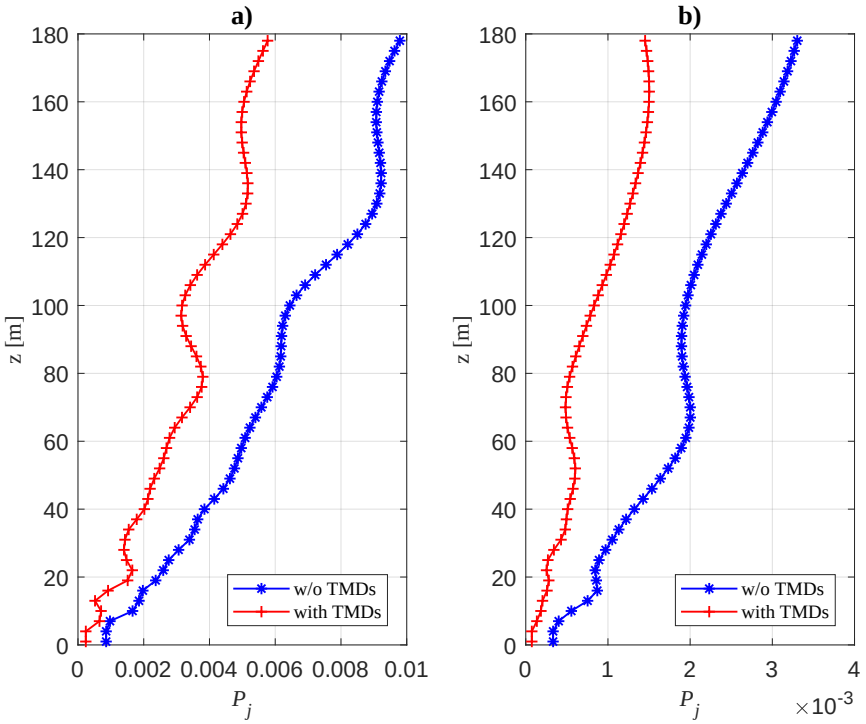

Fig. 6.13: Annual damage probability as a function of the floor height (z): a) partition walls (x direction); b) partition walls (y direction).

6.4.3 Cost accumulation results

In this Section, the life-cycle expected investment cost, accounting for wind-induced damage and intervention/repair cost, is illustrated. The total cost is evaluated as the sum, over all the floors, of drift-related costs and acceleration-related costs. Figure 6.15a) summarizes the evolution of the expected total cost value, normalized according to Equation 4.39 as a function of the lifetime and for the system with and without TMD. Estimation is carried out by Monte-Carlo sampling with $L(t)$ being a Poisson process with mean arrival rate equal to $\nu = 1$ event per year at the selected site (Section 5.5). The discount rate employed is $\lambda = 0.05$ (Section 5.5). It is noted that the normalization in Equation 4.39 is selected to highlight the relative differences between the two solutions; even though actual monetary values are dependent on the absolute value of the building estate, it is believed that this choice of normalization is particularly suitable during initial design as may provide assistance to the owner or the decision maker. Although the installation of the TMD induces a discontinuous "step" (cost increment) at $t = 0$, its presence provides a reduction

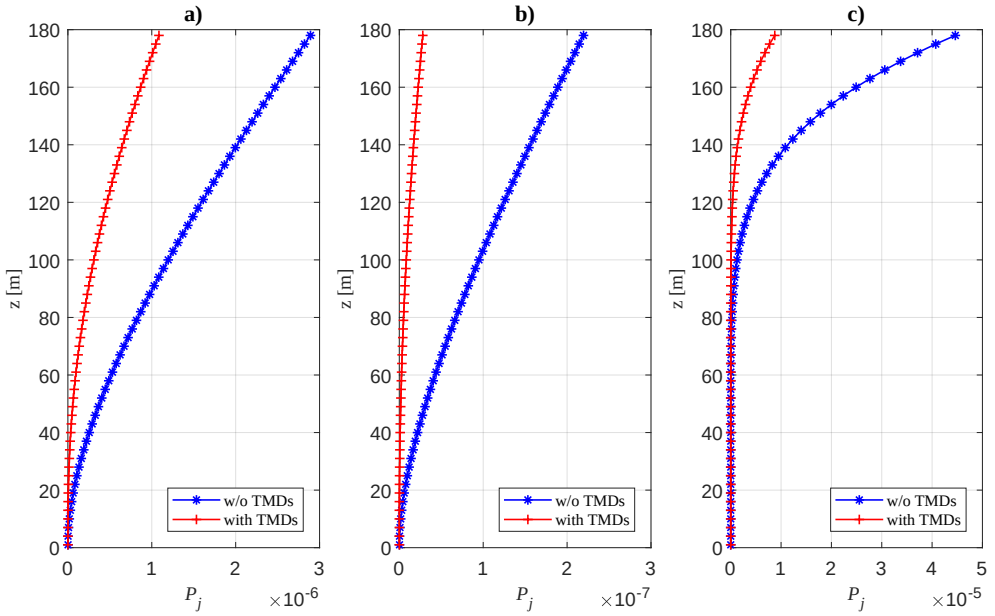

Fig. 6.14: Annual damage probability as a function of the floor height (z): a) glass façades (x direction); b) glass façades (y direction); c) suspended ceilings.

of damage occurrence and, consequently, a diminution of the intervention costs during the lifetime. Inspection of Figure 6.15a) reveals that, beyond a certain time duration (designated as *Break-even time*, BET), the adoption of the TMD becomes economically advantageous; the overall relative reduction of the investment cost progressively increases and is quantified around 40% at $t = 100$ years.

Figure 6.15b) reports a second example of calculation of the total expected normalized cost as a function of the lifetime. In this second case the TMD is installed 10 years after the building opening. Since a discounted initial cost of the TMD at $t = 0$ must be considered in the cost accumulation (Wen 2001; Wen and Kang 2001), the term $C_{0,cs}$ in Equation 4.39 is substituted with $C_{0,cs}e^{-\lambda t}$. It can be observed that the installation of the TMD after some time is not as advantageous as before, since the BET significantly increases in comparison with the case of installation at $t = 0$ and the cost overtime is not greatly reduced with respect to the uncontrolled case; this aspect depends on the choice of $c_{0,cs}$.

6.4.4 Parametric analyses on the variation of the cost model parameters

In the first part of the analysis, the initial installation cost ($C_{0,cs}$) of the TMD devices is assumed as a deterministic quantity and it is set equal to a fixed percentage of the initial

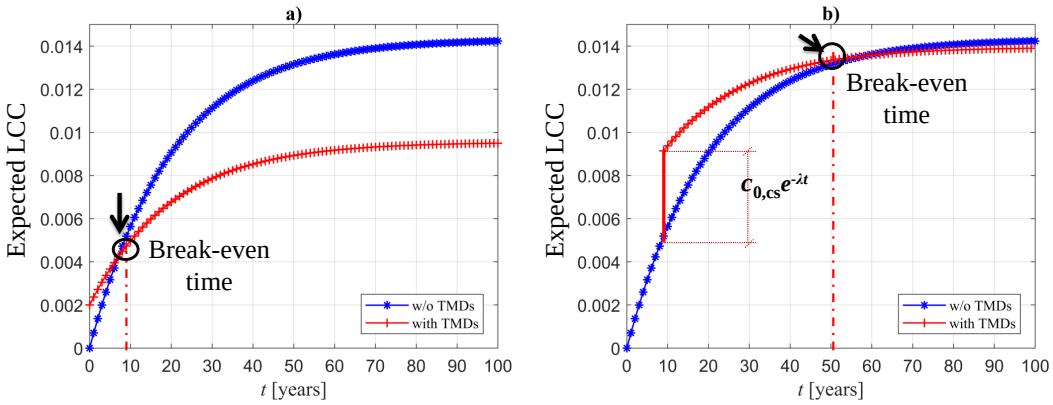

Fig. 6.15: Comparison between the expected values of the total life-cycle cost, accounting for wind-induced damage and intervention/repair cost, with and without TMDs: a) TMDs installed at $t = 0$ years; b) TMDs installed $t = 10$ years after building construction/opening.

structural cost, i.e. $c_{0,cs} = C_{0,cs}/C_{0,s} = 0.2\%$. This cost value is in line with the discussion in Section 4.8. To investigate the effect of the TMD installation cost, a parametric analysis is subsequently carried out by varying $c_{0,cs}$ between 0.2% and 0.6%. Figure 6.16 illustrates the expected normalized investment costs as a function of lifetime for different initial installation costs of the TMD. If $c_{0,cs}$ increases, the BET increases, as the time duration for which the initial investment is amortized, becomes longer. Figure 6.17 summarizes the BET values as a function of $c_{0,cs}$.

These considerations can be useful in the design phase since $c_{0,cs}$ becomes a design parameter to reach the best cost-saving solutions. On the basis of this consideration, as the cost of the TMD varies, BET becomes a key element for the best choice between different proposed solutions, for example, by different companies.

The mass ratio μ is a significant design variable of the TMD (Section 5.4) and in most applications the mass ratio is designed to be in the range of 1 to 10%. When the mass ratio increases, the TMD becomes more effective but an increased weight at the top of the building could cause high stress values, especially to the columns on the lower floors of the building. Moreover, an increase of the TMD mass corresponds to an increase in the terms of cost of the TMD. Interpolating cost data of TMDs with different mass ratios reported in Wang et al. (2016), a step cost increment of 1.2 is considered corresponding to an increase of 0.1% of μ. The TMD parameters and the normalized cost values with different μ are reported in Table 6.1.

As an example, Figure 6.18 illustrates the peak top floor IDR for directions x and y and the peak top floor a for different μ: from 0.01 to 0.03. From the Figures it is quite clear the

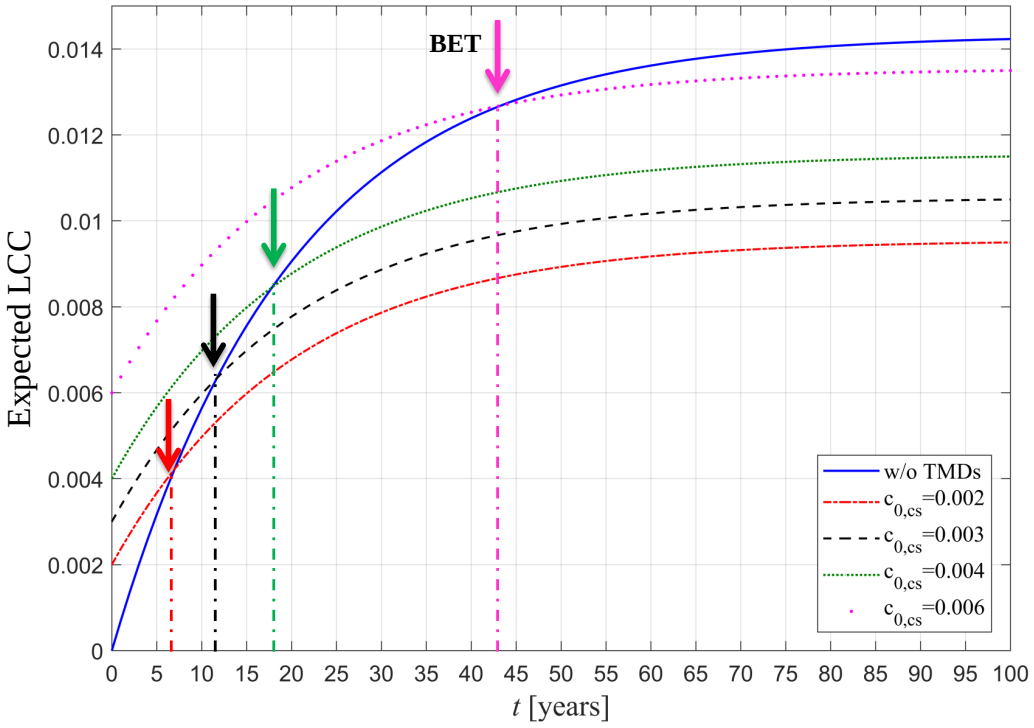

Fig. 6.16: Total normalized lifetime cost, accounting for wind-induced damage and intervention/repair cost, for different values of $c_{0,cs} = C_{0,cs}/C_{0,s}$.

fact that to the increase of μ corresponds a slight reduction in terms of structural response. The same trend is observed in Figure 6.19 as concerns the annual damage probability.
Figure 6.20 reports the total normalized lifetime investment costs by varying μ. The inspection of this Figure suggests that the cost increase is more relevant than the reduction of the structural response, for higher values of μ. Indeed, for values of μ between 0.01 and 0.02 no substantial variations in terms of cost are appreciated. Instead, for μ higher than 0.02, cost increases are significant enough to shift BET to the right until the installation of the device is no longer advantageous ($\mu = 0.03$). Considering these results it is reasonable to assume $\mu = 0.02$.

The effect of the discount rate λ on the cost estimation is studied through a parametric analysis. Table 6.2 summarizes the main results of this investigation and shows the expected normalized total cost for different lifetimes ($t = 10$ years, $t = 50$ years and $t = 100$ years), with and without installation of the TMD. As λ increases, it is observed a decrease

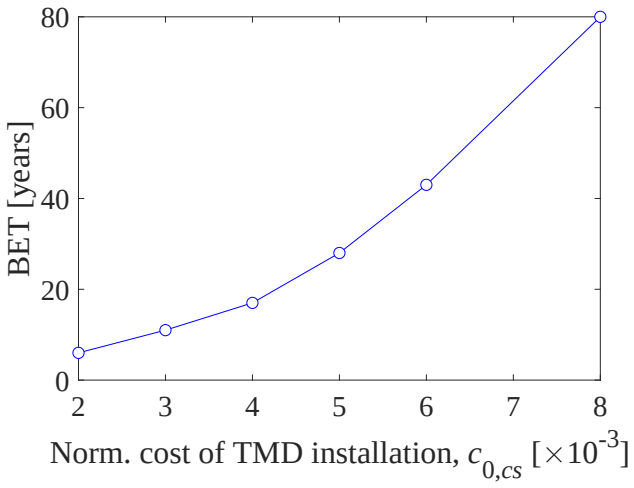

Fig. 6.17: Break-even time (BET) as a function of the initial normalized cost of the TMDs, $c_{0,cs} = C_{0,cs}/C_{0,s}$.

in the expected total cost, more pronounced for greater lifetimes. A non-negligible diminution of about 30% is noted at $t = 100$ years if the discount rate is increased from $\lambda = 0.04$ to $\lambda = 0.06$ with TMD system being installed.

Finally, Table 6.3 presents the separate contributions of the various damage types to the total normalized lifetime costs, for $t = 50$ years. In particular, the cost related to wind-induced damage to partition walls in x and y directions ($c_{pw,x}$, $c_{pw,y}$) and the cost related to the damage of suspended ceilings (c_{sc}) are separately reported. As previously observed,

Table 6.1: TMD parameters by varying the mass ratio μ

μ	Frequency ratio	Damping ratio	$c_{0,cs}[10^{-3}]$
0.01	0.9926	0.049	0.3
0.012	0.9911	0.054	0.5
0.014	0.9896	0.059	0.7
0.016	0.9882	0.063	0.9
0.018	0.9867	0.067	1.4
0.02	0.9853	0.070	2
0.022	0.9838	0.074	2.9
0.024	0.9824	0.077	4.1
0.03	0.9781	0.086	12.4

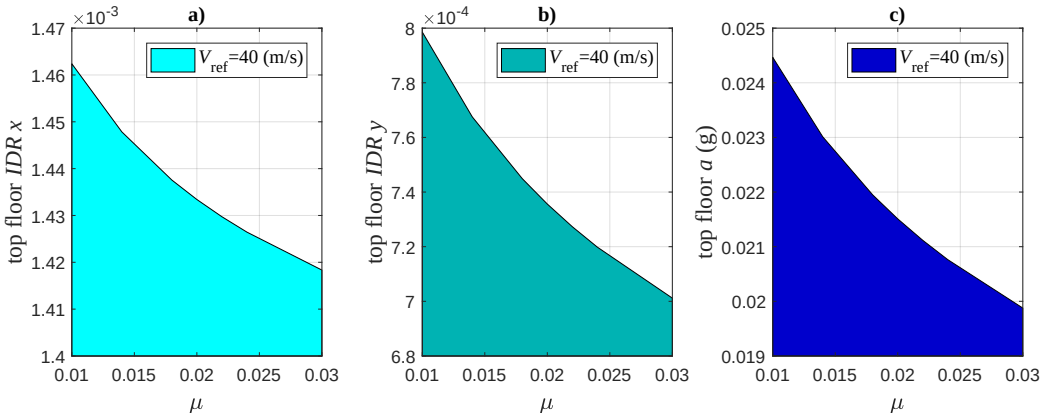

Fig. 6.18: Peak top floor IDR for directions x (a) and y (b) and peak top floor a (c) with respect to μ ($V_{ref} = 40$ m/s).

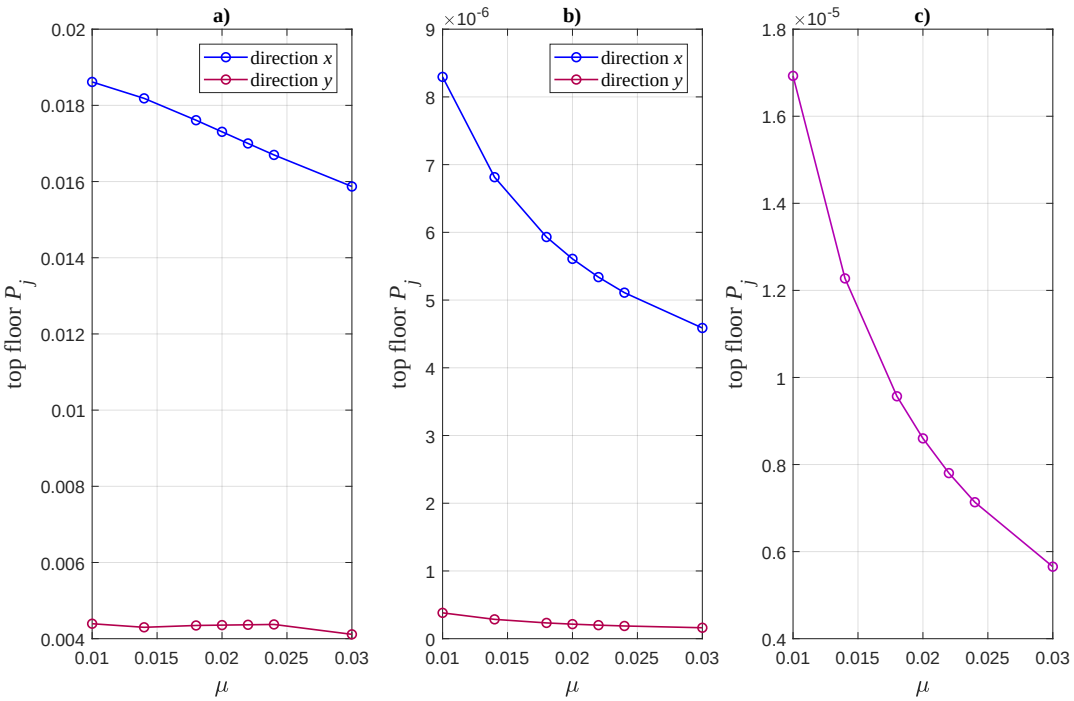

Fig. 6.19: Top floor annual damage probability for partition walls (a), glass façades (b) for directions x and y and suspendend ceilings (c).

the damage (i.e. intervention cost) related to suspended ceilings and glass façades is smaller than the one observed for partition walls. These results are not generalizable as they are based on the unit costs suggested by the FEMA guidelines and as they strictly depend

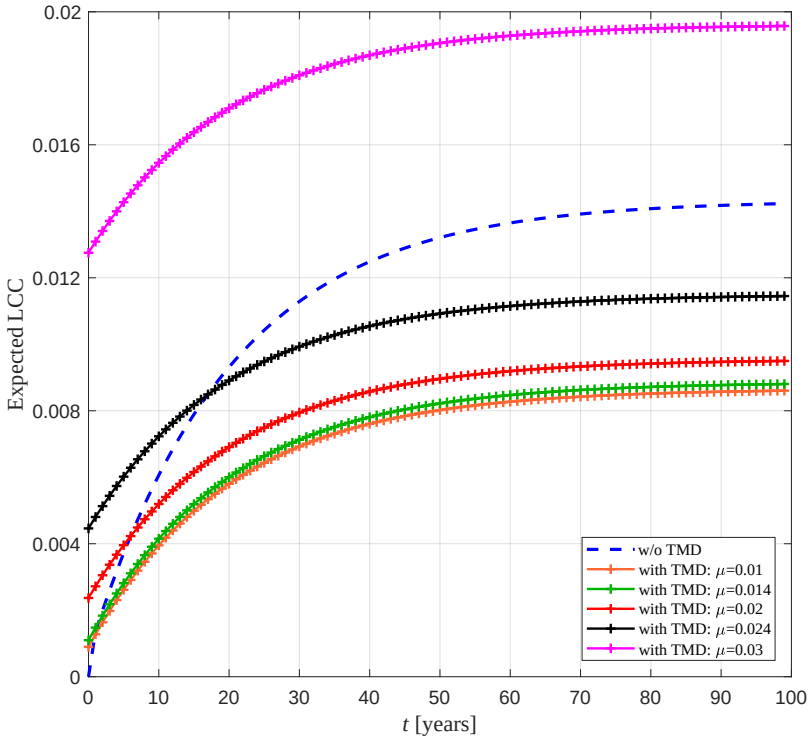

Fig. 6.20: Total normalized lifetime investment costs, accounting for wind-induced damage and intervention/repair cost, for different values of μ.

Table 6.2: Total normalized investment cost as a function of the discount rate λ for different lifetimes (*note*: t_{10}, ten years; t_{50}, fifty years; t_{100}, one hundred years).

	$\lambda = 0.04$		$\lambda = 0.05$		$\lambda = 0.06$	
t	w/o TMDs	with TMDs	w/o TMDs	with TMDs	w/o TMDs	with TMDs
t_{10}	0.0059	0.0052	0.0056	0.005	0.0051	0.0049
t_{50}	0.0165	0.0091	0.0132	0.0083	0.0119	0.0079
t_{100}	0.0176	0.0143	0.0141	0.0091	0.0113	0.0085

on the selected building. More investigation is possibly needed to better quantify the unit costs along with their estimation uncertainty. This item is beyond the scope of this study but may possibly be considered in future investigations.

Table 6.3: Total normalized life-cycle cost disaggregation for $t = 50$ years (*note*: $c_{pw,x}$, partition walls in x direction; $c_{pw,y}$, partition walls in y direction; c_{sc}, suspended ceilings).

$c_{gs,x}10^{-4}$		$c_{gs,y}10^{-4}$		$c_{pw,x}$		$c_{pw,y}$		$c_{sc}10^{-4}$	
w/o TMDs	with TMDs	w/o TMDs	with TMDs	w/o TMDs	with TMDs	w/o TMDs	with TMDs	w/o TMDs	with TMDs
0.135	0.007	.015	0.0002	0.01	0.006	0.003	0.0013	0.16	0.004

6.5 Design of nonstructural components

While glass façades are usually uniformly distributed over the building surface, the distribution of internal divisions can be considered related to the destination of use of a specific area inside the building. Consequently, considering the sensibility to the damage of nonstructural components, this aspect should be not neglected and it needs to be considered as a part of the design process. Once chosen the main characteristics of the building, the best building orientation and the adequate control system (previous steps), it is possible to investigate different design solution for nonstructural elements.

6.5.1 Indoor spaces distribution

The distribution of indoor spaces is linked to the destination of use of each setting. With the main objective of comparing different design alternatives, three destination of use groups are examined:

1. G1: sport area or relax area;
2. G2: meeting/conference area (open space);
3. G3: office area.

The sport/relax area is characterized by a central open space with separate rooms (fitness and changing rooms) distributed along the perimeter of the building (Figure 6.21). The meeting/conference area is composed of an open space with a minimal number of private rooms (Figure 6.22). The office area is developed with head offices distributed along the perimeter and employees offices clustered in the building core (Figure 6.23). Suspended ceilings are used for indoor areas that do not have windows and do not enjoy natural light and for open spaces that accommodate at same time many people (*Workplace Standards and Guidelines for office space*). The numbers of unit element for each group are summarized in Table 6.4.

Assuming the hypothesis that at the request of the client there is the need for 1 confer-

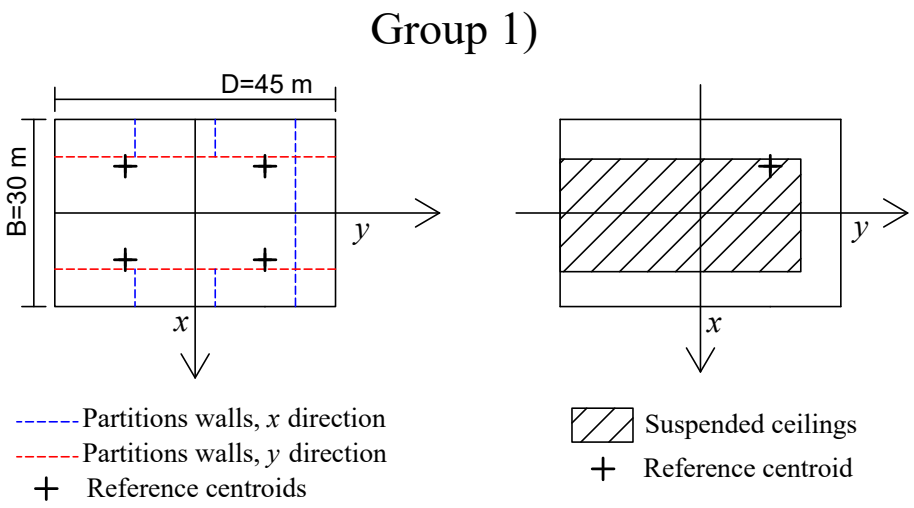

Fig. 6.21: Group 1 internal nonstructural components distribution (G_1).

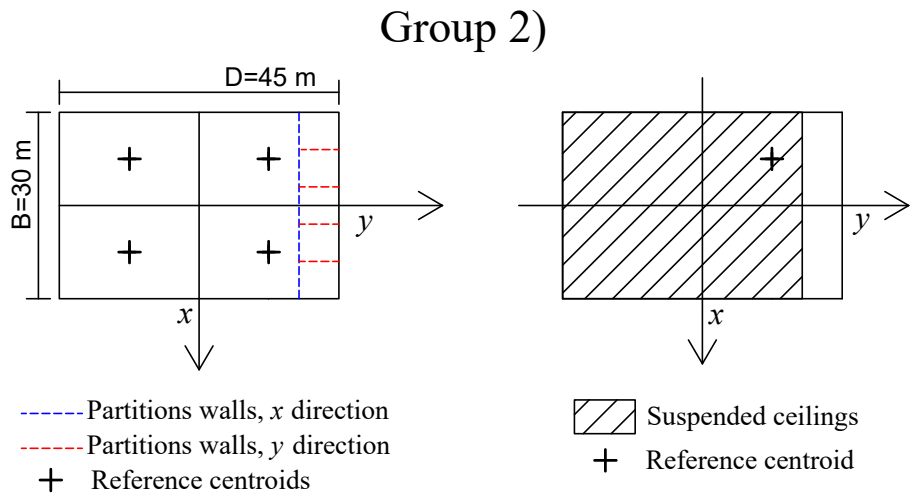

Fig. 6.22: Group 2 internal nonstructural components distribution (G_2).

ence area (G2) and 1 relax area (G1) at least every ten floors, two different distributions are compared:

- A): G1 group is considered for floors 9-19-29-39-49-59, G2 group for floors 10-20-30-

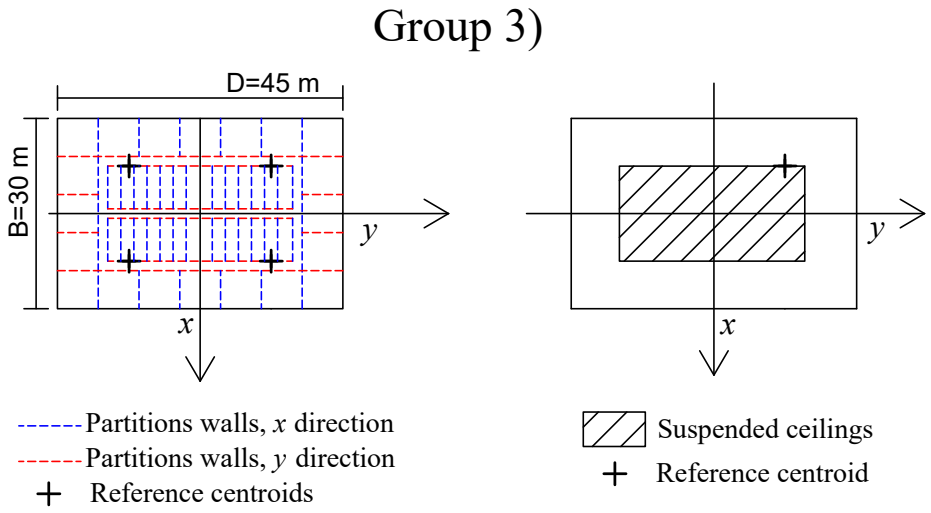

Fig. 6.23: Group 3 internal nonstructural components distribution (G_3).

Table 6.4: Nonstructural components number of units

Group	$\hat{n}_x(z)$	$\hat{n}_y(z)$	$\hat{n}_a(z)$
G1	1.8	3	3
G2	1	0.9	5
G3	10	7.8	1.9

40-50-60 and G3 group for floors 1:8, 11:18, 22:28, 32:38, 42:48, 52:58.

- B): G1 group is considered for floors 20:22, 55:57, G2 group for floors 23:25,58:60 and G3 group for floors 1:19, 26:54.

Figure 6.24 shows the total normalized lifetime expected costs, accounting for configurations A and B with respect to the initial design alternative described in Section 5.3. On the one hand it is clear that the location of areas with open spaces (G1 and G2) within the height of the building is not particularly influential. On the other hand, since the partition walls are particularly damage-sensitive, the increase in terms of numbers of units (Table 6.4) significantly contributes to the cost increase. This aspect confirms that the destination of use of a given area and consequently the distribution of nonstructural elements that are particularly damage-sensitive, can significantly influence the final design.

Figure 6.25 confirms the fact that the use of a control device like the TMD reduces costs

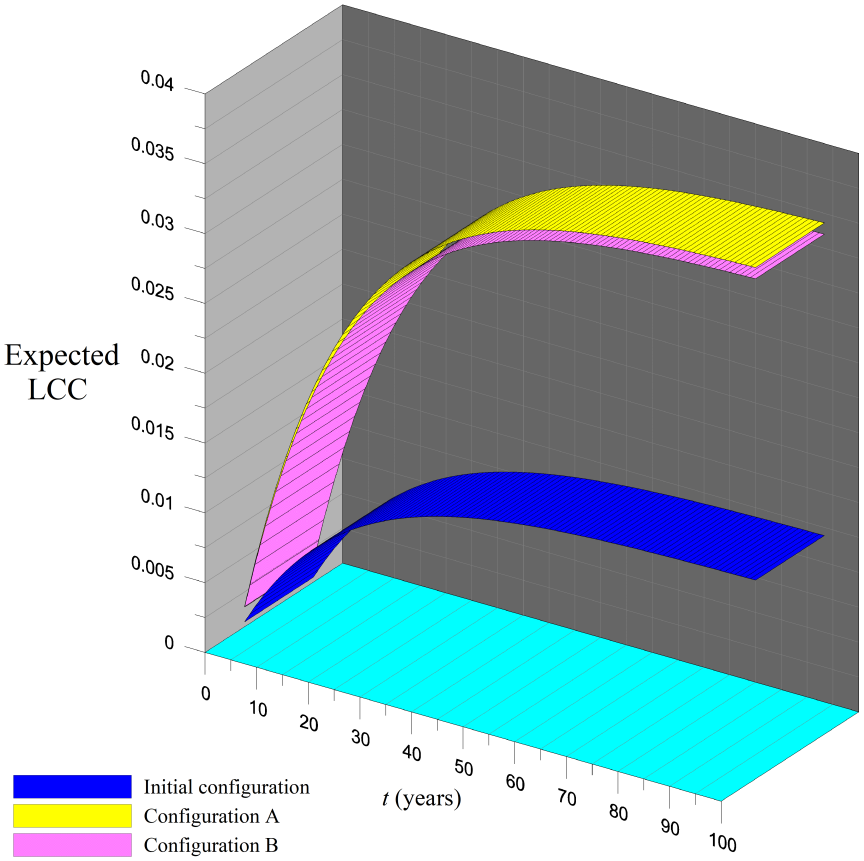

Fig. 6.24: Total normalized lifetime expected costs, accounting for the two different configurations of non structural elements (A,B) with respect to the initial one.

over time (Figure 6.25a). However, this assumption is tied to the initial cost of the device which should generally not exceed a certain percentage of the initial construction cost, as highlighted in Figure 6.25b).

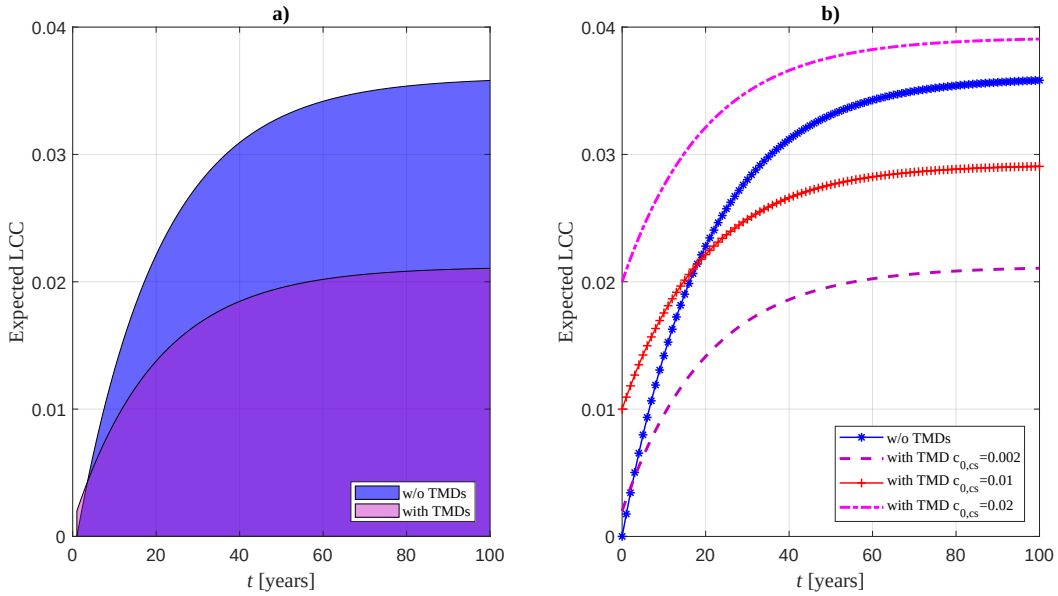

Fig. 6.25: Comparison between the expected values of the total investment cost, accounting for wind-induced damage and intervention/repair cost, with and without TMD: a) $c_{0,cs} = 0.002$, b) $c_{0,cs} = 0.002, 0.01, 0.02$.

6.6 LCCWD global results

According to Section 4.10 the LCCWD chart of the global results is here summarized. The comparative results are function of:

1. the design configuration (DC);
2. the expected cost evaluated for a lifetime of 100 years, calculated as described in Section 4.8;
3. parameters that characterize the control system: $c_{0,cs}$ and the time BET.

As a summary report, the following DCs (deeply investigated in previous Sections) are explored:

- different orientation by rotating the building between 0° and 360 with step increment of 22.5;
- controlled configuration for the best building orientation in the case of TMD installed at the top floor at the initial construction time, i.e. DC = 90°$cs(0)$. ;
- controlled configuration for the best building orientation in the case of TMD installed at the top floor after 10 years from the building construction7opening, i.e. DC = 90°$cs(10)$;
- controlled configuration for the best building orientation in the case of TMD installed at the initial construction time by varying the initial cost of the TMD, i.e. DC = 90°$cs(0)$. The column $c_{0,cs}$ identifies the different values of the initial costs. As underlined in Section 6.4.4 these alternatives are a key element for the best choice between different proposed solutions, for example, by different companies;
- different configuration for indoor nonstructural element distribution, i.e. DC = 90° A or B;
- controlled configuration for alternative B, i.e. DC = 90°$Bcs(0)$.

The main advantage of this approach is the possibility to explore different solutions that are easily comparable. The inspection of the global LCCWD chart in Figure 6.26 allows to:

- directly compare different design solutions on the basis of a common parameter, the expected life-cycle cost;
- create a connection between the designer and the stakeholder by putting together the methodology and an adequate representation of the results also suitable for a non-technical audience;
- choose between different alternatives by evaluating costs and benefits. For example, on the basis of the best cost-saved solution DC= 90°cs and $c_{0,cs} = 0.002$ should be selected;
- The client can decide whether the choice fully reflects his needs or if he wants to find a solution that agrees with both the principle of minimum cost and the benefits associated with a correct and complete usability of the construction over time.

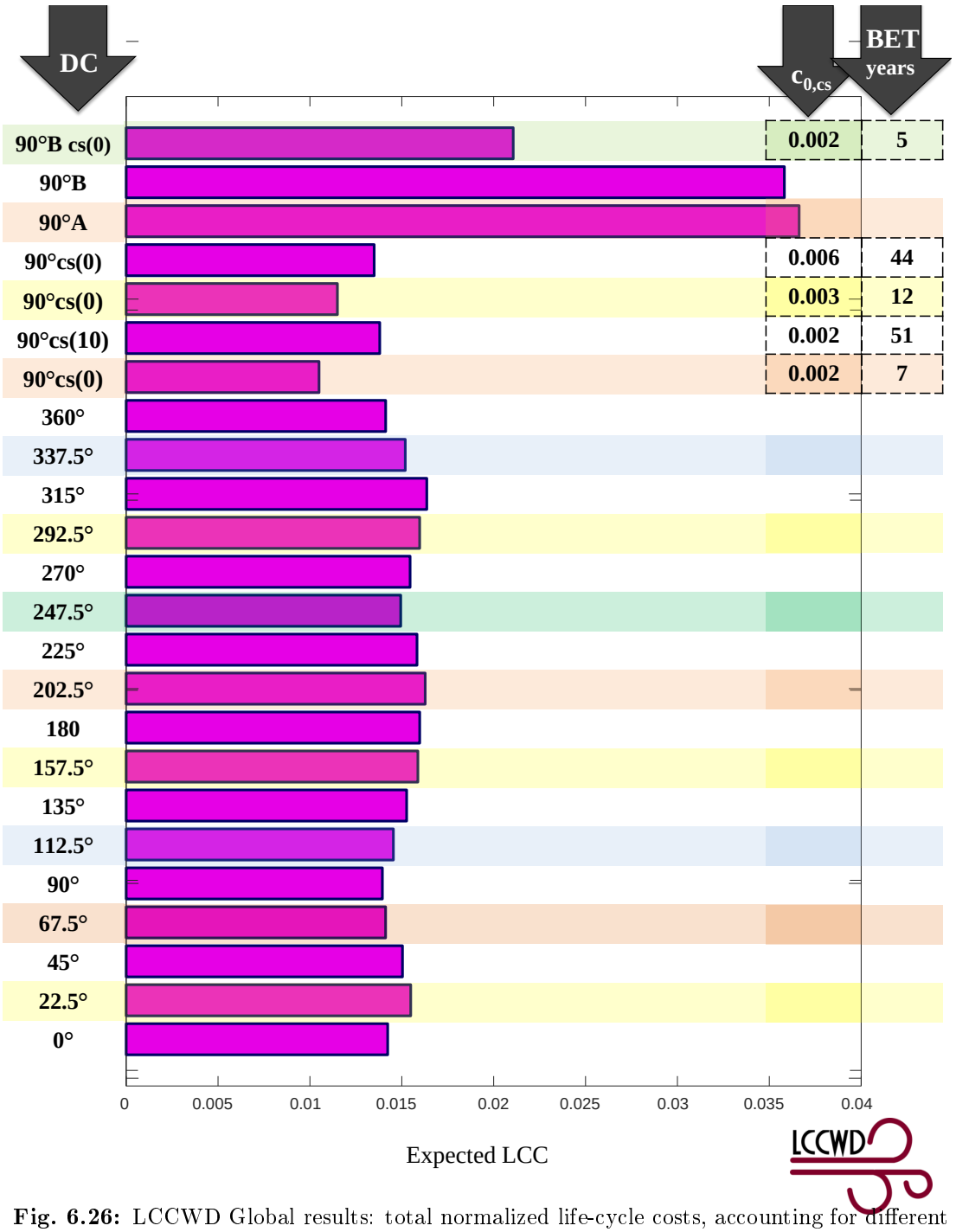

Fig. 6.26: LCCWD Global results: total normalized life-cycle costs, accounting for different design alternatives.

Chapter 7

Conclusions

This chapter summarizes the most important conclusions of the thesis responding appropriately to the research questions stated in Chapter 1:

(a) *it is possible to develop a life-cycle cost-based design method specific for tall buildings that responds to the needs of designer and stakeholders in terms of decision-making quantities that can be understood by both?*

(b) *how to account for all the uncertainties involved in the design process of tall buildings under wind load with an acceptable computational effort?*

In order to get answer to the research questions, a practical design approach named LC-CWD (life-Cycle Cost Wind Design) is proposed, that is tailored to tall buildings subjected to wind load.
Life-cycle cost approaches are widely used in the current practice of many disciplines for choosing the most economic design solution, by comparing different alternatives.
As an example, in earthquake engineering local standards are spreading out in order to give indication for the practical application of cost-based methodologies (Section 2.2.1).

As underlined in section 2.6, the applications in wind engineering are still few and deal with specific problems that make this design approach unattractive for the designers and not very understandable for the stakeholders. The LCCWD method provides the basics for using an automated design tool suitable for both parts.

7.1 Summary of the work

This research project is presented in 7 chapters. Chapter 1 presents the topic with the main research questions and the main research objectives. Chapter 2 illustrates a literature overview on LCCA for tall buildings also equipped with control devices and, upon the identified shortcomings, the LCCWD improvements are also indicated. Chapter 3 shows the basic theories on the characterization of the dynamic response of wind excited tall buildings. Chapter 4 describes the LCCWD approach for all the steps of the analysis. Chapter 5 illustrates the case study. Chapter 6 presents the numerical results by comparing different cost-effective design solutions. Finally, Chapter 7 summarizes the thesis.

7.2 Main outcomes

The efficiency of the LCCWD approach is demonstrated by making use of a case study of a 180-meters high rectangular building, for which wind tunnel data are available. In order to minimize the computational effort, wind tunnel records are directly converted to generalized forces, enabling the analysis in the frequency domain. Full-scale wind speeds and direction data records are evaluated for the specific site location of the building. In order to evaluate the influence of the orientation of the tall building, the empirical probability density functions of the annual maxima of wind speed and direction is numerically reconstructed by processing experimental data.
Empirical structural fragility curves are selected from the FEMA database. Damage to nonstructural elements of glass façades, partition walls and suspended ceilings are considered in the numerical application.
The control system consists in a bidirectional TMD, located at the elastic center of the top floor of the building. The structural analysis is carried out considering non linear mode shapes and torsional response. Costs related to both drift-sensitive and acceleration-sensitive nonstructural components are evaluated and the beneficial contribution of the TMD in reducing both types of damage is assessed in a life-cycle cost perspective.

The main results of the numerical application can be summarized as follows:

- to establish the best orientation of the building for a specific geographic location;
- to account for wind directionality;
- to determine most appropriate types of nonstructural elements by comparing different cost-based solutions;
- to provide indications about the possible use of the indoor spaces within the height of the building in relation to the distribution of nonstructural components;
- to estimate the time, called Break-Even Time (BET), after which the initial costs associated with the installation of the control system are absorbed, with a consequent significant lifetime costs reduction.

As concerns the research questions, a positive answer to question (a) can be provided considering that the final results of the procedure summarize in a clear and comprehensible manner the complexity of the analyses carried out. The global chart represented in Figure 6.26 considers, for all the proposed design alternatives, the relevant information over the period of analysis:

1. an identification code that describes the design configuration (DC);
2. the value of the expected cost calculated for a fixed lifetime;
3. parameters that justify the possible economic return (cost/benefit) to the expenses of a higher initial investment (BET).

The common decision (designer/stakeholder) variable is expressed in monetary value (life-cycle cost) and it is used as a parameter for comparison.
Based on the probabilistic PEER integral approach, the LCCWD allows to get answers also to question (b) by taking into account the uncertainties related to:

- the wind modeling: the uncertainty associated with the aerodynamic load estimation is efficiently taken into account by parsing the experimentally measured generalized wind forces.
- the structural modeling (aerodynamic structural response): the structural response is evaluated in probabilistic terms (PDF of EDP).

- the fragility models (probabilistic analysis of the damage associated to nonstructural elements). LCCWD relates the probability of exceeding a specific wind-induced non-structural damage state to the intervention and repair cost by incorporating specific structural fragility functions for nonstructural components.

In Chapter 4 all the previous aspects of the LCCWD procedure are deeply investigated.

The LCCWD is useful and easily adaptable to real applications in order to choose the best cost-based design solution on the basis of different alternatives that will simultaneously meet the need of customers and designers. Many sources of uncertainties are taken into account. Different design practical issues are explored. The long-term cost-effective aspect related to the installation of a structural control device are taken into account.

With the LCCWD it is possible to accept or reject design alternatives and select optimal and technically valid systems or decide for a particular structural control device that meets specific cost-based technical performance.

7.3 Future developments

On the basis of the present work, with the challenge of making even more comprehensive life-cycle cost-based design for tall buildings, some efforts are still necessary:

- since it is a general approach, LCCWD offer the base to develop large scale practical applications with the future challenge to provide dedicated databases and benchmarks (building's materials, geometry, shape and so on);
- given the lack of experimental campaigns to characterize the damage probability of non-structural elements, it is of primary importance to develop a fragility database (tool) regarding non structural components. Alternatively, specific studies on the adaptability of the FEMA fragility curves, largely used in earthquake engineering, need to be carried out;
- more complex models in the characterization of the wind effect on the building (for example aeroelastic effects or modifications in the aerodynamic damping) can be considered in the analysis;

- non-linear behavior under the action of high intensity winds (for different geographical locations), can be included in the procedure;
- building deterioration (i.e. the building cannot be repaired back to its original condition as time passes) can be considered. Under this hypothesis, damage probability curves might be not conservative over time;
- wind borne debris models can be considered as a source of damage in the case of strong wind events;
- the LCCWD procedure can be considered not only at the building level but also at the neighborhoods level contributing to the "community resilience" of specific areas;
- real cost data can be introduced in the numerical analyses with the aim of increasingly merging the two separate worlds of designers and investors.

Bibliography

Allemang, R.J. and D.L. Brown (1982). "A Correlation Coefficient for Modal Vector Analysis". In: *Proceedings of the 1st International Modal Analysis Conference in Orlando*, pp. 110–116.

Arditi, D. and M.M. Messiah (1996). "Life-Cycle Costing in Municipal Construction Projects". In: *Journal of Infrastructure Systems* 2(1), pp. –.

ASCE6/7-10 (2010). *Minimum Design Loads for Buildings and Other Structures*. American Society of Civil Engineers, Reston, Virginia (USA).

ASCE7-16 (2017). *Minimum Design Loads for Buildings and Other Structures*. American Society of Civil Engineers, Reston, Virginia (USA).

Aslani, H. and E. Miranda. "Probabilistic earthquake loss estimation and loss disaggregation in buildings, Report no. 157". In: *The John A. Blume Earthquake Engineering Center*.

Asprone, D., F. Jalayer, A. Prota, and G. Manfredi (2010). "Proposal of a probabilistic model for multi-hazard risk assessment of structures in seismic zones subjected to blast for the limit state of collapse". In: *Structural Safety* 32, pp. 25–34.

ASTM/E917-02 (2002). *Standard Practice for Measuring Life-Cycle Costs of Buildings and Building Systems*. Tech. rep. ASTM International, West Conshohocken, PA.

Aswegan, K., R. Larsen, R. Klemencic, J. Hooper, and J. Hasselbauer (2017). "Performance-based wind and seismic engineering: Benefits of considering multiple hazards". In: pp. 473–484.

Augusti, G. and M. Ciampoli (2008). "Performance-Based design in risk assessment and reduction". In: *Probabilstic Engineering Mechanics* 23.4, pp. 496–508.

Azioni ed effetti del vento su edifici alti. `https://www.unirc.it/documentazione/materiale_didattico/599_2010_264_8140.pdf`. Accessed: 2017-11-30.

Barbato, M., F. Petrini, V.U. Unnikrishnan, and M. Ciampoli (2013). "Performance-Based Hurricane Engineering (PBHE) framework". In: *Structural Safety* 45, pp. 24–35.

Barone, G. and D.M. Frangopol (2014). "Life-cycle maintenance of deteriorating structures by multi-objective optimization involving reliability, risk, availability, hazard and cost". In: *Structural Safety* 48, pp. 40–50.

Basile, S., R. Burlon, and F. Morales (2015). "Joint Probability Distributions for Wind Speed and Direction. A case study in Sicily." In: *4th International conference on Renewable Energy Research and Applications*. Palermo, Italy.

Beck, A.T., I.A. Kougioumtzoglou, and K.R.M. Dos Santos (2014). "Optimal performance-based design of non-linear stochastic dynamical RC structures subject to stationary wind excitation". In: *Engineering Structures* 78, pp. 145–153.

Bernardini, E., S.M.J. Spence, D.-K. Kwon, and A. Kareem (2015). "Performance-Based Design of High-Rise Buildings for Occupant Comfort". In: *Journal of Structural Engineering (United States)* 141.10.

Bjarnadottir, S., Y. Li, and M.G. Stewart (2014). "Regional loss estimation due to hurricane wind and hurricane-induced surge considering climate variability". In: *Structure and Infrastructure Engineering* 10.11, pp. 1369–1384.

Blaise, N., T. Canor, and V. Denöel (2016). "Reconstruction of the envelope of non-Gaussian structural responses with principal static wind loads". In: *Journal of Wind Engineering and Industrial Aerodynamics* 149, pp. 59–76.

Bluff-body aerodynamics. `http://windyn.dicca.unige.it/windenglist.php?id=8`. Accessed: 2017-11-30.

Bobby, S., S.M.J. Spence, E. Bernardini, and Kareem A. (2014). "Performance-based topology optimization for wind-excited tall buildings: A framework". In: *Engineering Structures* 74, pp. 242–255.

Borri, C. and S. Pastò (2006). *Lezioni di Ingegneria del Vento*. Firenze University Press (ITA).

Caracoglia, L (2014). "A stochastic model for examining along-wind loading uncertainty and intervention costs due to wind-induced damage on tall buildings". In: *Engineering Structures* 78, pp. 121–132.

Carta, J. A. and C. Ramirez P.and Bueno (2008). "A joint probability density function of wind speed and direction for wind energy analysis". In: *Energy Conversion and Management* 49, pp. 1309–1320.

Chen, J. and X. Zhang (2009). "An empirical joint probability density function of wind speed and direction". In: *the Seventh Asia-Pacific Conference on Wind Engineering*. Taipei, Taiwan.

Chen, J., Zeng. X., and Y. Peng (2017). "Probabilistic analysis of wind-induced vibration mitigation of structures by fluid viscous dampers". In: *Journal of Sound and Vibration* 409.Supplement C, pp. 287–305.

Chen, X. and G. Huang (2009). "Evaluation of peak resultant response for wind-excited tall buildings". In: *Engineering Structures* 31, pp. 858–868.

Chen, X. and A. Kareem (2005). "Coupled Dynamic Analysis and Equivalent Static Wind Loads on Buildings with Three-Dimensional Modes". In: *Journal of Structural Engineering* ASCE, pp. 1071–1082.

Chen, Y. (2011). "Optimal design of a complex high-rise building based on cost-effectiveness criterion". In: *Advanced Materials Research* 163–167, pp. 2295–2303.

Cheng, C.M., P.C. Lu, and M.S. Tsai (2002). "Acrosswind aerodynamic damping of isolated square-shaped buildings". In: *Journal of Wind Engineering and Industrial Aerodynamics* 90.12–15, pp. 1743–1756.

Chu, S.Y., T.T. Soong, and Reinhorn A.M. (2005). *Active, hybrid and semi-active structural control*. Wiley.

Chuang, W.C. and S.M.J. Spence (2017). "A performance-based design framework for the integrated collapse and non-collapse assessment of wind excited buildings". In: *Engineering Structures* 150, pp. 746–758.

Chung Yau, S., N. Lin, and E. Vanmarcke (2011). "Hurricane damage and loss estimation using an integrated vulnerability model". In: *Natural Hazards Review* 12.4, pp. 184–189.

Ciampoli, M. and F. Petrini (2012). "Performance-based Aeolian risk assessment and reduction for tall buildings". In: *Probabilistic Engineering Mechanics* 28.-, pp. 75–84.

Ciampoli, M., F. Petrini, and G. Augusti (2011). "Performance-based wind engineering: towards a general procedure". In: *Structural Safety* 32.-, pp. 367–378.

Constantinou, M.C., T.T. Soong, and Dargush (1998). *Passive Energy Dissipation Systems for Structural Design and Retrofit*. MCEER.

Cornell, C. and H. Krawinkler (2000). "Progress and Challenges in Seismic Performance Assessment". In: *PEER Center News* 3.2, pp. 1–3.

Council on Tall Buildings and Urban Habitat, CTBUH. `http://www.ctbuh.org/`. Accessed: 2017-11-20.

Cui, W. and L. Caracoglia (2015). "Simulation and analysis of intervention costs due to wind-induced damage on tall building". In: *Engineering Structures* 87, pp. 183–197.

— (2016a). "Exploring hurricane wind speed along US Atlantic coast in warming climate and effects on predictions of structural damage and intervention costs". In: *Engineering Structures* 112, pp. 209–225.

— (2016b). "Simulation and analysis of intervention costs due to wind-induced damage on tall buildings". In: *Engineering Structures* 87, pp. 183–197.

Davenport, A. G. (1961). "The application of statistical concepts to the wind loading to structures". In: *Proceedings of the Institution of Civil Engineering*. London, UK.

— (1964). "Note on the distribution of the largest value of a random function with application to gust loading". In: *Proceeding of the Institutions of civili Engineering* 28, pp. 187–196.

— (1967). "Gust loading factors". In: *Journal of the Structural Division,ASCE* 93, pp. 11–34.

— (1971). "Response of six building shapes to turbulent wind". In: *Philosophical Transactions of the Royal Society of London. Series A, Mathematical and Physical Sciences* 269.1199, pp. 385–394.

Den Hartog, J.P. (1956). *Mechanical vibrations*. McGraw Hill Book Company, New, York.

Denöel, V. (2014). "Multiple timescale spectral analysis". In: *Probabilistic Engineering Mechanics* 39.

Design guide for improving School Safety in Earthquakes, Floods and High Winds - Chapter 2. `https://www.fema.gov/media-library-data/20130726-1530-20490-8554/424_ch2_web.pdf`. Accessed: 2017-12-05.

Dyanati, M., Q. Huang, and D. Roke (2017). "Cost-benefit evaluation of self-centring concentrically braced frames considering uncertainties". In: *Structure and Infrastructure Engineering* 13.5, pp. 537–553.

FEMA-283 (1996). *Performance-Based Seismic Design of Buildings – An Action Plan for Future Studies*. Tech. rep. prepared by the Earthquake Engineering Research Center for the Federal Emergency Management Agency, Washington, D.C.

FEMA-349 (2000). *Action Plan for Performance-based Seismic Design*. Tech. rep. prepared by the Earthquake Engineering Research Center for the Federal Emergency Management Agency, Washington, D.C.

FEMA-356 (2000). *Guidelines for Seismic Rehabilitation of Buildings Vol. 1: Guidelines*. Tech. rep. prepared by the American Society of Civil Engineers for the Federal Emergency Management Agency, Washington DC.

FEMA-445 (2006). *Next-Generation Performance-Based Seismic Design Guidelines*. Tech. rep. prepared by the Applied technology Council for the Federal Emergency Management Agency, Washington DC.

FEMA-P-58 (2012a). *Performance Assessment Calculation Tool, Volume 1*. Tech. rep. URL: `http://www.fema.gov/media-library/assets/documents/90380`.

— (2012b). *Seismic Performance Assessment of Building, Volume 1*. Tech. rep. URL: http://www.fema.gov/media-library/assets/documents/90380.

— (2012c). *Seismic Performance Assessment of Building, Volume 2*. Tech. rep. URL: http://www.fema.gov/media-library/assets/documents/90380.

— (2012d). *Seismic Performance Assessment of Building, Volume 3*. Tech. rep. URL: http://www.fema.gov/media-library/assets/documents/90380.

Filliben, J.J., K. Gurley, J.P. Pinelli, and Simiu (2002). "Fragility curves, damage matrices, and wind induced loss estimation". In: *Third International Conference on Computer Simulation in Risk Analysis and Hazard Mitigation*. Sintra, Portugal, pp. 119–126.

Frangopol, D.M. and K. Maute (2003). "Life-cycle reliability-based optimization of civil and aerospace structures". In: *Computers and Structures* 81.7, pp. 397–410.

Griffis, L., V. Patel, S. Muthukumar, and Baldava S. (2013). "A Framework for Performance-Based Wind Engineering: Learning from Our Past". In: *Proceedings of the 2012 ATC and SEI Conference on Advances in Hurricane Engineering*. Sintra, Portugal, pp. 1205–12016.

Gu, M. and Y. Quan (2044). "Across-wind loads of typical tall buildings". In: *Journal of Wind Engineering and Industrial Aerodynamics* 92, 1147—1165.

Günel, M.H. and H.E. Ilgin (2014). *Tall Buildings structural systems and aerodynamic form*. London and New York: Routledge, Tayor & francis Group.

Hasançebi, O. (2017). "Cost efficiency analyses of steel framework for economical design of multi-storey buildings". In: *Journal of constructional steel research* 128, pp. 380–396.

Hayashida, H., Y. Mataki, and Y. Iwasa (1992). "Aerodynamic damping effects of tall building for a vortex induced vibration". In: *Journal of Wind Engineering and Industrial Aerodynamics* 43.1–3, pp. 1973–1983.

Hazus (2017). *Hazus MH-21 Techincal Report*. Tech. rep. URL: http://www.fema.gov/plan/prevent/hazus..

Hoang, N., Y. Fujino, and P. Warnitchai (2008). "Optimal tuned mass damper for seismic applications and practical design formulas". In: *Engineering Structures* 30, pp. 707–715.

Holmes, J.D. (1987). "Mode shape corrections for dynamic response to wind". In: *Engineering Structures* 9, pp. 210–212.

— (2007). *Wind loading of structures (second Edition)*. Taylor & Francis Group, New York.

Holmes, J.D., A. Rofail, and L. Aurelius (2003). "High frequency base balance methodologies for tall buildings with torsional and coupled resonant modes". In: *Proceedings of the* 11^{th} *International Conference on Wind Engineering*. Lubbock, USA, pp. 2381–2388.

Hoven, I. Van der (1957). "POWER SPECTRUM OF HORIZONTAL WIND SPEED IN THE FREQUENCY RANGE FROM 0.0007 TO 900 CYCLES PER HOUR". In: *Journal of meterology* 14, pp. 160–164.

Huang, M.F., Qiang Li, C.M. Chan, W.J. Lou, K.C.S. Kwok, and G. Li (2016). "Performance-based design optimization of tall concrete framed structures subject to wind excitations". In: *Journal of Wind Engineering and Industrial Aerodynamics* 139.Supplement C, pp. 70–81.

Huang, P., Y. Quan, and G. Ming (2013). "Experimental Study of Aerodynamic Damping of Typical Tall Buildings". In: *Mathematical Problems in Engineering* 2013, n.9.

Huang, R., A. Li, and Z. Zhang (2010). "MTMD wind-induced vibration control of Beijing Olympic Center Broadcast Tower based on its simplified model". In: *Jianzhu Jiegou Xuebao/Journal of Building Structures* 31.SUPPL. 2, pp. 131–136.

Irwin, P.A. (2008). "Bluff body aerodynamics in wind engineering". In: *Journal of Wind Engineering and Industrial Aerodynamics* 96, pp. 701–712.

ISO-15686 (2017). *Buildings and constructed assets: Service life planning part 1–10*. Technical Committee ISO/TC 59, Building construction – Subcommittee SC 14, Design life.

Jain, A., M. Srinivasan, and G.C. Hart (2001). "Performance based design extreme wind loads on a tall building". In: *The structural design of tall buildings* 10.-, pp. 9–26.

Jalayer, F., D. Asprone, A. Prota, and G. Manfredi (2011). "Multi-hazard upgrade decision making for critical infrastructure based on life-cycle cost criteria". In: *Earthquake engneering and structural dynamics* 40.10, pp. 1163–1179.

Jayachandran, P. (2009). "Design of Tall Buildings Preliminary Design and Optimization". In: *National Workshop on High-rise and Tall Buildings*. Hyderabad, India.

Johnson, R.A. and T.E. Wehrly (1978). "Some Angular-Linear Distributions and Related Regression Models". In: *Journal of the American Statistical Association* 73.363, pp. 602–606.

Kameshwar, S. and J.E. Padgett (2014). "Multi-hazard risk assessment of highway bridges subjected to earthquake and hurricane hazards". In: *Engineering Structures* 78, pp. 154–166.

Kareem, A. (1981). "Wind induced torsional loads on structures". In: *Engineering Structures* 3.2, pp. 85–86.

— (1982). "Acrosswind response of buildings". In: *ASCE J. Struct. Div.* 108.ST4, pp. 869–887.

Kareem, A. and Y. Zhou (2003). "Gust loading factor - past, present and future". In: *Journal of Wind Engineering and Industrial Aerodynamics* 91.12–15, pp. 1301–1328.

Kareem, A., T. Kijewski, and Y. Tamura (1999). "Mitigation of motions of tall buildings with specific examples of recent applications". In: *Wind and Structures* 2.3, pp. 201–251.

Kaveh, A., M. Kalateh-Ahani, and M. Fahimi-Farzam (2014). "Life-cycle cost optimization of steel moment-frame structures: Performance-based seismic design approach". In: *Earthquake and Structures* 7.3, pp. 271–294.

Kiani, A., B. Mansouri, and A.S. Moghadam (2016). "Fragility curves for typical steel frames with semi-rigid saddle connections". In: *Journal of Constructional Steel Research* 118, pp. 231–242.

Kim, Y.M., K.P. You, and N.H. Ko (2008). "Across-wind responses of an aeroelastic tapered tall building". In: *Journal of Wind Engineering and Industrial Aerodynamics* 96, pp. 1307–1319.

Kiureghian, A.M. (2005). "Life-cycle cost optimization of steel moment-frame structures: Performance-based seismic design approach". In: *Earthquake Engineering and Structural Dynamics* 34, pp. 1643–1652.

Kunnath, S.K. (2006). *Application of the PEER PBEE Methodology to the I-880 Viaduct*. Tech. rep. University of California, Davis.

Kwok, Kenny C.S. and William H. Melbourne (1981). "WIND-INDUCED LOCK-IN EXCITATION OF TALL STRUCTURES". In: *ASCE J Struct Div* 107.1, pp. 57–72.

LaFave, J.M., Z. Gao, D.E. Holder, M.J. Kuo, and L.A. Fahnestock (2016). "Commercial and residential building performance during the May 20, 2013, Tornado in Moore, Oklahoma". In: *Journal of Performance of Constructed Facilities* 30.2, p. 04014210.

Lagaros, N.D. (2007). "Life-cycle cost analysis of design practices for RC framed structures". In: *Bulletin of Earthquake Engineering* 5.3, pp. 425–442.

— (2013). "Life-cycle cost assessment of mid-rise and high-rise steel and steel–reinforced concrete composite minimum cost building designs". In: *The structural design of tall and special buildings* 22, pp. 954–974.

Lagaros, N.D. and M.G. Karlaftis (2016). "Life-cycle cost structural design optimization of steel wind towers". In: *Computers and Structures* 174, pp. 122–132.

Last, G. and M. Penrose (2017). *Lectures on the Poisson Process*. IMS Textbook by Cambridge University Press.

Le, T.-H. and L. Caracoglia (2017). "Computer-based model for the transient dynamics of a tall building during digitally simulated Andrews AFB thunderstorm". In: *Computers and Structures* 193, pp. 44–72.

Li, G. and H. Hu (2014). "Risk design optimization using many-objective evolutionary algorithm with application to performance-based wind engineering of tall buildings". In: *Structural Safety* 48, pp. 1–14.

Lienhard, J.N. (1996). *Synopsis of lift, drag, and vortex frequency data for rigid circular cylinders*. Tech. rep. Washington State University, Washington.

Life Cycle Costing. `http://ec.europa.eu/environment/gpp/pdf/WP-LifeCycleCosting.qx.pdf`. Accessed: 2017-12-11.

Lin, N., C. Letchford, Y. Tamura, B. Liang, and O. Nakamura (2005). "Characteristics of wind forces acting on tall buildings". In: *ournal of Wind Engineering and Industrial Aerodynamics* 93.3, pp. 217–242.

Liu, M. and M Boaxia (2017). "Life cycle cost analysis of energy-efficient buildings subjected to earthquakes". In: *Energy and Buildings* 154.Supplement C, pp. 581–589.

Liu, M., Y.K. Wen, and S.A. Burns (2004). "Life cycle cost oriented seismic design optimization of steel moment frame structures with risk-taking preference". In: *Engineering Structures* 26.10, pp. 1407–1421.

Mahmoud, H. and G. Cheng (2017). "Framework for lifecycle cost assessment of steel buildings under seismic and wind hazards". In: *Journal of Structural Engineering* 143.3, p. 040161.

Mannini, C., A.M. Marra, T. Massai, and G. Bartoli (2011). "Interference of vortex-induced vibration and transverse galloping for a rectangular cylinder". In: *Journal of Fluids and Structures* 66, pp. 403–423.

Marano, G.C., R. Greco, and S. Sgobba (2013). "A comparison between different robust optimum design approaches: Application to tuned mass dampers." In: *Probabilistic Engineering Mechanics* 25, pp. 108–118.

Marukawa, H., N. Kato, K. Fujii, and Y. Tamura (1996). "Experimental evaluation of aerodynamic damping of tall buildings". In: *Journal of Wind Engineering and Industrial Aerodynamics* 59.2–3, pp. 177–190.

Matsumoto, T. (1986). "On the across-wind oscillation of tall buildings". In: *Journal of Wind Engineering and Industrial Aerodynamics* 24.1, pp. 69–85.

Matta, E. (2015). "Seismic effectiveness of tuned mass dampers in a life-cycle cost perspective". In: *Earthquake and Structure* 9.1, pp. 73–91.

Melbourne, W.H. (1980). "Comparison of measurements on the CAARC standard tall building model in simulated model wind flows." In: *Journal of Wind Engineering and Industrial Aerodynamics* 6.1–2, pp. 73–78.

Mitropoulou, C.C., N.D. Lagaros, and M. Papadrakakis (2011). "Life-cycle cost assessment of optimally designed reinforced concrete buildings under seismic actions". In: *Reliability Engineering and System Safety* 96, pp. 1311–1331.

— (2015). "Generation of artificial accelerograms for efficient life-cycle cost analysis of structures". In: *Engineering Structures* 88, pp. 138–153.

Moon, K.S. (2010). "Vertically distributed multiple tuned mass dampers in tall buildings: Performance analysis and preliminary design". In: *Structural Design of Tall and Special Buildings* 19.3, pp. 347–366.

NERACOOS. *Northeastern Regional Association of Coastal and Ocean Observing Systems*. Tech. rep. URL: `http://www.neracoos.org/`.

Norton, T.R., M.M. Abdullah, and D. Stephens (2008). "Proposed Methodology for Performance-Based Vulnerability Assessment of Wind-Excited Tall Buildings". In: *The 4th International Conference on Advances in Wind and Structures(AWAS08)*, pp. 1228–1246.

Okasha, N.M. and D.M. Frangopol (2011). "Computational platform for the integrated life-cycle management of highway bridges". In: *Engineering Structures* 33.7, pp. 2145–2153.

Padgett, J.E., K. Dennemann, and J. Ghosh (2010). "Risk-based seismic life-cycle cost-benefit (LCC-B) analysis for bridge retrofit assessment". In: *Structural Safety* 32.3, pp. 165–173.

Pandey, M.D. and J.A.M. van der Weide (2017). "Stochastic renewal process models for estimation of damage cost over the life-cycle of a structure". In: *Structural Safety* 67.Supplement C, pp. 27–38.

Patil, V.B. and R.S. Jangid (2011). "Optimum multiple tuned mass dampers for the wind excited benchmark building". In: *Journal of Civil Engineering and Management* 17.4, pp. 540–557.

PEER-TBI (2010). *Tall Buildings Initiative, Guidelines for performance-based seismic design of tall buildings. Report No. 2010/05. TBI Guidelines Working Group*. PEER Center University of Berkeley California (USA).

Petrini, F., K. Gkoumas, and F. Bontempi (2013). "Damage and loss evaluation in the performance-based wind engineering". In: *Proceedings of the 11th International Conference on Structural Safety and Reliability ICOSSAR 2013*, pp. 1791–1797.

Piccardo, G. and G. Solari (2000). "Three-dimensional wind-excited response of slender structures: Closed-form solution". In: *Journal of Structural Engineering* 126.8, pp. 936–943.

Porter, K., R. Kennedy, and R. Bachman (2007). "Creating fragility functions for performance-based earthquake engineering". In: *Earthquake Spectra* 23.2, pp. 471–489.

Pozzuoli, C., G. Bartoli, U. Peil, and M. Clobes (2013). "Serviceability wind risk assessment of tall buildings including aerolastic effects". In: *Journal of Wind Engineering and Industrial Aerodynamics* 123.0, pp. 325–338.

Ramirez, C.M. and E. Miranda (2012). "Significance of residual drifts in building earthquake loss estimation". In: *Earthquake Engineering and Structural Dynamics* 41.11, pp. 1477–1493.

Ramirez, C.M., A.B. Liel, J. Mitrani-Reiser, C.B. Haselton, A.D. Spear, J. Steiner, Deierlein G.G., and Miranda E. (2012). "Expected earthquake damage and repair costs in reinforced concrete frame buildings". In: *Earthquake Engineering and Structural Dynamics* 41.11, pp. 1455–1475.

Seo, D.W. and L. Caracoglia (2013). "Estimating life-cycle monetary losses due to wind hazards: Fragility analysis of long-span bridges". In: *Engineering Structures* 56, pp. 1593–1606.

Shin, H. and M.P. Singh (2017). "Minimum lifecycle costbased optimal design of yielding metallic devices for seismic loads". In: *Engineering Structures* 144.Supplement C, pp. 174–184.

Simiu, E. and R.H. Scanlan (1996). *Wind effects on structures*. New York: Wiley.

Solari, G. (1982). "Alongwind response estimation: closed form solution". In: *ASCE J. Sruct. Div.* 108.7, pp. 225–244.

— (1987). "Turbulence Modeling for Gust Loading". In: *Journal of Structural Engineering* 113.7.

— (1994). *Gust-Excited Vibration (Wind Excited vibration of structures*. New York: Springer-Verlag Wien GMBH.

Soong, T.T. (1990). *Active Structural Control: Theory and Practice*. Longman Scientific & Technical.

Soong, T.T. and Dargush (1997). *Passive Energy Dissipation Systems in Structural Engineering*. John Wiley & Sons.

Spence, S.M.J. and A. Kareem (2014). "Performance-based design and optimization of uncertain wind-excited dynamic building systems". In: *Engineering Structures* 78, pp. 133–144.

Taflanidis, A. and J. Beck (2009). "Life-cycle cost optimal design of passive dissipative devices". In: *Structural Safety* 31.6, pp. 508–522.

Tallin, A. and B. Ellingwood (1985). "Analysis of torsional moments on tall buildings". In: *Journal of Wind Engineering and Industrial Aerodynamics* 18.2, pp. 191–195.

Taranath, B.S. (1998). *Steel, Concrete & Composite DEsign of Tall Buildings*. New York: McGraw-Hill Book Company.

— (2012). *Structural Analysis and Design of Tall Buildings*. Boca Raton, London, New York: CRC Press, Taylor & Francis Group.

Taylor, G.I. (1938). "The spectrum of turbulence". In: *Proceedings of the Royal Society of London. Series A, Mathematical and Physical Sciences* 164, pp. 476–490.

Tessari, R.K., H.M. Kroetz, and A.T. Beck (2017). "Performancebased design of steel towers subject to wind action". In: *Engineering Structures* 143.Supplement C, pp. 549–557.

Tschanz, T. and A.G. Davenport (1983). "The base balance technique for the determination of dynamic wind loads". In: *Journal of Wind Engineering and Industrial Aerodynamics* 13, pp. 429–439.

— (2016). "LCA of tall buildings: Still a long way to go". In: *Journal of Building Engineering* 7, pp. 379–381.

Tuned Mass Damper Applet. `http://web.mit.edu/jorloff/www/jmoapplets/secondorder/TunedMassDamper.html`. Accessed: 2017-11-30.

Venanzi, I. (2015). "Robust optimal design of tuned mass dampers for tall buildings with uncertain parameters". In: *Structural and Multidisciplinary Optimization* 51.1, pp. 239–250.

Venanzi, I. and A.L. Materazzi (2013). "Robust optimization of a hybrid control system for wind-exposed tall buildings with uncertain mass distribution". In: *Smart Structures and Systems* 12.6, pp. 641–659.

Venanzi, I., D. Salciarini, and Tamagnini C. (2014). "The effect of soil–foundation–structure interaction on the wind-induced response of tall buildings". In: *Engineering Structures* 79, pp. 117–130.

Venanzi, I., O. Lavan, and S. Fabrizi (2017). "Multi-hazard life-cycle performance of tall buildings under seismic and wind loads". In: *Life-Cycle of Engineering Systems: Emphasis on Sustainable Civil Infrastructure - 5th International Symposium on Life-Cycle Engineering, IALCCE 2016*, pp. 177–184.

Verma, S.K., A.K. Ahuja, and A.D. Pandey (2013). "Effects of wind incidence angle on wind pressure distribution on square plan tall buildings". In: *J. Acad. Indus. Res.* 1.12, pp. 747–752.

Vickery, B.J. and A. Steckley (1993). "Aerodynamic damping and vortex excitation on an oscillating prism in turbulent shear flow". In: *Journal of Wind Engineering and Industrial Aerodynamics* 49.1–3, pp. 121–140.

Vickery, P.J., P.F. Skerlj, J. Lin, L.A. Twisdale Jr., M.A. Young, and F.M. Lavelle (2006). "HAZUS-MH Hurricane Model Methodology. II:Damage and Loss Estimation". In: *Natural Hazards Review* 7.2, pp. 94–103.

Vision, 2000 (1995). *Performance Based Seismic Engineering of Buildings*. Tech. rep. University of California, Davis.

Wang, C.S., M.S. Zhai, H.T. Li, Y.Q. Ni, and T. Guo (2015). "Life-cycle cost based maintenance and rehabilitation strategies for cable supported bridges". In: *Advanced Steel Construction* 11.3, pp. 395–410.

Wang, L., X. Zhao, and Y.M. Zheng (2016). "A combined tuned damper and an optimal design method for wind-induced vibration control for super tall buildings". In: *The Structural Design of Tall and Special Buildings* 25.10, pp. 468–502.

Warburton, G.B. (1982). "Optimum absorber parameters for various combination of response and excitation parameters". In: *Earthquake Engineering and Structural Dynamics* 79, pp. 381–401.

Welch, P.D (1967). "The Use of Fast Fourier Transform for the Estimation of Power Spectra: A Method Based on Time Averaging Over Short, Modified Periodograms". In: *IEEE Trans. Audio Electroacoustics* AU.15, pp. 70–73.

Wen, Y.K. (2001). "Minimum lifecycle cost design under multiple hazards". In: *Reliability Engineering and System Safety* 73.-, pp. 223–231.

Wen, Y.K. and Y.J. Kang (2001). "Minimum building life-cycle cost design criteria. I: Methodology". In: *Journal of Structural Engineering, ASCE* 127.3, pp. 330–337.

Whitebread, R.E. (1975). "The measurement of non-steady wind forces on small-scale building models". In: *Proceedings of the fourth International Conference on Wind Effects on Buildings and Structures (Heathrow England)*, pp. 567–574.

Wong, K.K.F. and J.J. Harris (2013). "Seismic fragility and cost analyses of actively controlled structures". In: *The Structural Design of Tall and Special Buildings* 22, pp. 569–583.

Workplace Standards and Guidelines for office space. `http://www.mbie.govt.nz/info-services/nz-govt-procurement-and-property/government-property-group/document-image-library/workplace-standards-guidelines-office-space.pdf`. Accessed: 2017-12-10.

Xu, Y.L. and K.C.S. Kwok (1993). "Mode Shape corrections for wind tunnel tests of tall buildings". In: *Engineering Structures* 15.5, pp. 387–392.

Xu, YL, KCS Kwock, and B Samaly (1992). "Control of wind-induced tall building vibration by tuned mass damper". In: *Journal of Wind Engineering and Industrial Aerodynamics* 40, pp. 1–32.

Yamin, L.E., A. Hurtado, R. Rincon, Dorado J.F., and J.C. Reyes (2017). "Probabilistic seismic vulnerability assessment of buildings in terms of economic losses". In: *Engineering Structures* 138, pp. 308–323.

Yi, J. and Q.S. Li (2015). "Wind tunnel and full-scale study of wind effects on a super-tall building". In: *Journal of Fluids and Structures* 58, pp. 236–253.

Zhao, X. and T. Yu (2013). "Human comfort performance-based life cycle cost model of high-rise structures under wind load". In: *Tongji Daxue Xuebao/Journal of Tongji University* 41.12, pp. 1793–1798.

Zhou, Y., Kareem, and M. Gu (2002). "Mode Shape Corrections for Wind Load Effects". In: *Journal of Engineering Mechanics* 128.1, pp. 15–23.